



Democratic and Popular Republic of Algeria
Ministry of Higher Education and Scientific Research
University Mohamed Khider of Biskra



Faculty of Exact Sciences and Science of Nature and Life
Department of Matter Sciences

Ref :

Thesis Presented to obtain the degree of

Doctorate in Chemistry

Option: Pharmaceutical chemistry

Entitled:

Application of drug design strategies to predict new bioactive molecules

Presented by:
Bourougaa Lotfi

Publicly defended on: 24 / 10 / 2024

In front of the Jury committee composed of:

Mr. Belaidi Salah	Professor	University of Mohamed Khider of Biskra	President
Mrs. Ouassaf Mebarka	MCA	University of Mohamed Khider of Biskra	Supervisor
Mrs. Zekri Afaf	Professor	University of Mohamed Khider of Biskra	Examiner
Mrs. Kerassa Aicha	Professor	University of Echahid Hama Lakhdar of El Oued	Examiner

Abstract

Influenza is a pulmonary infection triggered by a virus that produces fever. Periodic epidemics can be fatal. Antiviral therapy shortens the length of sickness by around one day and will need to be explored especially for high-risk individuals. This work was focused on discovering and developing novel and effective anti-influenza medicines. Neuraminidase was chosen as the major target due to its critical activity and importance in the life of the influenza virus. Several compounds were created in the first stage using pharmacophore modeling, fragment-based drug design, Breed-Based De Novo Hybridization and 3D-QSAR (CoMFA model). The docking modeling data reveal that all of the designed compounds bind well to the Neuraminidase receptor in comparison with the clinical blockers. Moreover, each compound's pharmacokinetic profile has been verified, particularly its aqueous solubility, permeability, and bioavailability. The potential toxicity of each developed molecule was assessed using the ProTox II platform and the VEGA QSAR package. The atomic mobility of the generated complexes between the proposed compounds and Neuraminidase receptor was examined using molecular dynamics simulations performed for 100 ns via Gromacs package. All of the data show that the formed complexes (designed molecules_Neuraminidase) have high biomolecular stability. Finally, the results of molecular docking were confirmed by MM-BPSA calculations.

Key Word: *Influenza, Neuraminidase, Pharmacophore, Molecular docking, Fragment-based drug design, Breed-Based De Novo Hybridization, 3D-QSAR, CoMFA, Gromacs, MM-PBSA.*

Résumé

Influenza (la grippe) est un virus qui provoque une infection respiratoire et la fièvre. Les épidémies peuvent être mortelles. La période de la maladie est diminuée d'environ une journée par le traitement antiviral, qui devra être examiné en particulier chez les personnes à haut risque. Le but de ce travail était de trouver et de créer des médicaments efficaces antigrippaux. La Neuraminidase a été choisie comme cible principale en raison de son activité essentielle et de son impact sur la l'existence du virus. Dans un premier temps, plusieurs composés ont été créés à l'aide de la modélisation pharmacophore, de la conception de médicaments basée sur les fragments, de l'hybridation De Novo basée sur la race et du 3D-QSAR (modèle CoMFA). Les résultats de l'amarrage moléculaire indiquent que tous les composés générés se lient particulièrement au récepteur de la Neuraminidase par rapport aux inhibiteurs cliniques. De plus, le profil pharmacocinétique de chaque composé a été vérifié, notamment sa solubilité aqueuse, sa perméabilité et sa biodisponibilité. La toxicité potentielle de chaque molécule développée a été évaluée à l'aide de la plateforme ProTox II et du package VEGA QSAR. La mobilité atomique des complexes générés entre les composés proposés et le récepteur de la Neuraminidase a été examinée à l'aide de simulations de dynamique moléculaire réalisées pendant 100 ns via le package Gromacs. Toutes les données montrent que les complexes formés ont une grande stabilité structurelle et biomoléculaire. Enfin, les résultats de l'amarrage moléculaire ont été confirmés par les calculs MM-BPSA.

Mot clé : *Influenza, Neuraminidase, Pharmacophore, Fragments, L'hybridation De Novo basée sur la race, 3D-QSAR, CoMFA, Gromacs, MM-PBSA.*

المخلص

الأنفلونزا هي عدوى في الجهاز التنفسي يسبب الحمى. والأوبئة الدورية يمكن أن تكون قاتلة. العلاج المضاد للفيروسات يقلل مدة المرض بحوالي يوم واحد ويحتاج الى اكتشاف المرض مبكرا خاصة عند الأشخاص الذين لديهم أمراض مزمنة وكبار السن. ركز هذا العمل على إكتشاف وتطوير أدوية جديدة فعالة ضد الأنفلونزا. تم إختيار النورامينيداز كهدف عالجي بسبب أهميته ودوره الرئيسي في حياة الفيروس وانتشاره. في المرحلة الأولى تم تطوير العديد من الجزيئات النشطة باستخدام تصميم الفرماكوفور، تصميم الأدوية القائم على الأجزاء (الشظايا)، التهجين القائم على السلالة والعلاقة الكمية بين البنية والنشاط ثلاثية الأبعاد. تشير نتائج الالتحام الجزيئي أن جميع الجزيئات المصممة ترتبط إرتباطا قويا مع مستقبل النورامينيداز عند مقارنتها بالمتبطات السريرية. علاوة على ذلك، تم التحقق من الحركات الدوائية لكل مركب مصمم، وخاصة قابليته للذوبان في الماء ونفاذيته للأغشية البيولوجية والتوافر البيولوجي. من ناحية أخرى تم تقييم السمية المحتملة لكل جزيء مقترح باستخدام الأدوات الحاسوبية المختلفة. تم فحص الحركة الذرية للمعقدات المتولدة بين الجزيئات المتفرحة ومستقبل النورامينيداز باستخدام محاكاة الديناميكا الجزيئية لمدة 100 نانو ثانية عبر حزمة غروماكس، أشارت جميع البيانات الى أن جميع المعقدات المتشكلة بين الجزيئات المصممة والموقع الفعال للنورامينيداز تتمتع بثبات جزيئي وهيكل ممتاز وحركة ذرية ضعيفة. أخيرا تم التأكد من صحة نتائج الالتحام الجزيئي من خلال نهج الميكانيكا الجزيئية_ بواسون بولتزمان.

الكلمات المفتاحية: الأنفلونزا، النورامينيداز، الفرماكوفور، الالتحام الجزيئي، التصميم القائم على الأجزاء (الشظايا)، التصميم القائم على السلالة، العلاقة الكمية بين البنية والنشاط ثلاثية الأبعاد، غروماكس، الميكانيكا الجزيئية_ بواسون بولتزمان.

CONTENTS

ACKNOWLEDGMENT

TABLE OF CONTENTS

LIST OF FIGURS.....	I
LIST OF TABLES.....	VI
LIST OF ABBREVIATIONS.....	IX
General Introduction.....	1
References.....	4

Chapter I: Influenza Virus and Neuraminidase

I.1 Introduction.....	6
I.2 Neuraminidase Morphology.....	7
I.2.1 Transmembrane zone.....	7
I.2.2 Cytoplasmic tail ambit.....	8
I.2.3 Catalytic head.....	9
I.2.4 Stalk.....	9
I.3 Mechanism of Action of NAIs.....	10
I.4 Safety of Neuraminidase Inhibitors.....	11
I.4.1 Zanamivir.....	11
I.4.2 Oseltamivir.....	11
I.5 Neuraminidase Mutations Linked to NAI Resistance.....	13
I.6 Creating Neuraminidase-Inhibitors in Future Years.....	14
I.7 References.....	16

Chapter II: Drug Design Strategies

II.1 Introduction.....	21
II.2 Computer-Aided Drug Design Strategies.....	21
II.2.1 Structure-based drug design (SBDD).....	22
II.2.2 Ligand-based drug design (LBDD).....	23

II.2.2.1 Quantitative structure–activity relationship (QSAR).....	23
II.2.2.2 Pharmacophore modeling.....	24
II.2.2.3 BREED Based De Novo Hybridization strategy.....	25
II.3 ADME and Drug Likeness.....	26
II.3.1 Solubility.....	27
II.3.2 Lipophilicity.....	27
II.4 In Silico Toxicity Prediction.....	28
II.5 Molecular Dynamics Simulation (MDS).....	29
II.6 References.....	31

***Chapter III: Pharmacophore-Based Virtual Screening, Molecular Docking and
Molecular Dynamics Studies for the Discovery of Novel Neuraminidase
Inhibitors***

III.1 Introduction.....	35
III.2 Materials and Methods.....	36
III.2.1 Ligand preparation.....	36
III.2.2 Protein preparation.....	37
III.2.3 Generation of pharmacophore model.....	37
III.2.4 Construction of the 3D-QSAR model.....	37
III.2.5 Model validation.....	37
III.2.6 Virtual screening and docking study.....	38
III.2.7 ADMET study.....	38
III.2.8 Molecular dynamics simulation.....	38
III.2.9 Method of MMPBSA analysis.....	39
III.3 Results and Discussion.....	39
III.3.1 Pharmacophore and 3D-QSAR models.....	39
III.3.2 Model validation.....	40
III.3.3 3D-QSAR contour maps analysis.....	41

III.3.4 Virtual screening and docking studies.....	42
III.3.5 Prediction of ADME.....	46
III.3.6 Prediction of toxicity.....	46
III.3.7 Molecular dynamics study.....	47
III.3.8 MMPBSA analysis.....	50
III.4 Conclusion.....	52
III.5 References.....	53

Chapter IV: Discovery of Novel Potent Drugs for Influenza by Inhibiting the Vital Function of Neuraminidase via Fragment-Based Drug Design (FBDD) and Molecular Dynamics Simulation Strategies

IV.1 Introduction.....	56
IV.2 Computational Methods.....	58
IV.2.1 Protein and fragments preparation.....	58
IV.2.2 Fragment linking and molecular docking studies.....	58
IV.2.3 ADMET prediction.....	59
IV.2.4 Molecular dynamic simulation.....	59
IV.2.5 MM-PBSA calculations.....	60
IV.2.6 Reaction based enumeration.....	60
IV.3 Results and Discussion.....	60
IV.3.1 Fragment-based drug design and molecular docking.....	60
IV.3.2 ADMET and bioavailability.....	66
IV.3.3 Molecular dynamic simulation (MDS).....	68
IV.3.3.1 RMSD and RMSF analysis.....	68
IV.3.3.2 Radius of gyration (Rg) analysis.....	70
IV.3.3.3 Hydrogen bonds analysis.....	71
IV.3.3.4 Solvent accessible surface area (SASA) analysis.....	71
IV.3.4 MM-PBSA analysis.....	72

IV.3.5 Reaction based enumeration.....	74
IV.4 Conclusion.....	75
IV.5 Reference.....	77

***Chapter V: Pharmacoinformatics and Breed-Based De Novo Hybridization
Studies to Develop New Neuraminidase Inhibitors as Potential Anti-Influenza
Agents***

V.1 Introduction.....	80
V.2 Materials and Methods.....	81
V.2.1. Breed De Novo hybridization approach.....	81
V.2.2 Molecular docking study.....	83
V.2.3 ADME-Tox prediction.....	83
V.2.4 Molecular dynamic simulation.....	83
V.2.5 Binding free energy.....	84
V.2.6 Reaction-based enumeration.....	84
V.3 Result.....	85
V.3.1 Breed-based De Novo and molecular docking approaches.....	85
V.3.2 ADMET prediction.....	90
V.3.3 Study of molecular dynamics.....	91
V.3.3.1 RMSD and RMSF analysis.....	91
V.3.3.2 Radius of gyration (Rg).....	94
V.3.3.3 Hydrogen binding analysis.....	94
V.3.3.4 Solvent-accessible Surface area (SASA).....	95
V.3.4 MM-PBSA Analysis.....	96
V.3.5 Reaction-Based Enumeration.....	98
V.4 Discussion.....	102
V.5 Conclusion.....	103
V.6 References.....	105

Chapter VI: Comparative Molecular Field Analysis (CoMFA), Molecular Docking and ADMET Study on Thiazolidine-4-carboxylic acid Derivatives as New Neuraminidase Inhibitors

VI.1 Introduction.....	109
VI.2 Materials and Methods.....	111
VI.2.1 Experimental databases.....	111
VI.2.2 Structure preparation and alignment.....	111
VI.2.3 Generation of 3D-QSAR by CoMFA.....	111
VI.2.4 PLS analysis and validations.....	112
VI.2.5 Molecular docking.....	113
VI.1.6 Prediction of ADMET properties.....	114
VI.3 Results and Discussions.....	114
VI.3.1 Molecular alignment of dataset.....	114
VI.3.2 3D-QSAR model and validations.....	115
VI.3.3 CoMFA contour cap.....	116
VI.3.4 Design for new neuraminidase inhibitors.....	117
VI.3.5 Molecular docking.....	121
VI.3.6 ADMET and bioavailability prediction.....	124
VI.4 Conclusion.....	126
VI.5 References.....	127
General Conclusion.....	131

LIST OF FIGURES

Chapter I

Figure I. 1. <i>Viral structure of influenza virus.....</i>	7
Figure I. 2. <i>Neuraminidase structure and subdomains.....</i>	8
Figure I. 3. <i>The Neuraminidase catalytic head.....</i>	9
Figure I. 4. <i>The molecular structure of NAIs. All of these compounds have their origins on the configuration of DANA molecule.....</i>	10

Chapter II

Figure II. 1. <i>The most frequently employed drug design strategies.....</i>	21
Figure II. 2. <i>A graphical illustration of virtual screening (A), and de novo drug-design (B) strategies.....</i>	23
Figure II. 3. <i>Overview of QSAR modeling.....</i>	24
Figure II. 4. <i>Overview of pharmacophore modeling.....</i>	25
Figure II. 5. <i>Overview of breed based de novo hybridization strategy.....</i>	26
Figure II. 6. <i>Overview of molecular dynamics simulation via GROMACS package.....</i>	30

Chapter III

Figure III. 1. <i>(A) Pharmacophore model ADDPR_4 with their five-pharmacophore site points, and (B) Pharmacophore model ADRRR1 including an active molecule.....</i>	40
Figure III. 2. <i>The plot of the correlation between the experimental and predicted activity of based Neuraminidase inhibitors using pharmacophore-based QSAR model of training and test set.....</i>	41
Figure III. 3. <i>Contour maps for 3D-QSAR model: (A) Hydrogen Bond, (B) Hydrophobic, (C) Negative ionic, (D) Positive ionic, (E) Electron-withdrawing, where blue cubes represent favorable areas and red cubes represent unfavorable areas.....</i>	42
Figure III. 4. <i>The orientation of the hit molecules in the active site and hydrogen bonds and hydrophobic areas.....</i>	44

Figure III. 5. The binding interactions of the top hits with the active site of Neuraminidase, (a) CID 70139197, (b) CID 44428312, (c) CID 506047, (d) CID 3364666, (e) CID 5278285.....	45
Figure III. 6. The binding interactions of the Zanamivir and Oseltamivir with the active site of Neuraminidase.....	46
Figure III. 7. Root-mean-square deviation (RMSD) analysis of the backbone atoms of Neuraminidase and its complexes with CID 70139197 and CID 44428312.....	47
Figure III. 8. Root-mean-square fluctuation (RMSF) of the C-alpha atoms of Neuraminidase (NA) and its complexes with CID 70139197 and CID 44428312. A. RMSF of the C-alpha atoms of NA and its complexes. B. RMSF of the atoms of CID 44428312 and CID 70139197.....	48
Figure III. 9. Radius of gyration (Rg) of Neuraminidase and its complexes with CID 44428312 and CID 70139197.....	49
Figure III. 10. Hydrogen bond existence map of Neuraminidase complexes with CID 44428312 and CID 70139197 during 100 ns of simulation.....	49
Figure III. 11. Delta energy components for MMPBSA calculations for the complex (NA_44428312), receptor (NA) and ligand (CID 44428312).....	50
Figure III. 12. Delta energy components for MMPBSA calculations for the complex (NA_70139197), receptor (NA) and ligand (CID 70139197).....	51

Chapter IV

Figure IV. 1. SAR of Zanamivir, Peramivir and Oseltamivir drugs.....	56
Figure IV. 2. Fragment-based drug design (FBDD) strategy.....	58
Figure IV. 3. Chemical compositions of the top 10 compounds identified through the fragment-based drug design process and their constituent fragments.....	61
Figure IV. 4. Summary of structure-activity relationships of the best five hit inhibitors.....	62
Figure IV. 5. 2D diagram of the designed inhibitors and Zanamivir within Neuraminidase receptor.....	65

Figure IV. 6. The relative stability of the designed inhibitors with Neuraminidase receptor based on average root-mean-square deviation (RMSD).....	68
Figure IV. 7. The relative stability of the designed inhibitors with Neuraminidase receptor based on root-mean-square fluctuations (RMSFs).....	69
Figure IV. 8. Radius of gyration (Rg) of Neuraminidase and its complexes with Molecule 01-10, including Zanamivir.....	70
Figure IV. 9. Number of hydrogen bonds formed during 100 ns of simulation between NA, designed molecules and Zanamivir.....	71
Figure IV. 10. Solvent accessible surface area (SASA) for all complexes during 100 ns of simulation.....	72
Figure IV. 11. Graphic representation of total binding energies of the five systems.....	73
Figure IV. 12. Binding poses of the four complexes (NA_Molecule 01-04) over 100 ns of simulation.....	74
Figure IV. 13. Predicted synthetic pathway of the four designed Neuraminidase inhibitors (Molecule 01-04).....	75

Chapter V

Figure V. 1. Breed-based de novo hybridization strategy.....	81
Figure V. 2. The structures of compounds utilized in this research.....	82
Figure V. 3. Structures of the best fragments.....	86
Figure V. 4. Breed generation of top-scoring compounds from different fragments.....	87
Figure V. 5. The binding interactions of the seven new breed molecules, Zanamivir, Peramivir, and Oseltamivir within the active site of Neuraminidase.....	88
Figure V. 6. Root-mean-square deviation (RMSD) profile of the backbone atoms of Neuraminidase and its complexes with Breeds 1–7.....	92
Figure V. 7. Root-mean-square fluctuation (RMSF) of the C-alpha atoms of Neuraminidase (NA) and its complexes with Breeds 1–7.....	93

Figure V. 8. Radius of gyration (Rg) of Neuraminidase and its complexes with Breeds 1–7.....	94
Figure V. 9. Map of hydrogen bond existence of Neuraminidase complexes with Breeds 1–7.....	95
Figure V. 10. Solvent-accessible surface area (SASA) for Neuraminidase and its complexes during 100 ns of simulation.....	96
Figure V. 11. The Gibbs energy landscape maps over 100 ns of simulations for (A) NA, (B) NA_Breed 1, (C) NA_Breed 2, (D) NA_Breed 3, (E) NA_Breed 4, (F) NA_Breed 5, (G) NA_Breed 6, and (H) NA_Breed 7, with the extracted structures from the low-energy areas (in blue).	98
Figure V. 12. Predicted synthetic pathways of all the breed molecules (Breeds 1–7).....	102

Chapter VI

Figure VI. 1. Binding interaction illustration of Neuraminidase in complex with 1SJ.....	114
Figure VI. 2. The alignment of all molecules in the database.....	114
Figure VI. 3. The plot of the correlation between the experimental and predicted activity using 3D-QSAR model of training and test set.....	116
Figure VI. 4. CoMFA contour plot of compound binding to target: Visualization of (A) Steric and (B) Electrostatic Fields. Blue and green regions are favorable for inhibitory activity, red and yellow green regions are unfavorable for inhibitory activity.....	117
Figure VI. 5. Structural characteristics derived from CoMFA contour Map: Analysis of favorable and unfavorable regions for inhibitory activity. Blue and green regions are favorable for inhibitory activity, red and yellow green regions are unfavorable for inhibitory activity.....	118
Figure VI. 6. Proposed reaction: General form and chemical equations.....	118
Figure VI. 7. Proposed general mechanism for synthesizing the six compounds: Insights into reaction pathways and synthetic strategies.....	119
Figure VI. 8. Insights into ligand binding modes: Interactions of six designed compounds with Neuraminidase active site.....	123
Figure VI. 9. Comparative analysis of ligand binding modes: Interactions of 1SJ and Oseltamivir with Neuraminidase.....	123

Figure VI. 10. Assessing Drug-like properties: Bioavailability radar graphs of six designed molecules.....125

LIST OF TABLES

Chapter I

Table I. 1. Neuraminidase inhibitors used to combat the flu.....	12
Table I. 2. Resistance mutations in the Neuraminidase inhibitor.....	13

Chapter II

Table II. 1. Examples for the prediction of lipophilicity.....	28
---	----

Chapter III

Table III .1. Compounds structures with experimental activity.....	36
Table III. 2. Scores of different parameters of the best hypotheses.....	40
Table III. 3. Results of the 3D-QSAR, PLS statistical analysis for the chosen Pharmacophore model ADDPR_4.....	40
Table III. 4. Results of external validation for 3D-QSAR model.....	41
Table III. 5. All the interactions between top molecules and Zanamivir with the active site.....	43
Table III. 6. Docking scores of the selected hits and the Zanamivir.....	44
Table III. 7. Pharmacokinetic and physicochemical parameters calculated by SwissADME.....	46
Table III. 8. Toxicity prediction of the top hits molecules.....	47

Chapter IV

Table IV. 1. Docking results of the designed inhibitors and reference ligands.....	64
Table IV. 2. ADME features of newly designed compounds and drug-like characteristics.....	66
Table IV. 3. Evaluation of safety profiles and Predicted LD ₅₀ of newly designed molecules.....	67
Table IV. 4. Evaluation of safety profiles of the designed Neuraminidase inhibitors using VEGA QSAR.....	67

Table IV. 5. <i>The average values collected via MDS, including RMSD, RMSF, Rg, H-bonds and SASA.....</i>	<i>72</i>
Table IV. 6. <i>Table representing the ΔE_{VDW}, ΔE_{EEL}, ΔE_{PB}, ΔE_{NPOLAR}, ΔG_{GAS}, ΔG_{SOLV} and binding energy for Neuraminidase_Molecule 01-04 and Zanamivir complexes.....</i>	<i>73</i>

Chapter V

Table V. 1. <i>SP docking results for the best fragments.....</i>	<i>89</i>
Table V. 2. <i>Docking results of the breed molecules and Zanamivir, Peramivir, and Oseltamivir with the Neuraminidase receptor.....</i>	<i>90</i>
Table V. 3. <i>Pharmacokinetic and physicochemical parameters for the seven breed molecules.....</i>	<i>90</i>
Table V. 4. <i>Toxicity prediction of breed molecules.....</i>	<i>91</i>
Table V. 5. <i>The average values of various parameters, including RMSD, RMSF, Rg, and H-bonds.....</i>	<i>93</i>
Table V. 6. <i>Table representing the ΔE_{VDW}, ΔE_{EEL}, ΔE_{PB}, ΔE_{NPOLAR}, ΔE_{DISPER}, ΔG_{GAS}, ΔG_{SOLV}, and binding energy for Neuraminidase_Breed 1–7 complexes.....</i>	<i>97</i>

Chapter VI

Table VI. 1. <i>A Tabular analysis of relationship between structures of compounds and experimental Activity.....</i>	<i>112</i>
Table VI. 2. <i>Statistical parameters of partial Least Squares (PLS) analysis on the comparative molecular field analysis (CoMFA) model.....</i>	<i>115</i>
Table VI. 3. <i>Assessing the predictive performance by statistical parameters of external validation for the comparative molecular field analysis (CoMFA) model.....</i>	<i>115</i>
Table VI. 4. <i>Structures and pIC_{50} values of novel molecules predicted by the CoMFA model.....</i>	<i>120</i>
Table VI. 5. <i>Binding interactions and affinity values of six Neuraminidase inhibitors within the active site.....</i>	<i>122</i>

Table VI. 6. ADME properties of newly designed compounds: Evaluation of drug-like characteristics.....124

Table VI. 7. Evaluation of safety profiles: Toxicity prediction of newly designed compounds.....125

Table VI. 8. All the results obtained from VEGA QSAR.....126

LIST OF ABBREVIATIONS

- **ΔE_{EEL}** : Electrostatic interactions.
- **ΔE_{NPOLAR}** : Non-polar contribution of repulsive solute-solvent interactions to the solvation energy.
- **ΔE_{PB}** : Non-polar interactions in a solvated system.
- **ΔG_{GAS}** : Total gas phase molecular mechanics energy.
- **ΔG_{SOLV}** : Total solvation energy.
- **ΔE_{VDW}** : Van der Waals interactions.
- **3D**: three-dimensional.
- **3D-QSAR**: Three-dimensional quantitative structure activity relationship.
- **Å**: Angstrom.
- **ADME**: Absorption, Distribution, Metabolism and Excretion.
- **ADMET**: Absorption, Distribution, Metabolism, Excretion and Toxicity.
- **CADD**: Computer-aided drug design.
- **CoMFA**: Comparative molecular field analysis.
- **COPD**: Chronic obstructive pulmonary disease.
- **CYP450**: Cytochrome P450.
- **DANA**: N-acetyl-neuraminic acid.
- **FAD**: Food and drug administration.
- **FBDD**: Fragment-based drug design.
- **FEV1**: Forced expiratory volume.
- **Gromacs**: GRONingen machine for chemical simulations.
- **H-bonds**: Hydrogen bonds interactions.
- **HA**: Hemagglutinin.
- **IC₅₀**: half-maximal inhibitory concentration.
- **LBDD**: Ligand-based drug design.
- **LD₅₀**: Lethal dose.
- **LigPrep**: Ligand preparation.
- **LogP**: Partition coefficient.

- **LogS**: Aqueous solubility.
- **Log Kp** : Skin permeation.
- **MD**: Molecular dynamic.
- **MDS**: Molecular dynamics simulation.
- **MM-PBSA**: Molecular mechanics poisson-boltzmann surface area.
- **MW**: Molecular weight.
- **NA**: Neuraminidase.
- **NAI**: Neuraminidase inhibitor.
- **NAIs**: Neuraminidase Inhibitors.
- **NPT**: Number of molecules, volume and temperature are constant.
- **NVT**: Number of molecules, pressure temperature are constant.
- **Ns**: Nanosecond.
- **OPLS3e**: Optimized potential for liquid simulation.
- **PDB**: Protein data bank.
- **PLS**: Partial Least squares.
- **Ps**: Picosecond.
- **QSAR**: Quantitative structure activity relationship.
- **RMSD**: Root-mean-square deviation.
- **RMSF**: Root-mean-square fluctuation.
- **Rg**: Radius of gyration.
- **SAR**: Structure activity relationship.
- **SASA**: Solvent accessible surface area.
- **SP**: Standard precision.
- **TIP3P**: Transferable intermolecular potential with 3 points.
- **WHO**: World health organization
- **XP**: Extra-precision.

Acknowledgments

First of all, I thank GOD Almighty for giving me the will and the courage to complete this thesis. I also thank my parents, sisters, and brothers for their encouragement, support, and sacrifice.

I would like to express my profound gratitude to my thesis supervisor, **Dr. Ouassaf Mebarka**, for graciously accepting to oversee my research work and for her deep commitment to my study. I am deeply appreciative of her unwavering support, the confidence she has shown in me, and her continuous encouragement throughout the process.

I wish to extend my sincere gratitude to **Prof. Belaidi Salah**, Professor at Biskra University, for kindly accepting the role of president of my thesis committee. I am equally thankful to **Dr. Zekri Afaf**, MCA at Biskra University, for the honor of serving as an examiner for this work. Furthermore, I express my deepest appreciation to **Dr. Kerassa Aicha**, MCA at El-Oued University, for graciously agreeing to participate as a jury member and review my thesis.

Dedication

I dedicate this thesis:

To my dear parents

To my sisters and brothers

To all “BOUROUGAA” family

To all my friends.

Lotfi

1. General Introduction

Annually, respiratory viruses affect millions of people throughout the globe, producing a variety of symptoms and resulting in numerous deaths [1]. Influenza is an infectious virus that causes seasonal outbreaks, most of which occur in the winter [2]. Moreover, the World Health Organization estimates that yearly influenza outbreaks affect roughly four million severe illness cases and almost half a million fatalities per year [3]. The flu virus is usually spread from human to another by coughing and sneezing. The most common modes of propagation include physical contact with sick persons, coming into contact with tainted products, or inhaling aerosols contaminated with viruses [4]. Clinical justification, laboratory tests, epidemiological data, and infection symptoms are routinely used to make an accurate identification of influenza [5]. In addition, fever and coughing are particularly important clinical indicators of influenza illness until testing confirms it [6].

Neuraminidase (NA) is a main surface tetrameric glycoprotein that is bound to the viral membrane by sialidase. NA's primary role is to catalyze the breaking of the biomolecule bonds among sialic acid and neighboring sugar stains, resulting in the emission of freshly synthesized virions [7]. The FDA has authorized two NA inhibitors, Oseltamivir and Zanamivir as the most effective medicines for anti-influenza viruses [8]. Certain naturally generated influenza neuraminidase transformations, including H274Y variants in H1N1 and H5N1 influenza A types, have shown considerable resistance to the aforementioned medications [9]. As a result, the discovery of antiviral medications that are active against various strains of influenza virus, via developing novel Neuraminidase inhibitors or by increasing the inhibitory efficacy of current antiviral agents, is an active research topic.

Computer-aided drug design approaches are becoming important in the amelioration of drugs, particularly in the advantageous selection of potential therapeutic compounds. These computer programs are useful for minimizing the implementation of biological system in pharmaceutical studies, helping with the just design of innovative and secure compounds, and positioning commercial pharmaceuticals, therefore assisting medicinal scientists and pharmacologists throughout the drug design procedure [10, 11].

The fundamental objective of our research is to create novel and anti-flu compounds by Blocking physiological function of Neuraminidase via the application of different drug design methodologies.

The thesis consists of six chapters that are thematically separated into two sections. The first is the bibliographic context, which includes two chapters: (i) Influenza and the vital function of Neuraminidase, (ii) drug design approaches employed in this work. The next part will concentrate on the application of drug design methodologies to generate potent and novel Neuraminidase inhibitors that will be useful in virology and anti-influenza medications.

The first chapter, *Influenza virus and neuraminidase* will present the basic information related to this virus and the previous epidemics it has caused, the viral structure of Neuraminidase, and the major goal of exploiting Neuraminidase as a pharmacological and therapeutic target to develop new anti-flu treatment.

The second chapter, *Drug design strategies* offers the current state of the science in molecular modeling approaches, with an extra focus on ligand and structure-based drug development. It additionally offers an introduction to the different techniques employed during in silico drug development, with a focus on the algorithmic functions and bioinformatics tools utilized in this research.

The third chapter, *Pharmacophore-based virtual screening, molecular docking and molecular dynamics studies for the discovery of novel Neuraminidase inhibitors* reflects a pharmacophore based virtual screening for the aim of discovering powerful novel neuraminidase inhibitors. The pharmacophore model was validated by creating a 3D-QSAR model. By screening the PubChem database, several hit compounds were identified. A MD simulation investigation was carried out to confirm the biomolecular structure via Gromacs package.

The fourth chapter, *Discovery of novel potent drugs for influenza by inhibiting the vital function of neuraminidase via fragment-based drug design (FBDD) and molecular dynamics simulation strategies*, comprises the fragment-based design, which is an efficient and rapid modeling method for discovering bioactive molecules. Through docking modeling, ADMET predictions, MDS and MM-PBSA computations, the proposed molecules formed very good complexes with the Neuraminidase receptor.

The fifth chapter, *Pharmacoinformatics and breed-based De Novo hybridization studies to develop new Neuraminidase inhibitors as potential anti-influenza agents*, discusses how to design effective anti-influenza medications using pharmacoinformatics and bioinformatics methodologies. We employed breed De Novo Hybridization to develop potent anti-influenza

medicines. We have combined the atomic and biological features of empirical Neuraminidase inhibitors.

The sixth chapter, *Comparative molecular field analysis (CoMFA), molecular docking and ADMET study on thiazolidine-4-carboxylic acid derivatives as new Neuraminidase inhibitors*, describes the use of 3D quantitative structure-activity relationship (3D-QSAR) approach on thiazolidine-4-carboxylic acid derivatives to predict novel neuraminidase inhibitors.

2. Reference

- [1] Gaunt, E. R., Harvala, H., McIntyre, C., Templeton, K. E., & Simmonds, P. (2011). Disease burden of the most commonly detected respiratory viruses in hospitalized patients calculated using the disability adjusted life year (DALY) model. *Journal of Clinical Virology*, 52(3), 215-221.
- [2] Taubenberger, J. K., & Morens, D. M. (2008). The pathology of influenza virus infections. *Annu. Rev. Pathol. Mech. Dis.*, 3, 499-522.
- [3] Njouom, R., Monamele, G. C., Ermetal, B., Tchatchouang, S., Moyo-Tetang, S., McCauley, J. W., & Daniels, R. S. (2019). Detection of influenza C virus infection among hospitalized patients, Cameroon. *Emerging infectious diseases*, 25(3), 607.
- [4] Shao, W., Li, X., Goraya, M. U., Wang, S., & Chen, J. L. (2017). Evolution of influenza A virus by mutation and re-assortment. *International journal of molecular sciences*, 18(8), 1650.
- [5] Binnicker, M. J., Espy, M. J., Irish, C. L., & Vetter, E. A. (2015). Direct detection of influenza A and B viruses in less than 20 minutes using a commercially available rapid PCR assay. *Journal of clinical microbiology*, 53(7), 2353-2354.
- [6] Anderson, K. B., Simasathien, S., Watanaveeradej, V., Weg, A. L., Ellison, D. W., Suwanpakdee, D., ... & Jarman, R. G. (2018). Clinical and laboratory predictors of influenza infection among individuals with influenza-like illness presenting to an urban Thai hospital over a five-year period. *PLoS One*, 13(3), e0193050.
- [7] Bassetti, M., Castaldo, N., & Carnelutti, A. (2019). Neuraminidase inhibitors as a strategy for influenza treatment: pros, cons and future perspectives. *Expert Opinion on Pharmacotherapy*, 20(14), 1711-1718.
- [8] Zhao, Z. X., Cheng, L. P., Li, M., Pang, W., & Wu, F. H. (2019). Discovery of novel acylhydrazone neuraminidase inhibitors. *European Journal of Medicinal Chemistry*, 173, 305-313.
- [9] Laborda, P., Wang, S. Y., & Voglmeir, J. (2016). Influenza neuraminidase inhibitors: synthetic approaches, derivatives and biological activity. *Molecules*, 21(11), 1513.
- [10] Brogi, S., Ramalho, T. C., Kuca, K., Medina-Franco, J. L., & Valko, M. (2020). In silico methods for drug design and discovery. *Frontiers in chemistry*, 8, 612.

[11] Wang, Y., Xing, J., Xu, Y., Zhou, N., Peng, J., Xiong, Z., ... & Jiang, H. (2015). In silico ADME/T modelling for rational drug design. *Quarterly reviews of biophysics*, 48(4), 488-515.

Chapter I: Influenza Virus and Neuraminidase

1. Introduction

Influenza, which is frequently referred to as the flu, is a respiratory infection linked to viruses of the *Orthomyxoviridae* family. This particular species is composed of four seasonal influenza virus types (influenza viruses A, B, C, and D), which are differentiated by changes in the cellular glycoprotein functions and nucleoproteins. Influenza viruses can infect people, pigs, birds and other animals [1]. Each winter, influenza viruses cause periodic outbreaks that result in over 200,000 stays in hospitals and 30,000-50,000 fatalities [2]. Surprisingly, in line with statistics from the WHO, influenza viruses affect 5%–15% of humanity and cause 250,000–500,000 fatalities annually, therefore being the second-leading cause of death behind acquired immune deficiency syndrome [3].

The principal glycoproteins' surface of the flu, hemagglutinin (HA) and Neuraminidase (NA) characterize the virion area and function as the most important sites for these neutralizing antibodies. Aside from alterations caused by drift of antigenic, the NA and HA of influenza A viruses may appear in multiple configurations [4]. Both hemagglutinin and Neuraminidase collaborate by interacting with sialic acid, which has a final configuration linked to sugar remnants generated by glycolipids or glycoproteins at the cell membrane [5]. Neuraminidase plays a major function in the last phases of the infection. Neuraminidase eliminates sialic acids from the two cell surface receptors and newly produced NA and HA on budding virions that were previously sialylated as element of the host glycosylation cell processes [6].

The influenza M2 channel protein has become known as a significant target in the creation of anti-influenza drugs due to its role in viral transmission [7, 8]. When the virus penetrates affected cells, the tetrameric shape of the M2 protein creates a dependent on pH channel across the viral envelope that regulates proton permeability [9, 10]. M2 exists at approximately the same level as Neuraminidase and hemagglutinin but is detected at considerably lower numbers in the mature viral membrane, which is rich in cholesterol and sphingomyelin, since M2 is largely concentrated in liquid-crystalline portions of the cellular membrane over viral bud development [11]. **Figure I. 1** depicts the viral structure of the flu.

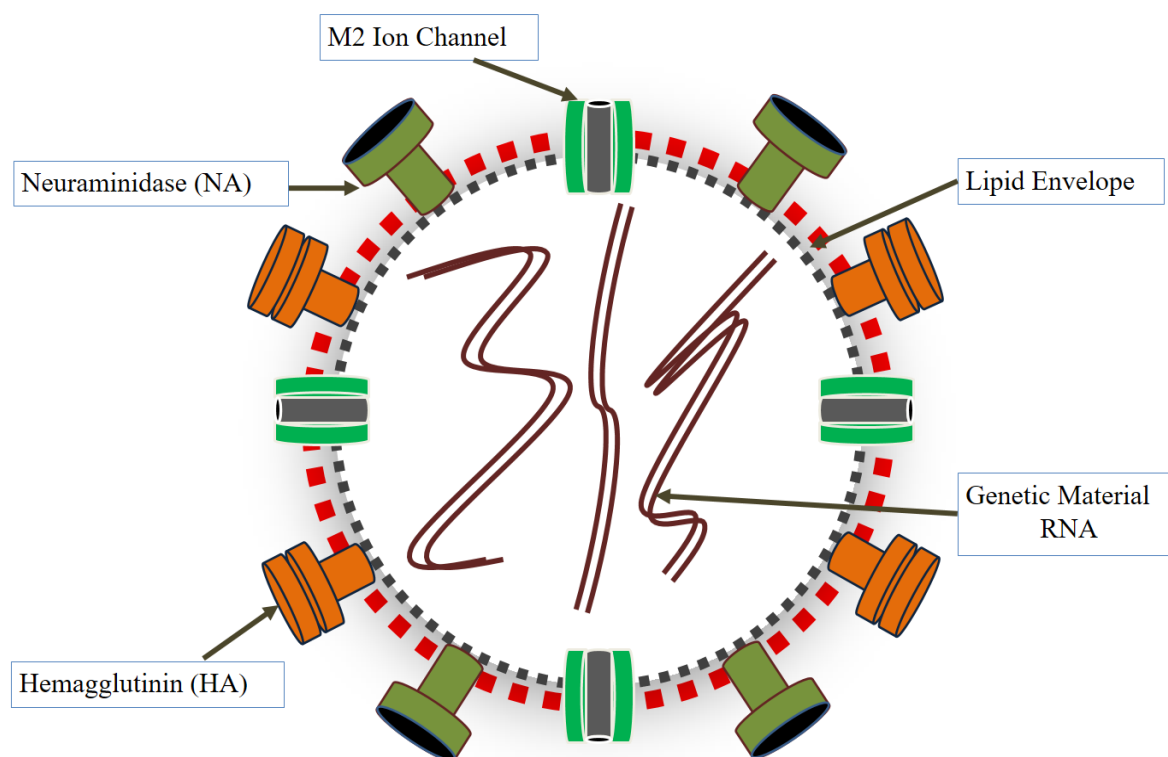


Figure I. 1. Viral structure of influenza virus.

2. Neuraminidase Morphology

The Neuraminidase integrates as a tetramer composed of four similar polypeptides. Once incorporated into the viral membrane, constitutes roughly 10-20% of the number of glycoproteins on the virus, with around 40-50 Neuraminidase spikes and a typical virion dimension of 120 nm [12, 13]. The Neuraminidase could extend somewhat or substantially above the viral membrane than the hemagglutinin due to the dimension of the stalk area, which may influence the virus's total enzyme function [14, 15]. The enzyme Neuraminidase arises is a tetramer composed of four homologous monomers. Every monomer is made up of four special structural subdomains called the transmembrane zone, the cytoplasmic tail, the catalytic cap (head) and the base (stalk). (**Figure I. 2**).

2.1 Transmembrane zone

The Neuraminidase is included to the hydrophobic transmembrane field at N-terminal, which has an irregular amino acid sequence including residual numbers 7-29 with anticipated to result in an alpha helix [16]. The transmembrane zone transmits information from the reticulum's endoplasmic to the apical region and facilitates interaction with rafts of lipids [17]. Implicating of the role of the transmembrane field involved in Neuraminidase movement

to the apical barrier. In without the presence of the stalk and head areas, membrane displacement is possible [18].

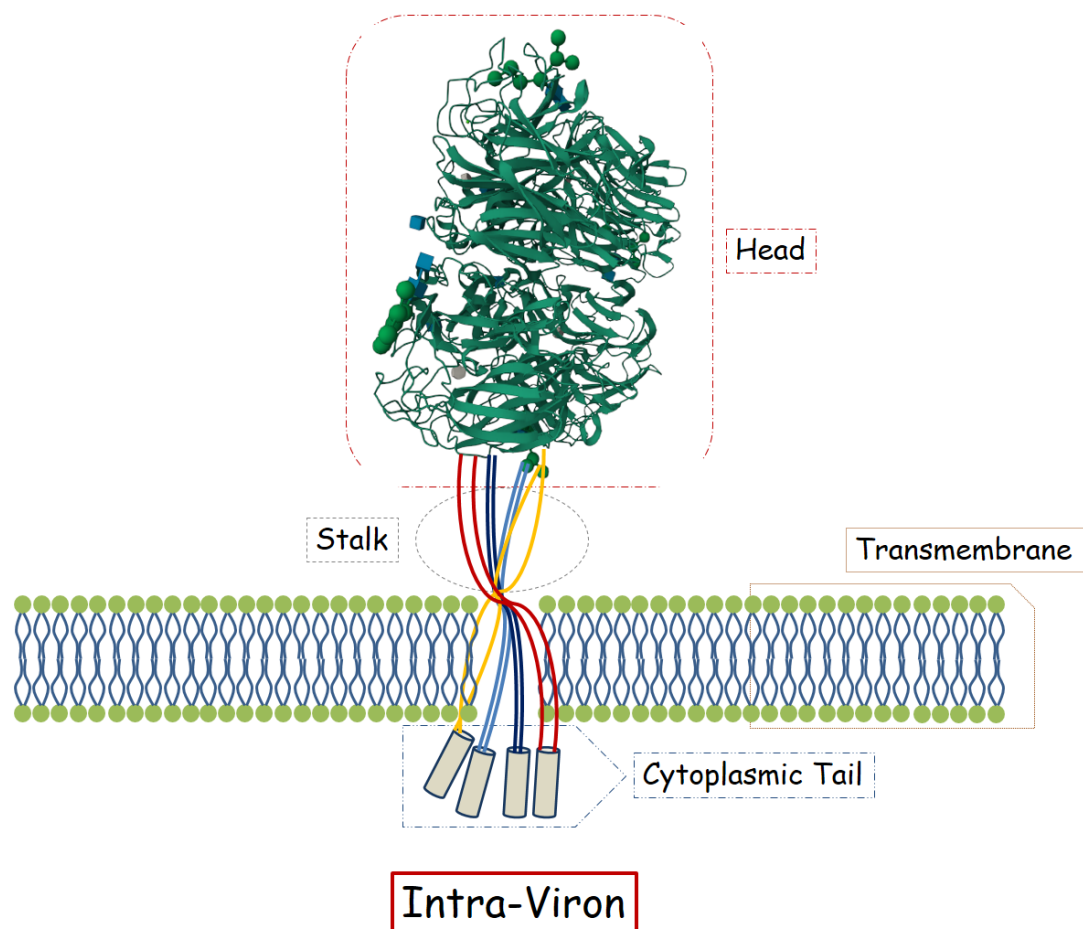


Figure I. 2. Neuraminidase structure and subdomains.

Particular amino acid mutation within the transmembrane domain may result in persistent morphological abnormalities in the placing signal area, resulting in decreased distribution to the plasma membrane [18].

2.2 Cytoplasmic tail ambit

The modified shape and reduced infectiousness of viruses producing Neuraminidase without the tail of the cytoplasm domain are assumed to be owing to an absence of association with the cell's membrane related matrix viral proteins [19]. The glycoprotein's movement to the close membrane of the plasma is influenced by factors associated with the transmembrane field and intracellular tail region the [20]. In addition, the function of the domain's tail in packing the surface Neuraminidase into unclear of virions remains [21].

A total deletion of the tail segment reduced the quantity of Neuraminidase in infected cells by 50%. This linked to a decrease in the quantity of Neuraminidase integrated into virions,

implying that existing Neuraminidase was packaged efficiently. While the lack of all tail amino acids except the starting methionine resulted in virus with significantly reduced incorporation of Neuraminidase into virions, yet Neuraminidase It appeared on the surface of the plasma membrane at comparable quantities to wild-type virus [21, 22].

2.3 Catalytic head

The catalytic head of every Neuraminidase has a box-shaped structure made up of four subunits as seen in **Figure I. 3**. Each subunit has a 6-bladed propeller design, with each one consisting of four oppositely b-sheets held together by disulphide bonds and linked by variable length loops [23]. Each subunit has a functioning catalytic site on its surface that is orientated towards the side rather than upwards, which is in accordance with the capacity to break sialic acids from surrounding glycoproteins' membrane to avoid viral entrapment [24]. A significant cavity with an exceptionally large amount of charged particles in the active site along the perimeter distinguishes these catalytic sites [24, 25]. When the Neuraminidase head field is effectively separated from the residual Neuraminidase tetrameric stalk lodged in the flu, the catalytic functions stay active and the head domains maintain their tetrameric configuration upon purification [26].

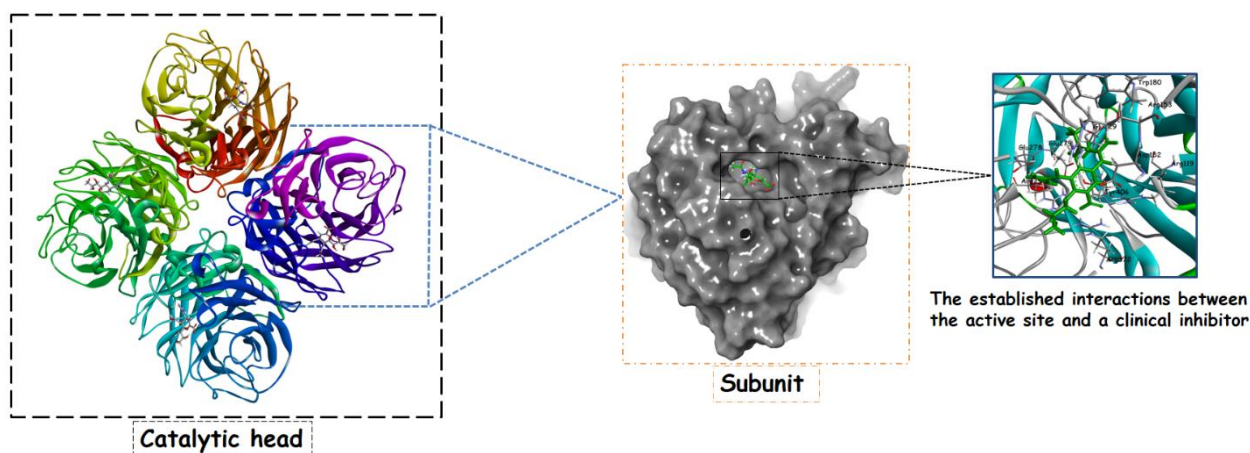


Figure I. 3. *The Neuraminidase catalytic head.*

2.4 Stalk

Various influenza Neuraminidase stalk regions although certain fundamental properties of a virus are shared, the amount and arrangement of amino acid residues can differ greatly [27]. The size of the stalk area in certain viral subtypes is capable of having a major influence on specific virus features. Modified viruses that were unable to form The Neuraminidase stalk could multiply in the culture of tissue cells at the same titer as the original host virus [28].

It was recently proposed that the restricted availability of substrate theory might not fully explain why stalk-deletion mutants have reduced sialidase activity, with the notion that grouping of NAs on the membrane's virion would lessen any obstructing effects of neighboring HA. The molecular dynamics computations confirmed this viewpoint, which showed that a smaller stalk affects the shape and dynamics of the enzyme active region, changing its attraction for sialic acids [29].

3. Mechanism of Action of NAIs

The molecular structure of the Neuraminidase receptor is substantially consistent throughout the two kinds of influenza viruses (A and B) because of its catalytic activity, this renders it an important target for anti-viral therapies.[30]. The NA viral background crystallographic information aided in the design and manufacturing of a range of molecule capable of simulating the original substrate of the Neuraminidase protein and competing for binding to pocket [31] (**Figure I. 4**). Considering that these Neuraminidase blockers depend on the configuration of the 2,3-didehydro derivative of DANA compound, they have a stronger binding capacity than Neu5Ac, inhibiting organic substrate cleavage. As an outcome, reproductive viruses struggle to be liberated via the sialic acid sensors and accumulate on the surfaces of the cell that has been infected, preventing infection from spreading among non-infected people. [32].

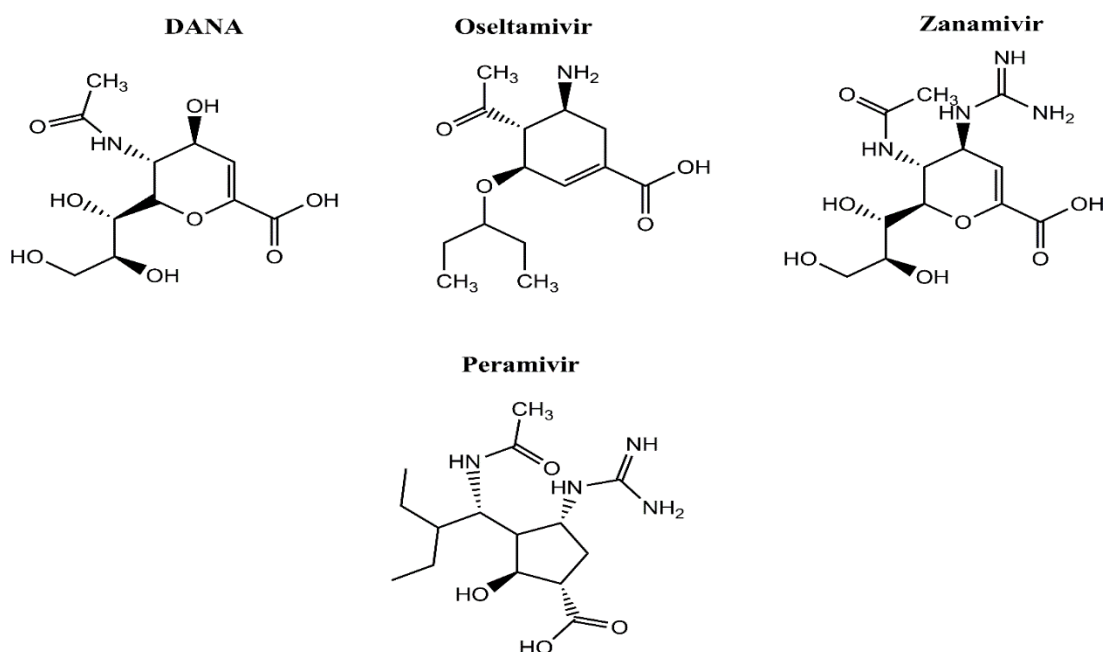


Figure I. 4. The molecular structure of NAIs.

All of these compounds have their origins on the configuration of DANA molecule.

Neuraminidase inhibitors suppress influenza virus multiplication from cells that have been damaged, reducing infection of neighboring cells and hence limiting infection transmission in the respiratory system [33]. Because flu multiplication in the respiratory system peaks from 24 to 70 hours after symptom start, medicines that act at the period of viral transmission, Neuraminidase inhibitors should be provided as soon as feasible [34].

4. Safety of Neuraminidase Inhibitors

Preclinical toxicology indicated that *Zanamivir* and *Oseltamivir* exhibit minimal acute side effects, with no significant endorgan harm seen at human-relevant dosages. Comprehensive carcinogenicity investigations with *Zanamivir* have yielded negative results, and investigations with *Oseltamivir* are ongoing, although neither medication is genotoxic or mutagenic. Because the vast majority of clinical research participants were adults in good health or those with established fundamental illnesses of moderate to average complexity, pharmacovigilance becomes critical if the medications grow more commonly used [35].

4.1. Zanamivir

In general, injectable *Zanamivir* (600 mg every day for five days) or inhalation *Zanamivir* (as much as to 96 mg everyday) were tolerated well [36]. In clinical trials, the most often reported side effects in treatment trials seem to be related to the existing influenza (diarrhea, headache, nasal symptoms, cough, nausea, throat pain, nosebleeds, dizziness), and few happened at a rate of more than 3% [37]. Preliminary data about a therapy study for individuals with COPD or asthma in addition to influenza show that on day 6, *Zanamivir* recipients had a higher proportion of FEV1 increases and decreases (35% as well as 15%, correspondingly) than placebo recipients (25% and 6%). Just one of 78 *Zanamivir*-treated individuals discontinued medication due to a non-respiratory dispute, and there were no changes in respiratory condition exacerbations during therapy (14% for *Zanamivir*). [38]. The conclusions of the United States FDA, certain individuals with underlying COPD or asthma have had significant worsening in respiratory activity after inhaling *Zanamivir*. Despite influenza produces such complications, Individuals with chronic respiratory illnesses should be closely monitored and given fast-acting bronchodilators when receiving *Zanamivir* treatment. Patients who have reduced function of the lung or bronchospasm should discontinue the medicine [39].

4.2. Oseltamivir

To date, *Oseltamivir* has proven to be tolerated effectively and is unlinked with clinical

test problems. Doses of up to 500 mg twice day for seven days have been tried in healthy people. The most common side effect is mild-to-moderate nausea; vomiting is less prevalent. In most persons, these effects are temporary, appearing most typically after the first dosage and resolving in 1-2 days despite continuing medication administration [40]. Investigations on animals show that it is well distributed throughout the respiratory system, but no equivalent human research have been recorded. The administration of *Oseltamivir* with meals has little effect on bioavailability or peak plasma levels, although it appears to reduce the possibility of gastric discomfort. The kidney excretes *Oseltamivir* carboxylate by filtration and tubular elimination after metabolization. Administration with probenecid increases the half-life, indicating anionic route secretion. Advanced renal failure necessitates dose modifications [41]. **Table I. 1** represents NAIs used in the therapy of influenza.

Table I. 1. *Neuraminidase inhibitors used to combat the flu.*

Period	Therapy	Individuals (% with confirmed flu)	Age group (mean)	illness's duration	diminution in time to alleviate the symptoms of individuals with influenza (median)	Observations	Ref
1993–1995	Nebulization <i>Zanami</i> . 10 mg (5 ds)	417 (63%)	13-32 years	≤ 48 hours	1 (5 vs 4) 3 (7 vs 4 in fever)	three days in patient treated for 30 hours	[41]
1997	Nebulization <i>Zanami</i> . 10 mg (5 ds)	455 (71%)	12-37 years	≤ 36 hours	1.5 (6.5 vs 5.0) 2.0 (6.5 vs 4.5 in febrile)	Complications and antibiotics were reduced in individuals with underlying illnesses (15% - 38%).	[42]
1996–1998	Nebulization <i>Zanami</i> . 10 mg (5 ds)	777 (73%)	12 years	≤ 48 hours	1 (6 vs 5)	fewer complications	[43]
1996–1998	Nebulization <i>Zanami</i> . 10 mg (5 ds)	356 (78%)	12 years	≤ 48 hours	2.5 (7.5 vs 5.0)	Problems and antibiotics were reduced (11% - 5%). There are no changes in dosage.	[44]
1996–1998	<i>Oseltami</i> . 75 mg or 150 mg (5 ds)	629 (60%)	18–65 years	≤ 36 hours	1.4 (4.3 vs 2.9 vs 2.9)	fewer complications	[44,45]

5. Neuraminidase mutations linked to NAI resistance.

Several great evaluations have addressed NAI resistance [46]. Neuraminidase inhibitors resistance is caused by mutations that modify the configuration of the NA receptor, leading in reduced linking of the NA inhibitors to the NA, or by alterations in amino acids that alter the interactions with the medication [47]. The bulk of resistance has been detected with *Oseltamivir*, *Zanamivir* resistance was identified in a small number of isolates [48]. This might be due *Zanamivir* is rather tightly linked to the original substrate, nevertheless, *Oseltamivir* is also considerably more often used. There have been no reports of *Laninamivir*-resistant strains [47]. A large number of NAI mutations are produced by modifications in the NA mutation. Mutations to the HA gene and product might additionally reduce vulnerability to Neuraminidase inhibitors. These modifications reduce the requirement for NA activity (**Table I. 2**) [49].

Table I. 2. Resistance mutations in the Neuraminidase inhibitor [47].

Influenza class	Transformation	Lower	Average	Higher	Hypersensitive
H1N1	H274Y			Osel, Pera	Zana
	Q136K			Zana	Osel
	N70S		Zana		Osel
	Y155H		Osel	Zana, Pera	
	I222V/M	Osel			Pera, Zana
H5N1	V116A	Pera	Osel, Zanz		
	H274Y			Pera, Osel	Zana
	E119G			Pera, Zana	Osel
	D198G		Osel, Zanz		Pera
	N294S			Osel	Pera, Zana
	S246N			Osel	Zana

	H252Y		Osel	Pera, Zana
	I222L		Osel	Zana
	I222v		Osel	Pera, Zana
	I222M/T		Osel	Pera, Zana
H3N2	N294S		Osel	Zana
	R292K	Zana	Osel, Pera	
	E119A/D		Osel, Pera, Zana	
	E119G		Pera	Zana
	E119I	Zana	Osel, Pera	
	E119v		Osel	Pera, Zanz
	Q136K		Zana	Osel
	R371K		Osel, Zana	
	D151A/D		Osel, Zana, Pera	

6. Creating Neuraminidase-inhibitors in future years

Considering the limits of existing medications (for example, the resistance), novel therapies are required. In addition to NAIs, various medicines with other viral sites are being investigated as well as recent trials of alternative combination therapies [50]. *Laninamivir* and other *Zanamivir* analogs have been produced. With the finding of the 150 cavity, new chemicals that might result in better binding of the NA and hence increased effectiveness are now being explored [51]. As a result, NA is present on the area of virions, there is growing desire in discovering molecules that interact with numerous NAs on virions' surfaces. Diverse

preparations that may show affinity that is more binding and potentially improved pharmacology, along with to higher effectiveness [52]. There is additionally speculation about producing peramivir analogues. Furthermore, benzoic acid is a low-cost chemical ingredient that might be used in future NAI production. Since present NAIs are costly to create and take an extended period to generate, the synthesis of cheaper benzoic acid derivatives with anti-influenza action might be very valuable in outbreaks of disease [53]. As flu resistance to present medicines rises, these pharmaceuticals as well as newer Neuraminidase inhibitors, will become increasingly relevant in the future.

7. Reference

- [1] Gopinath, S. C., Tang, T. H., Chen, Y., Citartan, M., Tominaga, J., & Lakshmipriya, T. (2014). Sensing strategies for influenza surveillance. *Biosensors and Bioelectronics*, 61, 357-369.
- [2] Vemula, S. V., & Mittal, S. K. (2010). Production of adenovirus vectors and their use as a delivery system for influenza vaccines. *Expert opinion on biological therapy*, 10(10), 1469-1487.
- [3] Vemula, S. V., Zhao, J., Liu, J., Wang, X., Biswas, S., & Hewlett, I. (2016). Current approaches for diagnosis of influenza virus infections in humans. *Viruses*, 8(4), 96.
- [4] McAuley, J. L., Gilbertson, B. P., Trifkovic, S., Brown, L. E., & McKimm-Breschkin, J. L. (2019). Influenza virus neuraminidase structure and functions. *Frontiers in microbiology*, 10, 39.
- [5] Palese, P., Tobita, K., Ueda, M., & Compans, R. W. (1974). Characterization of temperature sensitive influenza virus mutants defective in neuraminidase. *Virology*, 61(2), 397-410.
- [6] Basak, S., Tomana, M., & Compans, R. W. (1985). Sialic acid is incorporated into influenza hemagglutinin glycoproteins in the absence of viral neuraminidase. *Virus research*, 2(1), 61-68.
- [7] Holsinger, L. J., & Alams, R. (1991). Influenza virus M2 integral membrane protein is a homotetramer stabilized by formation of disulfide bonds. *Virology*, 183(1), 32-43.
- [8] Takeda, M., Pekosz, A., Shuck, K., Pinto, L. H., & Lamb, R. A. (2002). Influenza A virus M2 ion channel activity is essential for efficient replication in tissue culture. *Journal of virology*, 76(3), 1391-1399.
- [9] Pielak, R. M., & Chou, J. J. (2010). Flu channel drug resistance: a tale of two sites. *Protein & cell*, 1(3), 246-258.
- [10] Lin, T. I., & Schroeder, C. (2001). Definitive assignment of proton selectivity and attoampere unitary current to the M2 ion channel protein of influenza A virus. *Journal of virology*, 75(8), 3647-3656.
- [11] Rossman, J. S., Jing, X., Leser, G. P., & Lamb, R. A. (2010). Influenza virus M2 protein mediates ESCRT-independent membrane scission. *Cell*, 142(6), 902-913.

- [12] Moules, V., Ferraris, O., Terrier, O., Giudice, E., Yver, M., Rolland, J. P., ... & Lina, B. (2010). In vitro characterization of naturally occurring influenza H3NA- viruses lacking the NA gene segment: Toward a new mechanism of viral resistance?. *Virology*, 404(2), 215-224.
- [13] Ward, C. W., Colman, P. M., & Laver, W. G. (1983). The disulphide bonds of an Asian influenza virus neuraminidase. *Febs Letters*, 153(1), 29-33.
- [14] Harris, A., Cardone, G., Winkler, D. C., Heymann, J. B., Brecher, M., White, J. M., & Steven, A. C. (2006). Influenza virus pleiomorphy characterized by cryoelectron tomography. *Proceedings of the National Academy of Sciences*, 103(50), 19123-19127.
- [15] Matsuoka, Y., Swayne, D. E., Thomas, C., Rameix-Welti, M. A., Naffakh, N., Warnes, C., ... & Subbarao, K. (2009). Neuraminidase stalk length and additional glycosylation of the hemagglutinin influence the virulence of influenza H5N1 viruses for mice. *Journal of virology*, 83(9), 4704-4708.
- [16] Air, G. M. (2012). Influenza neuraminidase. *Influenza and other respiratory viruses*, 6(4), 245.
- [17] Barman, S., & Nayak, D. P. (2000). Analysis of the transmembrane domain of influenza virus neuraminidase, a type II transmembrane glycoprotein, for apical sorting and raft association. *Journal of virology*, 74(14), 6538-6545.
- [18] Ernst, A. M., Zacherl, S., Herrmann, A., Hacke, M., Nickel, W., Wieland, F. T., & Brügger, B. (2013). Differential transport of Influenza A neuraminidase signal anchor peptides to the plasma membrane. *FEBS letters*, 587(9), 1411-1417.
- [19] Enami, M., & Enami, K. (1996). Influenza virus hemagglutinin and neuraminidase glycoproteins stimulate the membrane association of the matrix protein. *Journal of virology*, 70(10), 6653-6657.
- [20] Kundu, A., Avalos, R. T., Sanderson, C. M., & Nayak, D. P. (1996). Transmembrane domain of influenza virus neuraminidase, a type II protein, possesses an apical sorting signal in polarized MDCK cells. *Journal of virology*, 70(9), 6508-6515.
- [21] García-Sastre, A., & Palese, P. (1995). The cytoplasmic tail of the neuraminidase protein of influenza A virus does not play an important role in the packaging of this protein into viral envelopes. *Virus research*, 37(1), 37-47.
- [22] Mitnaul, L. J., Castrucci, M. R., Murti, K. G., & Kawaoka, Y. (1996). The cytoplasmic tail of influenza A virus neuraminidase (NA) affects NA incorporation into virions, virion

morphology, and virulence in mice but is not essential for virus replication. *Journal of virology*, 70(2), 873-879.

[23] Varghese, J. N., Laver, W. G., & Colman, P. M. (1983). Structure of the influenza virus glycoprotein antigen neuraminidase at 2.9 Å resolution. *Nature*, 303(5912), 35-40.

[24] Burmeister, W. P., Ruigrok, R. W., & Cusack, S. (1992). The 2.2 Å resolution crystal structure of influenza B neuraminidase and its complex with sialic acid. *The EMBO journal*, 11(1), 49-56.

[25] Colman, P. M., Hoyne, P. A., & Lawrence, M. C. (1993). Sequence and structure alignment of paramyxovirus hemagglutinin-neuraminidase with influenza virus neuraminidase. *Journal of virology*, 67(6), 2972-2980.

[26] McKimm-Breschkin, J. L., Caldwell, J. B., Guthrie, R. E., & Kortt, A. A. (1991). A new method for the purification of the influenza A virus neuraminidase. *Journal of virological methods*, 32(1), 121-124.

[27] Blok, J., & Air, G. M. (1982). Variation in the membrane-insertion and "stalk" sequences in eight subtypes of influenza type A virus neuraminidase. *Biochemistry*, 21(17), 4001-4007.

[28] Castrucci, M. R., & Kawaoka, Y. O. S. H. I. H. I. R. O. (1993). Biologic importance of neuraminidase stalk length in influenza A virus. *Journal of virology*, 67(2), 759-764.

[29] Durrant, J. D., Bush, R. M., & Amaro, R. E. (2016). Microsecond molecular dynamics simulations of influenza neuraminidase suggest a mechanism for the increased virulence of stalk-deletion mutants. *The Journal of Physical Chemistry B*, 120(33), 8590-8599.

[30] Samson, M., Pizzorno, A., Abed, Y., & Boivin, G. (2013). Influenza virus resistance to neuraminidase inhibitors. *Antiviral research*, 98(2), 174-185.

[31] Talele, T. T., Khedkar, S. A., & Rigby, A. C. (2010). Successful applications of computer aided drug discovery: moving drugs from concept to the clinic. *Current topics in medicinal chemistry*, 10(1), 127-141.

[32] Ikram, N. K. K., Durrant, J. D., Muchtaridi, M., Zaaludin, A. S., Purwitasari, N., Mohamed, N., ... & Wahab, H. A. (2015). A virtual screening approach for identifying plants with anti H5N1 neuraminidase activity. *Journal of chemical information and modeling*, 55(2), 308-316.

- [33] Hayden, F. G. (2004). Pandemic influenza: is an antiviral response realistic?. *The Pediatric infectious disease journal*, 23(11), S262-S269.
- [34] Meindl, P., Bodo, G., Palese, P., Schulman, J., & Tuppy, H. (1974). Inhibition of neuraminidase activity by derivatives of 2-deoxy-2, 3-dehydro-N-acetylneuraminic acid. *Virology*, 58(2), 457-463.
- [35] Gubareva, L. V., Kaiser, L., & Hayden, F. G. (2000). Influenza virus neuraminidase inhibitors. *The Lancet*, 355(9206), 827-835.
- [36] Cass, L. M., Efthymiopoulos, C., & Bye, A. (1999). Pharmacokinetics of zanamivir after intravenous, oral, inhaled or intranasal administration to healthy volunteers. *Clinical pharmacokinetics*, 36, 1-11.
- [37] Freund, B., Gravenstein, S., Elliott, M., & Miller, I. (1999). Zanamivir: a review of clinical safety. *Drug Safety*, 21, 267-281.
- [38] Cass, L. M. R., Gunawardena, K. A., Macmahon, M. M., & Bye, A. (2000). Pulmonary function and airway responsiveness in mild to moderate asthmatics given repeated inhaled doses of zanamivir. *Respiratory medicine*, 94(2), 166-173.
- [39] US Food and Drug Administration. Public health advisory: safe and appropriate use of influenza drugs (Jan 12, 2000).
- [40] Massarella, J. W., He, G. Z., Dorr, A., Nieforth, K., Ward, P., & Brown, A. (2000). The pharmacokinetics and tolerability of the oral neuraminidase inhibitor oseltamivir (Ro 64-0796/GS4104) in healthy adult and elderly volunteers. *The Journal of Clinical Pharmacology*, 40(8), 836-843.
- [41] Hayden, F. G., Atmar, R. L., Schilling, M., Johnson, C., Poretz, D., Paar, D., ... & Oseltamivir Study Group. (1999). Use of the selective oral neuraminidase inhibitor oseltamivir to prevent influenza. *New England Journal of Medicine*, 341(18), 1336-1343.
- [42] The, M. I. S. T. (1998). Randomised trial of efficacy and safety of inhaled zanamivir in treatment of influenza A and B virus infections. *The Lancet*, 352(9144), 1877-1881.
- [43] Gravenstein, S., Drinka, P., Osterweil, D., Schilling, M., Krause, P., Elliott, M., ... & Keene, O. (2005). Inhaled zanamivir versus rimantadine for the control of influenza in a highly vaccinated long-term care population. *Journal of the American Medical Directors Association*, 6(6), 359-366.

- [44] Hayden, F. G., Gubareva, L. V., Monto, A. S., Klein, T. C., Elliott, M. J., Hammond, J. M., ... & Ossi, M. J. (2000). Inhaled zanamivir for the prevention of influenza in families. *New England Journal of Medicine*, 343(18), 1282-1289.
- [45] Treanor, J. J., Hayden, F. G., Vrooman, P. S., Barbarash, R., Bettis, R., Riff, D., ... & US Oral Neuraminidase Study Group. (2000). Efficacy and safety of the oral neuraminidase inhibitor oseltamivir in treating acute influenza: a randomized controlled trial. *Jama*, 283(8), 1016-1024.
- [46] Ferraris, O., & Lina, B. (2008). Mutations of neuraminidase implicated in neuraminidase inhibitors resistance. *Journal of Clinical Virology*, 41(1), 13-19.
- [47] Samson, M., Pizzorno, A., Abed, Y., & Boivin, G. (2013). Influenza virus resistance to neuraminidase inhibitors. *Antiviral research*, 98(2), 174-185.
- [48] Thorlund, K., Awad, T., Boivin, G., & Thabane, L. (2011). Systematic review of influenza resistance to the neuraminidase inhibitors. *BMC infectious diseases*, 11, 1-13.
- [49] Ison, M. G. (2013). Clinical use of approved influenza antivirals: therapy and prophylaxis. *Influenza and other respiratory viruses*, 7, 7-13.
- [50] Das, K. (2012). Antivirals targeting influenza A virus. *Journal of medicinal chemistry*, 55(14), 6263-6277.
- [51] Yamashita, M., Tomozawa, T., Kakuta, M., Tokumitsu, A., Nasu, H., & Kubo, S. (2009). CS-8958, a prodrug of the new neuraminidase inhibitor R-125489, shows long-acting anti-influenza virus activity. *Antimicrobial agents and chemotherapy*, 53(1), 186-192.
- [52] Kiso, M., Takahashi, K., Sakai-Tagawa, Y., Shinya, K., Sakabe, S., Le, Q. M., ... & Kawaoka, Y. (2010). T-705 (favipiravir) activity against lethal H5N1 influenza A viruses. *Proceedings of the National Academy of Sciences*, 107(2), 882-887.
- [53] Escuret, V., Cornu, C., Boutitie, F., Enouf, V., Mosnier, A., Bouscambert-Duchamp, M., ... & Lina, B. (2012). Oseltamivir–zanamivir bitherapy compared to oseltamivir monotherapy in the treatment of pandemic 2009 influenza A (H1N1) virus infections. *Antiviral research*, 96(2), 130-137.

Chapter II: Drug Design Strategies

1. Introduction

A medication is defined as any chemical that is employed in the diagnosis, treatment, or prevention of disease or that aims to change the vital function of the body. Years of scientific research are required to discover the biochemistry of an illness for which pharmacological intervention is viable [1]. The research and development of novel drugs takes both resources and time, and it currently requires around twelve years and an average of \$1.8 billion to market a novel medicine. In addition, the number of innovative medications that have achieved market authorization has decreased throughout the years. [2].

The design of small molecules that are able to controlling or modifying specific vital functions in the body that are closely associated with human illnesses is made possible by a comprehension of the biomolecular structural and chemical binding properties of significant drug targets in biologically pertinent pathways. This is done via numerous interactions with a specific target [3, 4]. Computer-aided drug design (CADD) refers to computer methods for identifying, developing, and evaluating drug and active molecules with comparable biological features [4]. The major components of computer-aided drug design are virtual screening, molecular docking, quantitative structure activity relationship, homology modeling and pharmacophore modeling [6]. The application of three-dimensional protein structure data in the generation of novel bioactive molecules, known as structure-based drug design, is a successful and effective strategy employed by pharmaceutical research globally [7]. This certified data may be used immediately for the identification of new ligands, also the improvement of lead compounds. This offers up new avenues for accelerating the hunt for lead molecules while reducing the number of compounds that must be evaluated experimentally [8]. **Figure I. 1** depicts the most frequently employed drug design strategies.

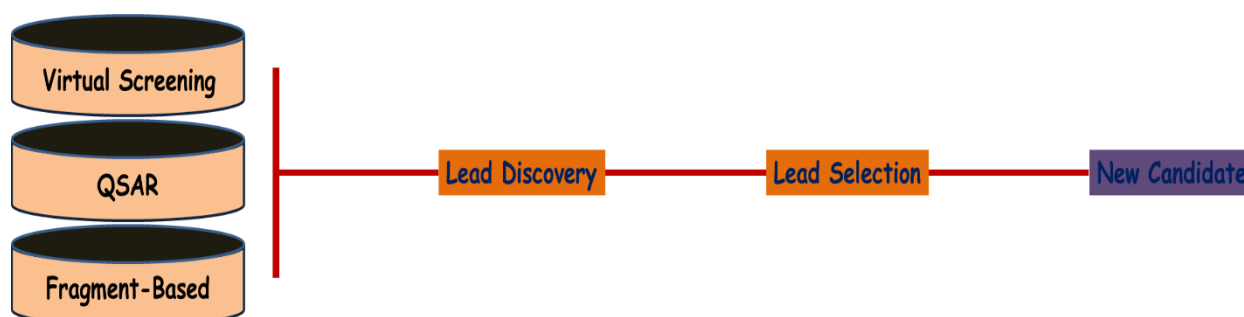


Figure II. 1. The most frequently employed drug design strategies.

2. Computer-Aided Drug Design Strategies

The primary condition for starting a CADD work requires a precise 3D configuration of the medicine and the protein. To produce novel lead molecules, a ligand-based (QSAR, CoMFA,

Pharmacophore) or structure-based (Virtual screening, docking modeling) technique can be employed. The particularly interesting compounds can be produced and tested for affinity and activity [9, 10]. The obtainability of three-dimensional structures of disease-related therapeutic targets allows for the examination of molecular interactions and dynamics of ligand-receptor binding, as well as their link with resistance mutation [11].

2.1. Structure-based drug design (SBDD)

During SBDD, the generated ligands were evaluated according to their displayed biomolecular interactions with the enzyme receptor, which is derived from the protein structure [12]. As a result, the first critical step in SBDD are the choosing of a valid therapeutic target and the collection of structural data about it. In structural and computational biology research, the use of X-ray crystallography and nuclear magnetic resonance aided in the creation of a protein structures [13]. There are two categories of structure-based drugs design: the virtual screening approach and de novo approach [13, 14].

Virtual screening approach implement accessible molecule libraries to determine molecules with specific biological activity to function as substitutes ligands for target or to develop molecules for undiscovered recognized targets with accessible configuration [15]. Following library and protein preparation, a docking software is used to realistically dock each molecule in the library into the target active site. Docking attempts for predicting the receptor-ligand complex structures by examining the configuration space of the ligands inside the active site of the target. After that, a scoring function is run to estimate the free energy of the complex and the ligand in every docking pose [16]. After docking and scoring, ranking molecules are examined for estimated binding scores, desirable physicochemical features, lead-likeness, and chemical diversity. Following post-processing, a limited number of chosen compounds are subjected to experimental testing [17].

The expression *de novo* indicates "at the start," indicating that this technology may produce unique molecules without the necessity for a starting reference [18]. The benefits of de novo drug development are creating molecules that represent original property, the creation of therapeutic candidates in an economical and quick way, the ability to explore larger chemical groups, and the possibility for innovative and better treatments. The process of synthesis of the produced compounds is the fundamental hurdle in de novo drug design [19, 20]. De novo design uses data from the three-dimensional structure of the active site to find fragments which fit the receptor well. These fragments should be connected using linking rules to assure synthetic availability, resulting

in a structurally unique ligand that be produced for more examinations [21]. **Figure II. 2** illustrates a graphical representation of de novo drug design process and virtual screening.

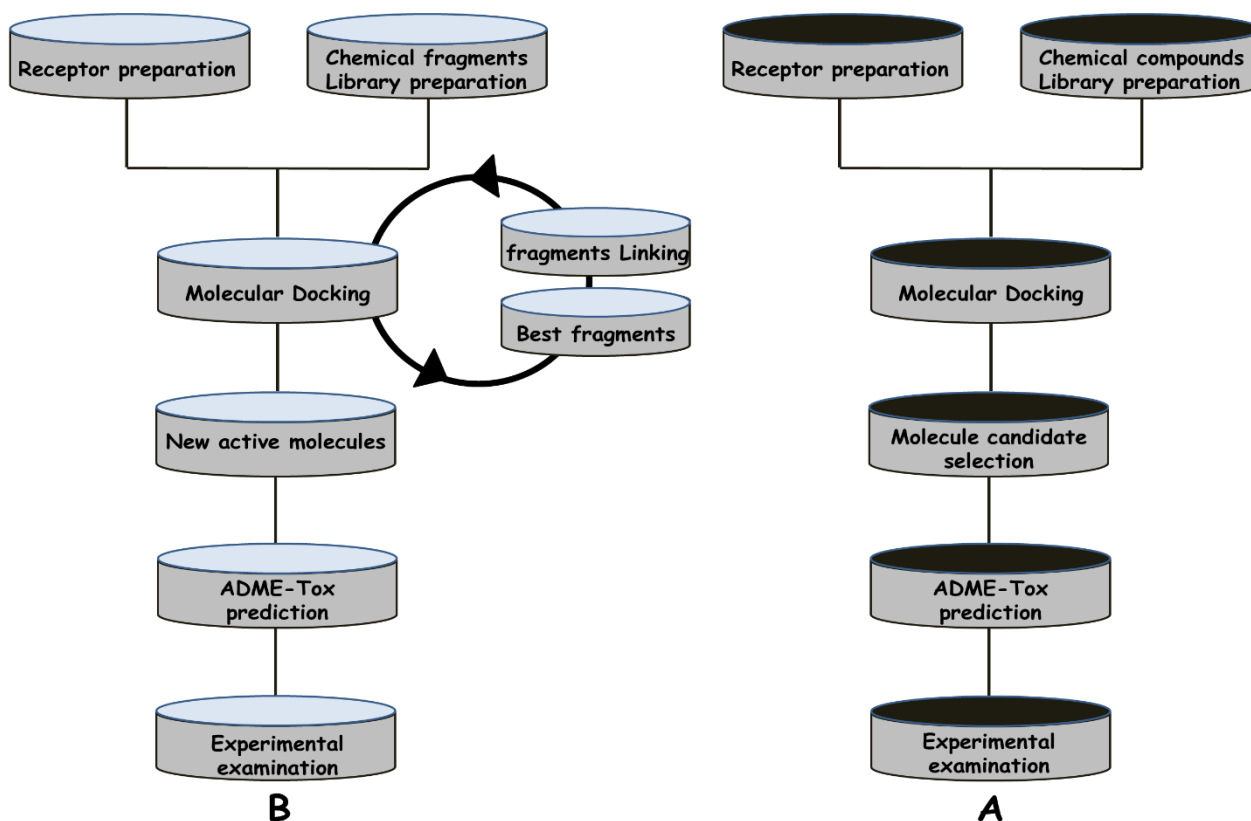


Figure II. 2. A graphical illustration of virtual screening, (A) de novo drug-design (B) strategies.

2.2. Ligand-based drug design (LBDD)

In the absence of a 3D configuration of the enzyme, data derived from a group of bioactive compounds inhibiting an important target might prove useful to determine the important features and biochemical characteristics accountable for the experimental activities. There is a presumption that two identical molecule structures have comparable biological responses with the target [22]. To create a good predictive power the ligand-based hypothesis, the molecule library must contain an extensive variety of concentrations [23]. In addition, pharmacophore-based and quantitative structure-activity relationships methodologies are the common ligand-based drug development approaches.

2.2.1. Quantitative structure–activity relationship (QSAR)

The concept of QSAR investigations posits that variations of biological activity correlate with structural and molecular variations in a group of compounds. To create an excellent QSAR model, it is necessary to follow a number of rules: (i) the bioactivity data must be large enough and obtained from an identical experimental process and selected in a manner in which the

effectiveness values are comparable; (ii) the training and test sets need to be properly chosen; (iii) to prevent over-fitting, the molecular descriptors of ligands shouldn't contain any autocorrelation, (iv) To assess its predictive power, the model needs to be evaluated either internally or externally. [23, 24].

Among the oldest and greatest known 3D-QSAR methodologies is CoMFA, which was developed over three decades back [25]. Numerous parameter options for are provided (as in CoMFA), the steric and electrostatic values are adjusted using cut-offs (± 30 kcal/mol) based on the location of the grid point. Following pretreatment, the data is scaled, which gives equal weight to all molecular descriptors and sets them on a similar platform for useful statistical analysis [26].

Figure II. 3 depicts an overview of QSAR modeling.

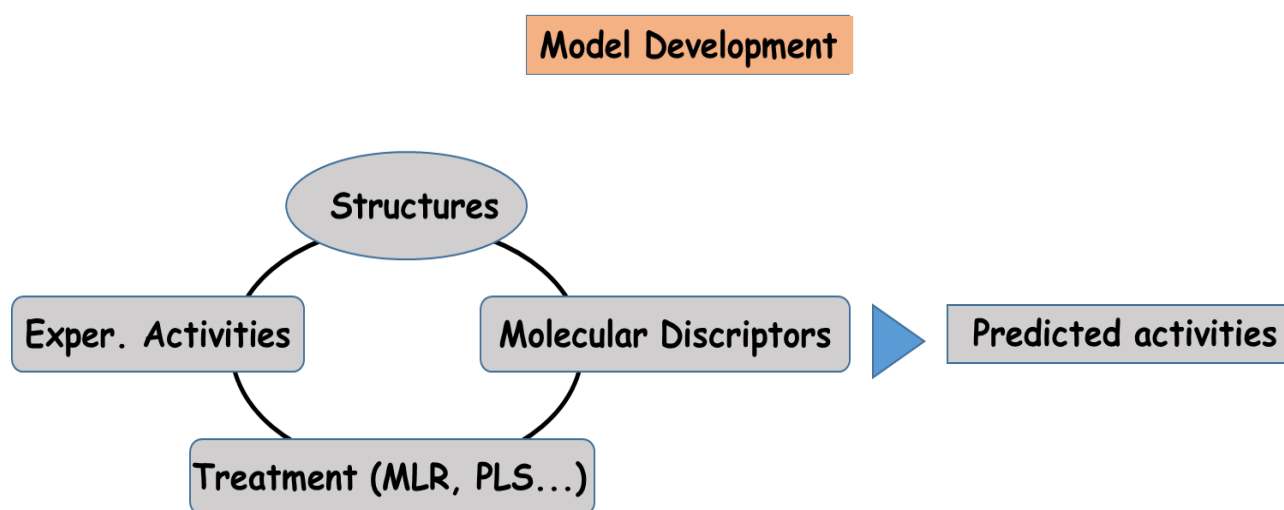


Figure II. 3. Overview of QSAR modeling.

2.2.2. Pharmacophore modeling

The goal of pharmacophore modeling is to identify compounds with different structures but a similar three-dimensional configuration of essential interacting functional groups [27]. Furthermore, pharmacophore modeling (**Figure II. 4**) is commonly employed in the molecular alignment step of QSAR modeling research [23]. More importantly, characteristics that are not consistently observed in active molecules ought to be rendered optional or removed from the hypothesis. After model refining, validation is necessary to evaluate the capacity of the model and its predictive power with an external validation [28]. On the other hand, the generation of pharmacophore models via various ligands entails two important phases: (i) building the configuration space for every ligand in the training set to symbolize ligand configuration flexibility, (ii) Alignment of all compounds in the training set to discover the needed common characteristics to generate a pharmacophore hypothesis [29]. It is worth mentioning that ligand arrangement flexibility and structural alignment constitute crucial strategies and major difficulties

in pharmacophore modeling [30]. Considering significant progress, some major problems in pharmacophore modeling remain. The first challenging aspect is ligand flexibility modeling. To address this issue, a solution has been developed: is the pre-enumeration method, where several configurations of each molecule are calculated than recorded in the database [31].

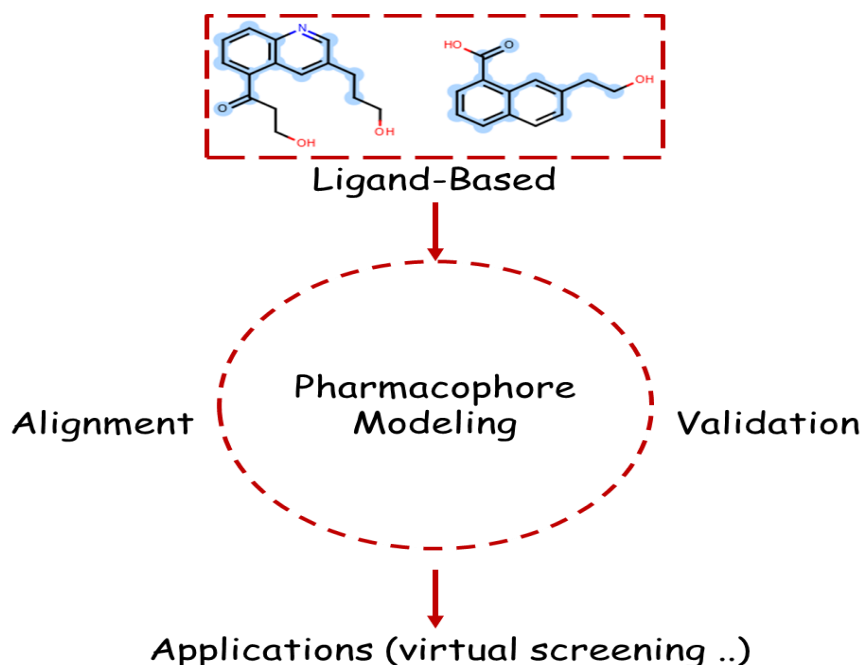


Figure II. 4. Overview of pharmacophore modeling.

2.2.3. BREED Based De Novo Hybridization process

The quantity of structural data usable in inhibitor design has increased dramatically as the identification of enzyme-inhibitor complex configurations is now frequently occurring. However, as the availability of this data grows, it becomes more and more challenging to fully exploit it [32]. The collection of all of this data from a group of complex structures is far more challenging, and comparing a number of structures at the same time is nearly impossible [32]. Using the known features of a couple of ligands to combine different fragments from each to make an individual ligand is one easy way for utilizing structural knowledge [32, 33]. The newly created compound would be a combination two scaffolds. In addition, BREED was created to facilitate this procedure by employing a bond-matching and fragment-swapping algorithm analogous to that of *Ho and Marshall* [34]. As seen in **Figure II. 5**, the generation of two new compounds for each set of matching bonds between two compounds. If the original molecules are divided into two 'halves' at the matching bond, one new molecule is created by the first half of molecule one and the second half of molecule two. The remaining new compound is formed of the second half of compound one and the initial half of compound two [32, 33].

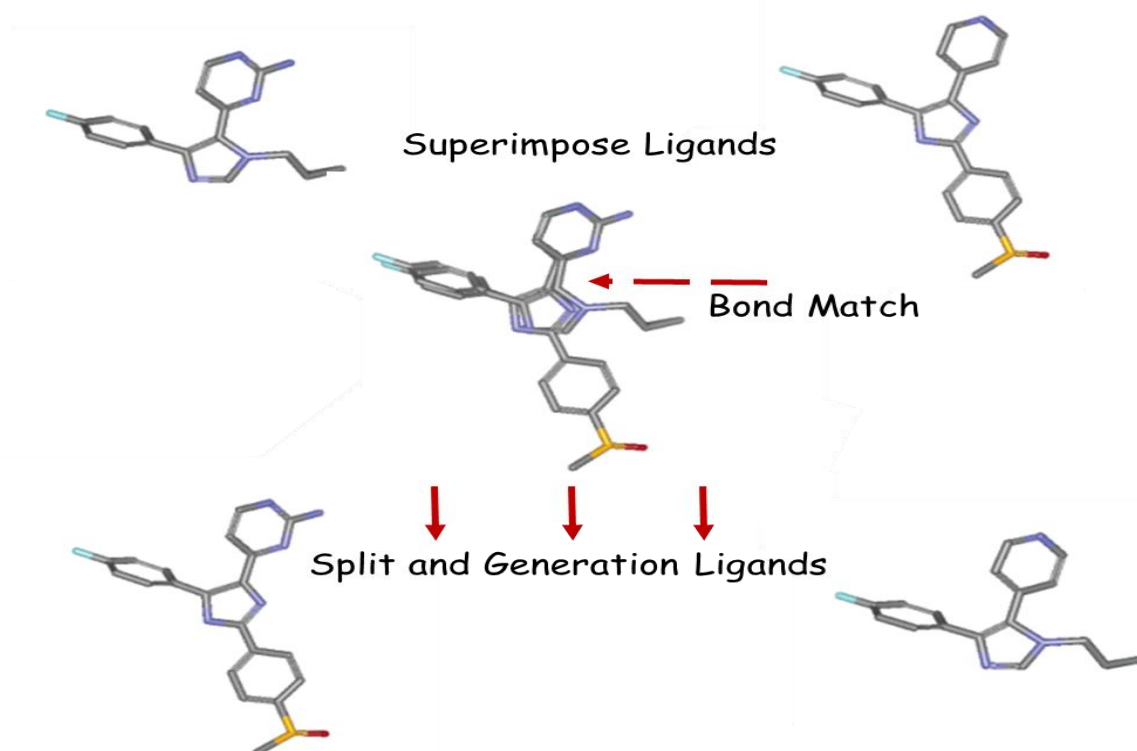


Figure II. 5. Overview of breed based de novo hybridization strategy.

3. ADME and drug likeness

Potent and secure drugs show a perfectly adjusted combination of pharmacodynamics and pharmacokinetics, comprising excellent effectiveness, affinity and specificity towards the atomic target, as well as sufficient absorption, distribution, metabolism, excretion and minimal toxicity. The integrated optimization of these factors is a key challenge in medication development [35, 36]. Since performing elaborate and expensive ADMET, testing processes for a significant amount of molecules is impracticable, *in silico* ADMET prediction is the alternative approach preference during initial drug development. The construction of excellent *in silico* ADMET models will make it possible for multiple optimizations of substance effectiveness and drug features, which is projected to not only enhance the general effectiveness of therapeutic candidates and thus their likelihood of success but also contribute to lower overall costs [37 - 39]. The technique of converting leads to drugs, on the other hand, is more difficult. This example becomes clear when we compare the variety of newly identified active substances to the number of newly authorized medications within the exact same time. *ChEMBL*, for illustration, is a collection of databases including a significant number of bioactive compounds retrieved from publications. The total variety of chemicals in *ChEMBL* was 629 943 in 2012, however by November 2014, it had risen to 1 638 394 [40].

3.1. Solubility (LogS)

Particularly evident relationship is that between solubility and lipophilicity. As a result, *Yalkowsky* and his colleagues published the experimentally obtained global solubility the formula, which characterizes a compound's solubility as a combination of LogP and melting point, where melting point quantifies the lattice energy produced on dissolution. For organic molecules, a more current version of this equation is [41 - 43]:

$$\text{LogS} = 0.5 - \text{LogP} - 0.01 (\text{MP} - 25)$$

Whereas MP indicates the melting point in degrees Centigrade. In addition, the compound's solubility is still reliant on LogP, and for significant LogP compounds, poor solubility might still show as pH dependent solubility and limited absorption.

3.2. Lipophilicity (LogP)

Lipophilicity is a critical metric in drug development since it influences a compound's solubility, permeability, potency, selectivity. The lipophilicity of organic compounds is commonly expressed as $\text{LogP}_{o/w}$, when P represents the proportion of a compound's concentrations in a mixture in equilibrium of water and octanol phases [44, 45]. The total solvation Gibbs free energies in various phases at constant temperature (T) and pressure (P) that are predicted with molecular dynamics utilizing the thermodynamic methodology which used to build ab initio methods for LogP prediction [46].

$$\text{LogP}_{o/w} = (\Delta G^{(oct/sol)} - \Delta G^{(w/sol)}) / 2.303 RT$$

Wherever $\Delta G^{(oct/sol)}$ reflects Gibbs' free energies for solvation of molecules in water-saturated octanol, $\Delta G^{(w/sol)}$ represents Gibbs' free energies for solvation of molecules in water, R represents the molar gas constant and T represents the temperature (298 K). **Table II. 1** highlights the various ways for estimating LogP [46].

Table II. 1. Examples for the prediction of lipophilicity.

Methods	Models	Illustrations
Ab initio models	$LogP_{o/w} = (\Delta G^{(oct/sol)} - \Delta G^{(w/sol)}) / 2.303 RT$	GBLogP, QLogP
Property-based methods	Empirical models: Estimation of perturbed molecular orbitals, linear solvation energy relationship, molecular size and H-bond strength	ABSOLV, SLIPPER
Statistical-based models	Developed based on numerous descriptions, such as topological parameters, graph molecular connectivity, and machine-learning approach, estate descriptors,	MLogP, TLogP

4. In silico toxicity prediction

An immediate evaluation of a chemical structure's risky qualities is vital not only for the development of medicines, but also additionally for decisions made by regulatory organizations like the United States FDA [47]. Furthermore, because of duration, expense, and moral issues with animal testing, it is difficult to examine each of these molecules on experimental systems. As a result, in silico toxicity is quickly growing to be a vital tool for anticipating the toxicity of compounds that may be detrimental to animals, plants, humans and natural world [48]. The toxicity of drugs is directly tied to their structure. SARs have recently been used extensively in nations such as Europe and the United States to forecast toxicity using computers. In addition, biostatistics, toxicology, systems biology, computer technology and numerous other related subjects are all included in the in-silico toxicity framework [49]. A molecules' toxicity could be quantified using toxicity outcomes that include mutagenicity, carcinogenicity and a variety of other parameters. It may Also to be evaluated numerically, as in LD₅₀ (lethal dosage) numbers, and in a qualitative manner as in binary (active or inactive) for particular kinds of cells and tests or signal areas including cytotoxicity, immunotoxicity, and hepatotoxicity [50].

5. Molecular dynamics simulation (MDS)

Several scientific fields, including chemical physics, biomaterials and biophysics have benefited greatly from MDS. This computational approach has shown to be quite helpful for the explained analysis of biomolecular structures, including balance with empirical information, optimization and prediction of experimental design of pertinent features for molecular structures that are costly or hard to analyze empirically [51].

Independent atom trajectories (configurations as a function of time) are created in MD simulations by simultaneously combining Newton's theorem of movement. Force fields are potential energy distributions that are employed to determine the atoms' shifts and then adjust their positions and motions at every phase of the simulation. This modeling of a protein's energy area is simple in theory but difficult in practice [52]. CHARMM, AMBER, and GROMOS are the three most common types of force fields from the numerous that available. The CHARMM 27 force field's energy equation is [53, 54, 55]:

$$\begin{aligned}
 V = & \sum_{bonds} k_B (b - b_0)^2 + \sum_{angles} k_\theta (\theta - \theta_0)^2 + \sum_{dihedrals} k_\phi [1 - \cos(n\phi - \delta)] \\
 & + \sum_{impropers} k_\omega (\omega - \omega_0)^2 + \sum_{UB} k_u (u - u_0)^2 \\
 & + \sum_{Nonbonded}^{i>j} \epsilon_{ij} \left[\left(\frac{R_{minij}}{r_{ij}} \right)^{12} - \left(\frac{R_{minij}}{r_{ij}} \right)^6 \right] + \sum_{i>j} \frac{q_i q_j}{4\pi\epsilon_0 \epsilon r_{ij}}
 \end{aligned}$$

- While V represents total potential energy.
- k_B Indicates the bond force constant, and $b - b_0$ signifies the distance the atom has shifted from equilibrium.
- k_θ Represents the angle force constant, and $\theta - \theta_0$ denotes the angle from equilibrium between three attached atoms.
- k_ϕ Indicates the dihedral force constant, n is the function multiplicity, ϕ indicates the dihedral angle and δ represents the phase shift.
- k_ω Denotes the force constant, and $\omega - \omega_0$ is the out-of-plane angle.
- k_u Is the relevant force constant, and u is the distance between the 1,3 atoms in the harmonic potential.

The van der Waals (VDW) energy is computed using a conventional 12-6 Lennard-jones potential, and the electrostatic energy is calculated using a coulombic potential.

The most frequent simulation packages are NAMD, CHARMM, AMBER, and GROMACS. These sets share fundamental characteristics but differ in their functionality and underlying perspectives, and it is worth noting that GROMACS is the only open source suite of the four, having been ported from its initial FORTRAN code to C. [56, 57, 58, 59]. **Figure II. 6** depicts an illustration of the MD simulation approach (as implemented by the Gromacs package).

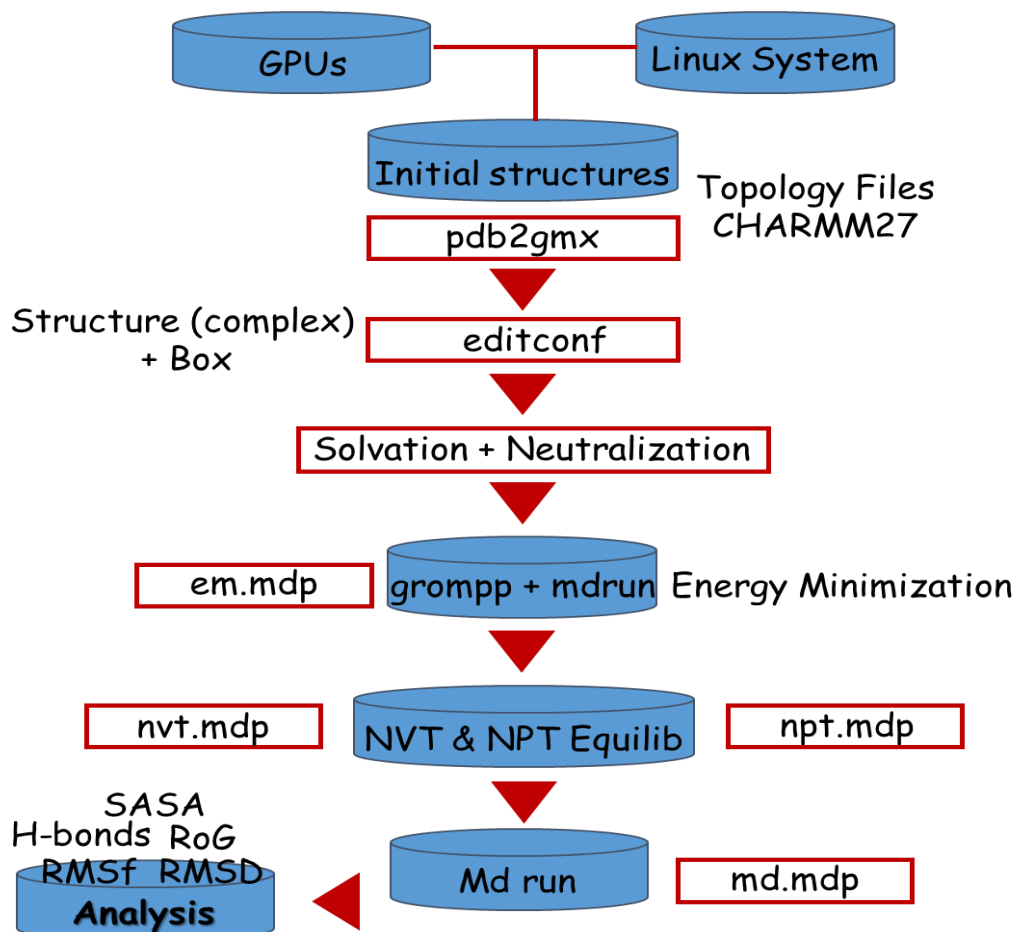


Figure II. 6. Overview of molecular dynamics simulation via GROMACS package.

6. Reference

- [1] Baldi, A. (2010). Computational approaches for drug design and discovery: An overview. *Systematic reviews in Pharmacy*, 1(1), 99.
- [2] Sinha, S., & Vohora, D. (2018). Drug discovery and development: An overview. *Pharmaceutical medicine and translational clinical research*, 19-32.
- [3] Hajduk, P. J., Huth, J. R., & Tse, C. (2005). Predicting protein druggability. *Drug discovery today*, 10(23-24), 1675-1682.
- [4] Cavasotto, C. N., & W Oorry, A. J. (2007). Ligand docking and structure-based virtual screening in drug discovery. *Current topics in medicinal chemistry*, 7(10), 1006-1014.
- [5] Veselovsky, A. V., & Ivanov, A. S. (2003). Strategy of computer-aided drug design. *Current Drug Targets-Infectious Disorders*, 3(1), 33-40.
- [6] Kore, P. P., Mutha, M. M., Antre, R. V., Oswal, R. J., & Kshirsagar, S. S. (2012). Computer-aided drug design: an innovative tool for modeling.
- [7] Jorgensen, W. L. (2004). The many roles of computation in drug discovery. *Science*, 303(5665), 1813-1818.
- [8] Andricopulo, A. D., Salum, L. B., & Abraham, D. J. (2009). Structure-based drug design strategies in medicinal chemistry. *Current topics in medicinal chemistry*, 9(9), 771-790.
- [9] Taft, C. A., & Da Silva, V. B. (2008). Current topics in computer-aided drug design. *Journal of pharmaceutical sciences*, 97(3), 1089-1098.
- [10] Griffith, R., Luu, T. T., Garner, J., & Keller, P. A. (2005). Combining structure-based drug design and pharmacophores. *Journal of Molecular Graphics and Modelling*, 23(5), 439-446.
- [11] Cao, Z. W., Han, L. Y., Zheng, C. J., Ji, Z. L., Chen, X., Lin, H. H., & Chen, Y. Z. (2005). Computer prediction of drug resistance mutations in proteins. *Drug discovery today*, 10(7), 521-529.
- [12] Grinter, S. Z., & Zou, X. (2014). Challenges, applications, and recent advances of protein-ligand docking in structure-based drug design. *Molecules*, 19(7), 10150-10176.
- [13] Kalyaanamoorthy, S., & Chen, Y. P. P. (2011). Structure-based drug design to augment hit discovery. *Drug discovery today*, 16(17-18), 831-839.
- [14] Lionta, E., Spyrou, G., K Vassilatis, D., & Cournia, Z. (2014). Structure-based virtual screening for drug discovery: principles, applications and recent advances. *Current topics in medicinal chemistry*, 14(16), 1923-1938.
- [15] Lavecchia, A., & Di Giovanni, C. (2013). Virtual screening strategies in drug discovery: a critical review. *Current medicinal chemistry*, 20(23), 2839-2860.
- [16] Meng, X. Y., Zhang, H. X., Mezei, M., & Cui, M. (2011). Molecular docking: a powerful approach for structure-based drug discovery. *Current computer-aided drug design*, 7(2), 146-157.

- [17] Cheng, T., Li, Q., Zhou, Z., Wang, Y., & Bryant, S. H. (2012). Structure-based virtual screening for drug discovery: a problem-centric review. *The AAPS journal*, 14, 133-141.
- [18] Devi, R. V., Sathya, S. S., & Coumar, M. S. (2015). Evolutionary algorithms for de novo drug design—A survey. *Applied Soft Computing*, 27, 543-552.
- [19] Schneider, G., & Fechner, U. (2005). Computer-based de novo design of drug-like molecules. *Nature Reviews Drug Discovery*, 4(8), 649-663.
- [20] Mouchlis, V. D., Afantitis, A., Serra, A., Fratello, M., Papadiamantis, A. G., Aidinis, V., ... & Melagraki, G. (2021). Advances in de novo drug design: from conventional to machine learning methods. *International journal of molecular sciences*, 22(4), 1676.
- [21] Rodrigues, T., & Schneider, G. (2014). Flashback forward: reaction-driven de novo design of bioactive compounds. *Synlett*, 25(02), 170-178.
- [22] Prathipati, P., Dixit, A., & Saxena, A. K. (2007). Computer-aided drug design: Integration of structure-based and ligand-based approaches in drug design. *Current Computer-Aided Drug Design*, 3(2), 133-148.
- [23] Melo-Filho, C. C., Braga, R. C., & Andrade, C. H. (2014). 3D-QSAR approaches in drug design: perspectives to generate reliable CoMFA models. *Current computer-aided drug design*, 10(2), 148-159.
- [24] Cherkasov, A., Muratov, E. N., Fourches, D., Varnek, A., Baskin, I. I., Cronin, M., ... & Tropsha, A. (2014). QSAR modeling: where have you been? Where are you going to?. *Journal of medicinal chemistry*, 57(12), 4977-5010.
- [25] Cramer, R. D. (2003). Topomer CoMFA: a design methodology for rapid lead optimization. *Journal of medicinal chemistry*, 46(3), 374-388.
- [26] Patel, H. M., Noolvi, M. N., Sharma, P., Jaiswal, V., Bansal, S., Lohan, S., ... & Bhardwaj, V. (2014). Quantitative structure–activity relationship (QSAR) studies as strategic approach in drug discovery. *Medicinal chemistry research*, 23, 4991-5007.
- [27] Vuorinen, A., & Schuster, D. (2015). Methods for generating and applying pharmacophore models as virtual screening filters and for bioactivity profiling. *Methods*, 71, 113-134.
- [28] Dixon, S. L., Smondyrev, A. M., & Rao, S. N. (2006). PHASE: a novel approach to pharmacophore modeling and 3D database searching. *Chemical biology & drug design*, 67(5), 370-372.
- [29] Yang, S. Y. (2010). Pharmacophore modeling and applications in drug discovery: challenges and recent advances. *Drug discovery today*, 15(11-12), 444-450.
- [30] Shepphird, J. K., & Clark, R. D. (2006). A marriage made in torsional space: using GALAHAD models to drive pharmacophore multiplet searches. *Journal of computer-aided molecular design*, 20, 763-771.
- [31] Seidel, T., Wieder, O., Garon, A., & Langer, T. (2020). Applications of the pharmacophore concept in natural product inspired drug design. *Molecular Informatics*, 39(11), 2000059.
- [32] Pierce, A. C., Rao, G., & Bemis, G. W. (2004). BREED: Generating novel inhibitors through hybridization of known ligands. Application to CDK2, p38, and HIV protease. *Journal of medicinal chemistry*, 47(11), 2768-2775.

- [33] Patel, H. M., Shaikh, M., Ahmad, I., Lokwani, D., & Surana, S. J. (2021). BREED based de novo hybridization approach: generating novel T790M/C797S-EGFR tyrosine kinase inhibitors to overcome the problem of mutation and resistance in non small cell lung cancer (NSCLC). *Journal of Biomolecular Structure and Dynamics*, 39(8), 2838-2856.
- [34] Ho, C. M., & Marshall, G. R. (1993). SPLICE: a program to assemble partial query solutions from three-dimensional database searches into novel ligands. *Journal of Computer-Aided Molecular Design*, 7, 623-647.
- [35] Segall, M. (2014). Advances in multiparameter optimization methods for de novo drug design. *Expert opinion on drug discovery*, 9(7), 803-817.
- [36] Ferreira, L. L., & Andricopulo, A. D. (2019). ADMET modeling approaches in drug discovery. *Drug discovery today*, 24(5), 1157-1165.
- [37] Cheng, F., Li, W., Liu, G., & Tang, Y. (2013). In silico ADMET prediction: recent advances, current challenges and future trends. *Current topics in medicinal chemistry*, 13(11), 1273-1289.
- [38] Clark, D. E., & Pickett, S. D. (2000). Computational methods for the prediction of 'drug-likeness'. *Drug discovery today*, 5(2), 49-58.
- [39] Moroy, G., Martiny, V. Y., Vayer, P., Villoutreix, B. O., & Miteva, M. A. (2012). Toward in silico structure-based ADMET prediction in drug discovery. *Drug discovery today*, 17(1-2), 44-55.
- [40] Gaulton, A., Bellis, L. J., Bento, A. P., Chambers, J., Davies, M., Hersey, A., ... & Overington, J. P. (2012). ChEMBL: a large-scale bioactivity database for drug discovery. *Nucleic acids research*, 40(D1), D1100-D1107.
- [41] Dearden, J. C. (2006). In silico prediction of aqueous solubility. *Expert opinion on drug discovery*, 1(1), 31-52.
- [42] Yalkowsky, S. H., & Valvani, S. C. (1980). Solubility and partitioning I: solubility of nonelectrolytes in water. *Journal of pharmaceutical sciences*, 69(8), 912-922.
- [43] Ran, Y., Jain, N., & Yalkowsky, S. H. (2001). Prediction of aqueous solubility of organic compounds by the general solubility equation (GSE). *Journal of chemical information and computer sciences*, 41(5), 1208-1217.
- [44] Arnott, J. A., & Planey, S. L. (2012). The influence of lipophilicity in drug discovery and design. *Expert opinion on drug discovery*, 7(10), 863-875.
- [45] Waring, M. J. (2010). Lipophilicity in drug discovery. *Expert Opinion on Drug Discovery*, 5(3), 235-248.
- [46] Waring, M. J. (2010). Lipophilicity in drug discovery. *Expert Opinion on Drug Discovery*, 5(3), 235-248.
- [47] Zhang, L., McHale, C. M., Greene, N., Snyder, R. D., Rich, I. N., Aardema, M. J., ... & Venkatachalam, S. (2014). Emerging approaches in predictive toxicology. *Environmental and molecular mutagenesis*, 55(9), 679-688.
- [48] Raies, A. B., & Bajic, V. B. (2016). In silico toxicology: computational methods for the prediction of chemical toxicity. *Wiley Interdisciplinary Reviews: Computational Molecular Science*, 6(2), 147-172.

- [49] Banerjee, P., Eckert, A. O., Schrey, A. K., & Preissner, R. (2018). ProTox-II: a webserver for the prediction of toxicity of chemicals. *Nucleic acids research*, 46(W1), W257-W263.
- [50] Lea, I. A., Gong, H., Paleja, A., Rashid, A., & Fostel, J. (2017). CEBS: a comprehensive annotated database of toxicological data. *Nucleic acids research*, 45(D1), D964-D971.
- [51] Filipe, H. A., & Loura, L. M. (2022). Molecular dynamics simulations: Advances and applications. *Molecules*, 27(7), 2105.
- [52] Godwin, R. C., Melvin, R., & Salsbury, F. R. (2016). Molecular dynamics simulations and computer-aided drug discovery. *Computer-aided drug discovery*, 1-30.
- [53] MacKerell Jr, A. D., Bashford, D., Bellott, M. L. D. R., Dunbrack Jr, R. L., Evanseck, J. D., Field, M. J., ... & Karplus, M. (1998). All-atom empirical potential for molecular modeling and dynamics studies of proteins. *The journal of physical chemistry B*, 102(18), 3586-3616.
- [54] Ponder, J. W., & Case, D. A. (2003). Force fields for protein simulations. *Advances in protein chemistry*, 66, 27-85.
- [55] Oostenbrink, C., Villa, A., Mark, A. E., & Van Gunsteren, W. F. (2004). A biomolecular force field based on the free enthalpy of hydration and solvation: the GROMOS force-field parameter sets 53A5 and 53A6. *Journal of computational chemistry*, 25(13), 1656-1676.
- [56] Phillips, J. C., Braun, R., Wang, W., Gumbart, J., Tajkhorshid, E., Villa, E., ... & Schulten, K. (2005). Scalable molecular dynamics with NAMD. *Journal of computational chemistry*, 26(16), 1781-1802.
- [57] Brooks, B. R., Brooks III, C. L., Mackerell Jr, A. D., Nilsson, L., Petrella, R. J., Roux, B., ... & Karplus, M. (2009). CHARMM: the biomolecular simulation program. *Journal of computational chemistry*, 30(10), 1545-1614.
- [58] Case, D. A., Cheatham III, T. E., Darden, T., Gohlke, H., Luo, R., Merz Jr, K. M., ... & Woods, R. J. (2005). The Amber biomolecular simulation programs. *Journal of computational chemistry*, 26(16), 1668-1688.
- [59] Hess, B., Kutzner, C., Van Der Spoel, D., & Lindahl, E. (2008). GROMACS 4: algorithms for highly efficient, load-balanced, and scalable molecular simulation. *Journal of chemical theory and computation*, 4(3), 435-447.

***Chapter III: Pharmacophore-Based Virtual Screening,
Molecular Docking and Molecular Dynamics Studies for the
Discovery of Novel Neuraminidase Inhibitors***

1. Introduction

Since emerging influenza can start a worldwide pandemic, it still poses a severe threat to public health [1]. Despite regular vaccinations annually, we could provide only limited protection to the elderly or immunocompromised individuals. In other words, current vaccines are ineffective against the rapidly emerging novel influenza A subtype responsible for the 2009 pandemic [2].

The surface of the influenza virus (IV) composes two crucial transmembrane glycoproteins, hemagglutinin (HA) and neuraminidase (NA) [3]. During (IV) infections, NA plays three major roles: it facilitates virus access to epithelial cells by degrading mucins rich in sialic acids of the respiratory tract, it desialilates the virion and the cytoplasmic membrane, optimizing the fusogenic potential of the HA, it encourages the production of new virions and inhibits their accumulation on the host cell surface [4].

The application of rational drug design in CADD provides an experience and understanding strategy that can give significant information regarding the interaction pattern and binding affinity between protein and ligand (complex) [5]. One of the most common approaches is molecular docking, which predicts various binding modes of a drug at a specific target-binding site and evaluates affinity based on its own conformation and complementarity with the features detected in the binding pocket [6].

The characteristics of absorption, distribution, metabolism, elimination, and toxicity (ADMET) are essential for determining the safety and efficacy of medication candidates. It is necessary to execute ADMET prediction to avert medication rejections in later phases of clinical trials [7].

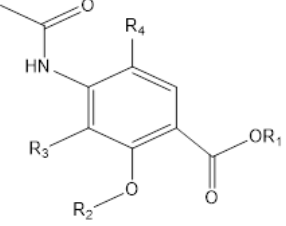
In this study, we have utilized *in silico* approaches to predict and search for new potential Neuraminidase inhibitors, which could be used to treat influenza infection.

2. Materials and Methods

2.1 Ligand Preparation

For this study, the biological data of a series of neuraminidase inhibitors containing twenty-seven *p*-aminosalicylic acid derivatives (**Table III. 1**) were extracted from the available published research [8]. The IC₅₀ value of each compound was converted into a pIC₅₀ value for in silico analysis using the provided formula: pIC₅₀ = -Log (IC₅₀) [9]. The LigPrep module using Schrodinger software [10] optimizes the 3D structures of ligands.

Table III .1. Compounds structures with experimental activity (*, Test set).



Compounds	R ₁	R ₂	R ₃	R ₄	MW	pIC ₅₀
01	Me	Et	NO ₂	NO ₂	327.25	5.939
02*	Me	Et	N=C(NH ₂) ₂	N=C(NH ₂) ₂	351.36	7.444
03	H	Et	N=C(NH ₂) ₂	N=C(NH ₂) ₂	337.15	7.495
04*	Me	i-Pr	H	H	251.28	5.274
05	Me	i-Pr	H	N=C(NH ₂) ₂	308.33	6.921
06*	H	i-Pr	H	N=C(NH ₂) ₂	294.31	7.309
07	Me	n-Pr	H	H	251.28	5.033
08	Me	n-Pr	H	NO ₂	296.28	5.447
09*	Me	n-Pr	H	NH ₂	266.29	5.899
10	H	n-Pr	H	N=C(NH ₂) ₂	294.31	6.143
11	Me	s-Bu	H	H	265.13	5.527
12	Me	s-Bu	H	NO ₂	310.31	5.799
13*	Me	s-Bu	H	N=C(NH ₂) ₂	322.36	6.131
14*	H	s-Bu	H	N=C(NH ₂) ₂	308.33	7.134
15	Me	n-Bu	H	N=C(NH ₂) ₂	322.36	7.284
16	H	n-Bu	H	N=C(NH ₂) ₂	308.33	7.409
17	Me	isopentyl	H	H	279.33	5.419
18*	Me	isopentyl	H	NO ₂	324.33	5.529
19*	Me	isopentyl	H	N=C(NH ₂) ₂	336.39	6.745
20	H	isopentyl	H	N=C(NH ₂) ₂	322.36	7.387
21	Me	Methylcyclopentane	H	N=C(NH ₂) ₂	334.37	7.032
22	H	Methylcyclopentane	H	N=C(NH ₂) ₂	320.34	7.252
23	Me	Cetyl (C ₁₆ H ₃₃)	H	H	433.62	5.570
24	Me	Cetyl (C ₁₆ H ₃₃)	H	NO ₂	478.62	5.727
25*	Me	Cetyl (C ₁₆ H ₃₃)	H	NH ₂	448.64	5.995
26*	Me	Cetyl (C ₁₆ H ₃₃)	H	N=C(NH ₂) ₂	490.68	6.059
27	H	Cetyl (C ₁₆ H ₃₃)	H	N=C(NH ₂)	476.65	6.159

2.2 Protein Preparation

The crystal structure of the neuraminidase protein utilized in this study was obtained from the Protein Data Bank (PDB ID: 5L17, in complex with *Zanamivir*) [11]. The structure was optimized and minimized utilizing the OPLS3e force field. Partial atomic charges were assigned at pH7.0 and potential ionization states were generated. Then geometry refinement was carried out using restrained minimization so that the junction of atoms had an RMSD default value of 0.3 Å [12].

2.3 Generation of Pharmacophore Model

Any number of ligands with their activity value (IC_{50}) can be employed to develop a common pharmacophore. The pharmacophoric model uses geometric concepts like spheres, planes, and vectors to depict the chemical properties of a molecule that can interact with its target protein [13]. Each hypothesis has certain traits, a maximum of six of which are H bond acceptor, hydrophobic, negatively charged, Aromatic, H-bond donor and positively charged moieties., The latter are typical pharmacophoric properties defined by a given chemical structure group [14]. The number of pharmacophoric site points was set between 4 and 6. Based on the threshold, active and inactive compounds have been classified as follows (Active $pIC_{50} > 6$, Inactive $pIC_{50} < 6$).

2.4 Construction of the 3D-QSAR model

In comparison to the pharmacophore-based alignment, an atom-based alignment was used to develop the QSAR model, which is more useful in explaining the structure-activity relationship [15]. The partial least squares (PLS) regression approach was used to create 3D-QSAR models [16]. The pictorial representation of the contours was used to visualize the 3D-QSAR results. The blue cubes represent favorable regions for activity, while the red cubes represent unfavorable regions [17]. In our study, 60% and 40% of the ligands were distributed to the training and test sets.

2.5 Model Validation

If the QSAR model is not tested, it may result in erroneous predictions of biological activity. As a result, validation of QSAR models is the most important element of QSAR investigations [18]. We employed external validation for this purpose. Golbraikh and Tropsha used the following statistical parameters of the test set to evaluate the predictive power of a QSAR model [17]: $q^2 > 0.5$, $r^2 > 0.6$, $(r^2 - r_0^2) / r^2 < 0.1$, or $(r^2 - r^{20}) / r^2 < 0.1$ and $0.85 \leq k \leq 1.15$ or $0.85 \leq k' \leq 1.15$. In addition, Roy and colleagues developed the new r_m^2 metrics as a fundamental set of validation parameters [19].

2.6 Virtual Screening and docking study

For our study, we filtered the PubChem library by searching for compounds having 80% similarity (Compared to the most active compound). Then we obtained 415420 small molecules, imported them into the project, and prepared for screening using the LigPrep model. The screening of the data was completed using pharmacophore fitness and Lipinski rules. Molecular docking is one of the most effective drug design filtering strategies. The best orientation and interaction of each lead at the active site of the protein was determined by docking [20]. We applied the docking approach with standard precision (SP), and extra precision (XP) to verify the accuracy of the results obtained.

2.7 ADMET study

We examined ADME properties of each compound, particularly the solubility and absorbability, the most important factors influencing activity [21]. We studied the ADME properties using SwissADME [22]. The ProTox-II platform was used to estimate the potential toxicity [23]. Then, the lethal dose (LD₅₀) was quantified for both active and inactive cell types in order to explore hepatotoxicity, immunotoxicity, and cytotoxicity [24].

2.8 Molecular dynamics simulation

The methodology presented in this study outlines the detailed steps for conducting molecular dynamics (MD) simulations of two compounds. The rationale for selecting these two compounds (CID 70139197 and CID 44428312) was based on the best binding affinities for Neuraminidase and good pharmacokinetic profiles. The first step involved the selection of two compounds based on their high binding affinities and good pharmacokinetic profiles. To prepare the ligand and protein topology files, the SwissParam server was used, and the protein topology file was created using the CHARMM27 all-atom force field [25]. The next step involved solvating the system with the TIP3P water model and adding Na⁺ and Cl⁻ ions to neutralize the system's charge. The solvated system was then subjected to energy minimization using the steepest descent minimization algorithm until the maximum force was less than 10.0 kJ/mol. The equilibration process was then carried out in two stages, namely the NVT equilibration and the NPT equilibration. During the NVT equilibration phase, the system was coupled with a v-rescale algorithm at 300 K with a coupling value of 0.1 ps and a duration of 100 ps. The NPT equilibration was then performed with a Berenson pressure-coupling algorithm for 100 ps and a coupling constant of 2.0 ps. After the equilibration process, the production MD simulation was performed for 100 ns using the Gromacs-2022.4 package with the CHARMM27 force field [26].

The MD simulation data were analyzed to gain insights into the stability, flexibility, compactness, and binding affinity of the protein-ligand complex. The Root Mean Square Deviation (RMSD) was calculated to determine the structural stability of the protein-ligand complex during the simulation, and the Root Mean Square Fluctuation (RMSF) was calculated to evaluate the flexibility of the protein residues. The radius of gyration was calculated to measure the compactness of the protein-ligand complex. Hydrogen bond analysis was performed to identify the hydrogen bonding interactions between the protein and ligand. Finally, the Molecular Mechanics Poisson-Boltzmann Surface Area (MM-PBSA) calculation was performed to calculate the binding free energy of the protein-ligand complex.

2.9 Method of MMPBSA Analysis

The molecular mechanics Poisson-Boltzmann surface area (MMPBSA) method was used to analyze the energetic contribution of different energy components in the protein-compounds (4428312 and 70139197) interaction. The structures of the protein-ligand complex, receptor, and ligand were prepared and optimized using the molecular dynamics simulation with the Gromacs software. The molecular mechanics force field ff14SB was used for the protein, and the GAFF force field was used for the ligand. The Poisson-Boltzmann equation was used to calculate the solvation energy, and the nonpolar solvation energy was estimated using the surface area model. The energy decomposition was performed using the MMPBSA.py script of the Gromacs software.

3. Results AND Discussion

3.1 Pharmacophore and 3D-QSAR models

The main objective of this study was to develop the pharmacophore of neuraminidase inhibitors for the influenza virus using fifteen known active and twelve inactive molecules. Then, using pharmacophore hypotheses, we aim to search new neuraminidase inhibitors. We chose the best of these hypotheses based on Survival score, Inactive score, Site, Victor, and Volume. The best four hypotheses are presented in **Table III. 2**. Survival scores with higher values improve the current mapping of pharmacophores with active molecules. However, the model with the highest inactive score can differentiate between active and inactive molecules. Very close results were recorded for the best four-pharmacophore hypotheses, as the survival score ranged between 6.415 and 6.365. In addition, the inactive score ranged from 2.098 to 2.128.

Table III. 2. Scores of different parameters of the best hypotheses

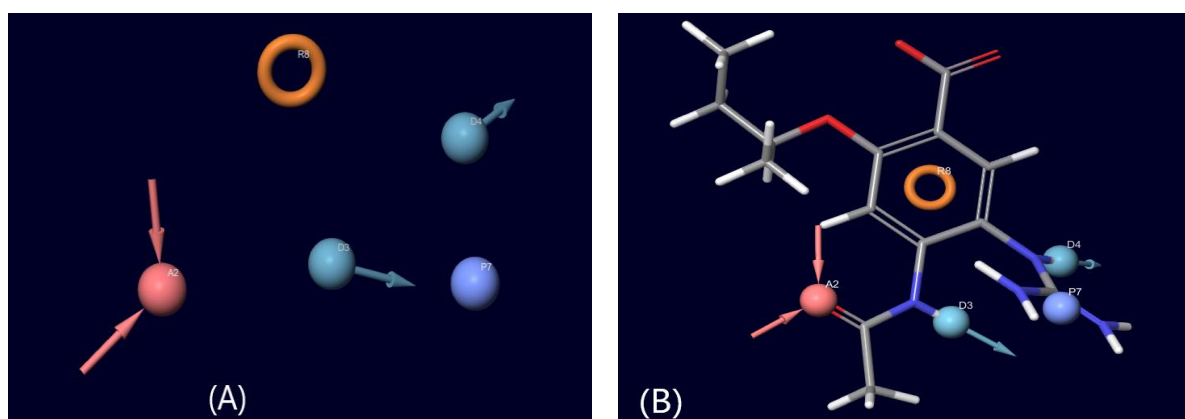
	Survival	Site	Vector	Volume	Inactive	PhaseHypo
ADDPR_1	6.415	1.000	0.968	0.881	2.098	1.385
ADDPR_2	6.405	1.000	0.968	0.871	2.099	1.384
ADDPR_3	6.373	1.000	1.000	0.882	2.130	1.382
ADDPR_4	6.365	1.000	1.000	0.874	2.128	1.382

We used atom-based 3D-QSAR for all the pharmacophore hypotheses to identify and predict the best pharmacophore hypothesis. After this step, we found the hypothesis ADDPR_4 has a high R^2 value for the training set (0.974), exceptional and best predictive potential (Q^2 , 9.05), outstanding Pearson-R coefficient (0.953), RMSE (0.230) and SD (0.160), (**Table III. 3**).

Table III. 3. Results of the 3D-QSAR, PLS statistical analysis for the chosen Pharmacophore model ADDPR_4.

ID	PLS factors	SD	R^2	F	P	RMSE	Q^2	Pearson-R
ADDPR_4	1	0.387	0.796	58.8	0.942	0.29	0.851	0.949
	2	0.249	0.921	82.4	0.850	0.26	0.878	0.949
	3	0.188	0.958	99.4	0.890	0.25	0.891	0.951
	4	0.165	0.970	98.1	0.903	0.23	0.904	0.995
	5	0.160	0.974	83.5	0.897	0.23	0.905	0.953

The spatial arrangement of the best pharmacophore hypothesis ADDPR_4 with their five-pharmacophore site is shown in **Figure III. 1**. Based on the above, we have selected the pharmacophore hypothesis ADDPR_4 for the next part of the studies.

**Figure III. 1.** (A) Pharmacophore model ADDPR_4 with their five-pharmacophore site points, and (B) Pharmacophore model ADRRR1 including an active molecule.

3.2 Model Validation

Based on the statistical analysis, we observed a high R^2_{pred} (0.9056) value was considered to be a sign of excellent external predictability. The linear regression values of r^2_0 and r'^2_0 were close

to r^2 , and $[r^2-r^2_0]/r^2$ and $[r^2-r^2_0]/r^2$ were less than 0.1. We obtained a higher value of r^2_m , (0.8613). According to the external validation results (Table III. 4), the developed 3D-QSAR model is valid and could be employed to predict the activities of new inhibitors.

Table III. 4. Results of external validation for 3D-QSAR model.

R^2_{pred}	r^2	r^2_0	r'^2_0	K	K'	$[r^2-r^2_0]/r^2$	$[r^2-r'^2_0]/r^2$	r^2_m
0.9056	0.9088	0.9060	0.9071	0.9965	1.0020	0.0030	0.0018	0.8613

3.3 3D-QSAR Contour Maps Analysis

The 3D-QSAR contour map analysis was carried out to explain the diverse vital pharmacophoric sites. It includes H-bond donor, hydrophobic/non-polar, negative ionic, positive ionic, and electron-withdrawing regions on their Neuraminidase inhibition. The blue cubes show favorable regions for activity, and the red cubes show unfavorable regions for activity. A comparison was performed using the 3D-QSAR model to compare favorable and unfavorable regions for activity, using the most active compound (compound 3, pIC₅₀: 7.495). Figure III. 2 represents the correlation plot between the experimental and predicted activity of Neuraminidase inhibitors, illustrating the strong correlation between experimental and predicted activity.

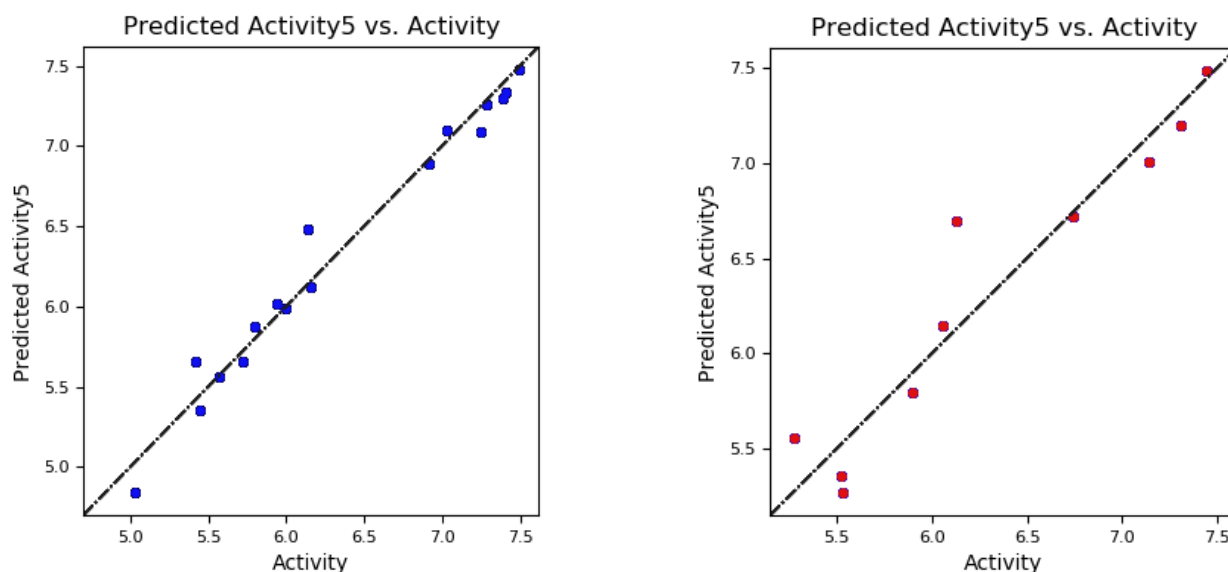


Figure III. 2. The plot of the correlation between the experimental and predicted activity of based Neuraminidase inhibitors using pharmacophore-based QSAR model of training and test set.

The red zone has not been observed for hydrogen bonds; the blue cubes were localized around the $N=C(NH_2)_2$ groups. We observed a few red cubes near the NH of the two groups of $N=C(NH_2)_2$ for the hydrophobic interaction, also the blue cubes are observed around the aromatic ring, in all regions of the ethyl radical, methyl group, for all NH_2 group, and the hydrogen atom of

the aromatic ring. Only a blue area indicated for the negative ionic presented by the, C=O of the carboxylic acid group. In addition, the presence of the blue cubes around two NH₂ of N=C(NH₂)₂ group from the positively charged ionic groups, confirmed Neuraminidase inhibition. As for the electron-withdrawing groups, the red cubes near the carboxylic acid signified as unfavorable area for inhibition activity. The appearance of blue cubes around the two N=C(NH₂)₂ groups in the most active compound contour plot revealed the preference for the electron-withdrawing group at these positions. Based on the above analysis, the QSAR model indicated that the substitution of different groups, such as hydrogen bonds, positive and negative ionic, electron-withdrawing and hydrophobic groups, at N=C(NH₂)₂, C=O of carboxylic acid, hydrogen of the aromatic ring, and the ethyl group, play a significant role in the inhibitory activity. Substitution at the OH position of the carboxylic acid had no significant contribution to the inhibitory activity. A QSAR model visualized in the context of favorable and unfavorable effects on the most active compound is presented in **Figure III. 3**.

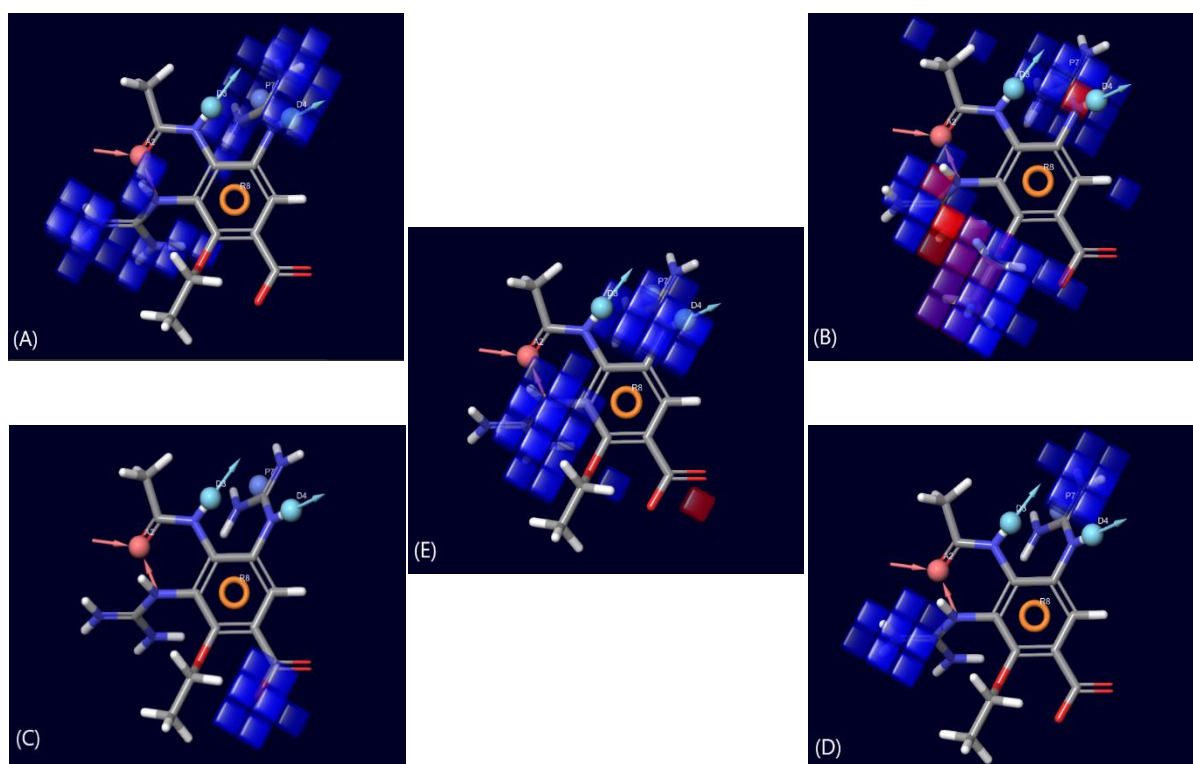


Figure III. 3. Contour maps for 3D-QSAR model: (A) Hydrogen Bond, (B) Hydrophobic, (C) Negative ionic, (D) Positive ionic, (E) Electron-withdrawing, where blue cubes represent favorable areas and red cubes represent unfavorable areas.

3.4 Virtual screening and docking studies

Virtual Screening approaches play an important role in the discovery of novel bioactive compounds [27]. Initially, we selected the PubChem library to search for new potent

Neuraminidase inhibitors. We applied a similarity of 80% and the Lipinski filter to 415420 compounds in our virtual screening process. In the next step, the pharmacophore model (ADDP_R_4) was used to screen all the 415420 molecules. Following the screening process, all compounds with a fitness score more than 2.0 were subjected to docking study. Then we filtered to obtain 1927 compounds for the following phase. It includes docking of these hits and analysis of the docking scores using Glide/SP. The docking was completed with Glide tool on Maestro 11.8 software. The details of virtual screening compounds are shown in **Table III. 5**. We used *Zanamivir*, clinically approved anti-influenza [28], as a reference ligand in our study. In the treatment of influenza, Neuraminidase inhibitors such as *Zanamivir* and *Oseltamivir* are more commonly used. To estimate the inhibitory power of hits more thoroughly, we perform molecular docking for *Oseltamivir* with Neuraminidase.

Table III. 5. All the interactions between top molecules and *Zanamivir* with the active site.

CID	H-Bond	Distance (Å)	Electrostatic	Distance	Hydrophobic	Distance (Å)
7013919 7	Arg119, Arg153, Glu278, Glu279, Arg294, Arg372	[1.6 – 2.7]	Arg119, Asp152, Glu279, Arg294	[3.7-5.0]	Trp180, Ile224, Arg226	[3.5-5.3]
4442831 2	Arg119, Arg153, Trp180, Glu229, Glu279, Arg294, Arg372	[1.5 – 2.8]	Arg119, Glu120, Asp152, Glu229, Glu279, Arg294	[3.5 – 5.4]		
506047	Arg119, Arg153, Trp180, Glu278, Glu279, Arg294, Arg372	[1.6 – 2.9]	Arg119, Glu120, Asp152, Glu229, Glu278, Glu279, Arg294	[3.2 – 5.5]		
3364666	Arg119, Arg153, Glu278, Arg294, Arg372	[1.6 – 2.6]	Arg119, Asp152, Glu279	[3.7 – 5.1]		
5278285	Arg119, Glu120, Asp152, Arg153, Trp180, Glu229, Glu278, Arg294, Arg372	[1.6 – 3]	Arg119, Glu120, Glu229, Glu279, Arg294	[4 – 5.1]		
<i>Zanamivir</i>	Arg119, Glu120, Asp152, Arg153, Trp180, Glu229, Glu278, Arg294, Arg372	[1.6 – 3.1]	Glu120, Glu229, Glu279, Arg294	[4 – 5.1]		
<i>Oseltamivir</i>	Asp151, Glu229, Glu278, Glu279	[1.7-3.1]				

The docking score of *Zanamivir* and *Oseltamivir* complexes with Neuraminidase was -9.873 and -6.244 kcal/mol respectively. The highest-scoring hit molecule was CID 70139197, with a binding energy of -11.549 kcal/mol. The second best-scored hit molecules was CID 44428312 with a binding energy of -10.682 kcal/mol. Then it was followed by CID 506047, the third best hit molecule with a binding energy of -10.506 kcal/mol. Docking scores of the screened hits using Glide/SP, XP are represented in **Table III. 6**.

Table III. 6. Docking scores of the selected hits and the *Zanamivir*.

Compound Names CID	SP Score (kcal/mol)	XP Score (kcal/mol)	Glide E Model
70139197	-8.704	-11.549	-58.009
44428312	-8.255	-10.682	-44.704
506047	-8.251	-10.506	-52.938
3364666	-8.650	-10.460	-60.477
5278285	-8.631	-10.217	-60.577
<i>Zanamivir</i>	-8.053	-9.873	-56.249
<i>Oseltamivir</i>	-5.506	-6.244	-68.653

For the five hits molecules, we noticed similar interactions with the amino acids Arg119, Arg153, Arg294 and Arg372, by hydrogen bond interactions with a distance from 1.5 to 3.1 Å (Table 6). We also observed another interaction by hydrogen bonding between the three best molecules only with the amino acid Glu279. It confirms that the interaction with the amino acid (Glu279) plays a vital role in the inhibitory activity of Neuraminidase. Docking analysis indicated the best-hit molecule CID 70139197 interacted with the active site by hydrophobic interaction with the amino acids Trp180, Ile224, and Arg226 with a distance from 3.5 to 5.3 Å. It confirms the importance of this interaction for the inhibitory activity (**Figure III. 4**).

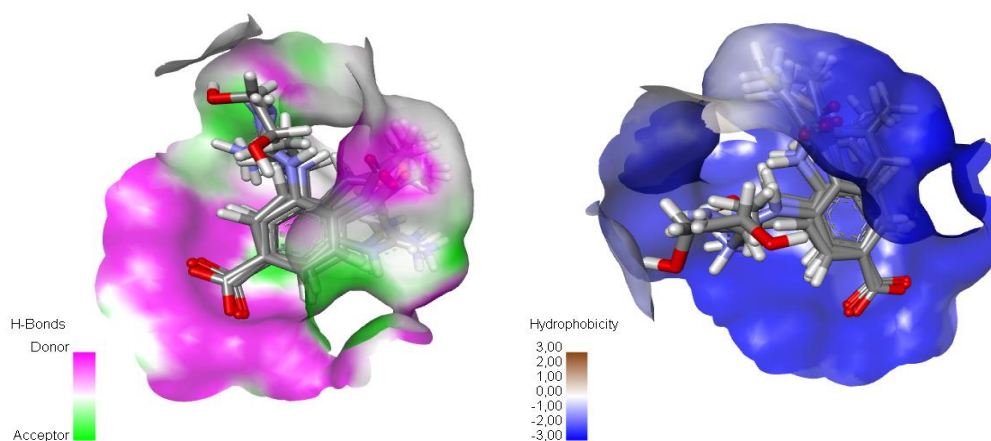


Figure III. 4. The orientation of the hits molecules in the active site and hydrogen bonds and hydrophobic areas.

In general, we remarked a similarity of interactions for the five best molecules with the active site for electrostatic interactions observed between the hits molecules and the residues Arg119, Asp152, Glu279, and Arg294 (**Figure III. 5**). However, the molecule *Zanamivir* interacted with Glu120, Glu229, Glu279 and Arg294 amino acids from a distance of 4 to 5.1. *Oseltamivir* interacted with Asp151, Glu229, Glu278, Glu279 by hydrogen bond interactions only, at about the same distance (**Figure III. 6**). According to the results obtained by the Molecular Docking study, all hit molecules are more stable in the active site of Neuraminidase than *Zanamivir* and *Oseltamivir*.

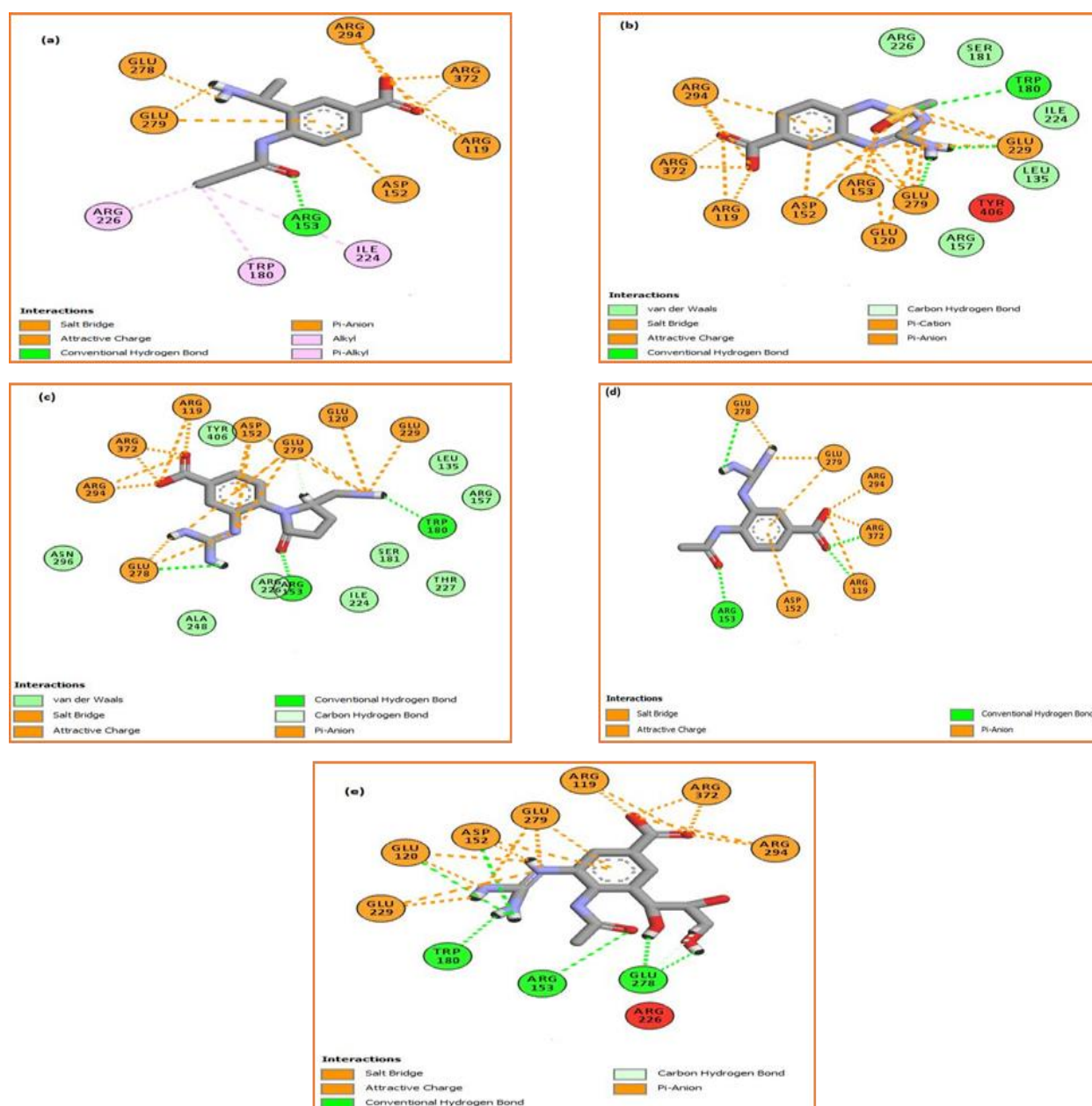


Figure III. 5. The binding interactions of the top hits with the active site of Neuraminidase, (a) CID 70139197, (b) CID 44428312, (c) CID 506047, (d) CID 3364666, (e) CID 5278285.

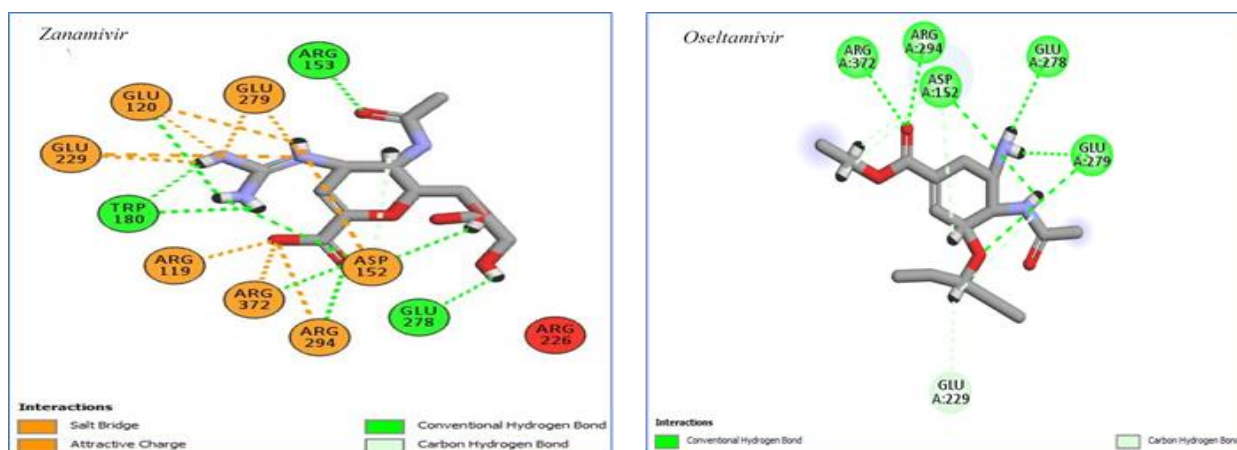


Figure III. 6. The binding interactions of the Zanamivir and Oseltamivir with the active site of Neuraminidase.

3.5 Prediction of ADME

The aqueous solubility and the permeability to the biological membranes are the two pharmacokinetic parameters responsible for optimal activity. According to SwissADME analysis, all hits presented consensus $\log P_{o/w}$ values between -1.40 and 0.71 and Log S between -0.03 and 0.82. Therefore, the five hits molecules have the best aqueous solubility and good permeability to the biological membranes. The best-hit molecule (CID 70139197) and (CID 3364666) were estimated to have a high GI absorption, plasma proteins binding ability, good distribution, and acceptable elimination profile due to increased aqueous solubility. The bioavailability score for all hits was 0.55, more than 10%, and the predictions related to skin permeability (LogKp) showed values close to -10, as shown in **Table III. 7**. Finally, all pharmacokinetic parameters support Lipinski's guideline.

Table III. 7. Pharmacokinetic and physicochemical parameters calculated by SwissADME.

CID	MW (g/mol)	Consensus Log $P_{o/w}$	Log S	Bioavailability	GI absorption	Cytochrome P450 inhibitor	Log Kp	Synthetic accessibility
70139197	236.27	0.71	-0.37	0.55	High	No	-8.71	2.39
44428312	256.28	-0.29	-1.03	0.55	Low	No	-8.31	3.05
506047	291.31	-0.87	0.80	0.55	Low	No	-10.77	2.97
3364666	238.24	-1.28	0.82	0.55	High	No	-10.09	2.03
5278285	326.31	-1.40	-0.03	0.55	Low	No	-10.06	3.64

3.6 Prediction of Toxicity

The toxicity of the five hits predicted by ProToxII is presented in **Table III. 8**. In summary, five distinct undesirable drug effects, such as hepatotoxicity, immunotoxicity, carcinogenicity, mutagenicity, and cytotoxicity, were calculated for all selected top hits to predict potential toxicity. In addition, all of the five hits molecules presented calculated LD_{50} between 1000 and 5000 mg/kg, which is also a toxicity class of 4 to 5, which signifies low toxicity.

Table III. 8. Toxicity prediction of the top hits molecules.

CID	Hepatotoxicity	Carcinogenicity	Immunotoxicity	Mutagenicity	Cytotoxicity	LD50	Class
70139197	Inactive	Inactive	Inactive	Inactive	Inactive	1782	4
44428312	Inactive	Inactive	Inactive	Inactive	Inactive	5000	5
506047	Inactive	Inactive	Inactive	Inactive	Inactive	1000	4
3364666	Inactive	Inactive	Inactive	Inactive	Inactive	3918	5
5278285	Inactive	Inactive	Inactive	Inactive	Inactive	1517	4

3.7 Molecular dynamics study

The present study aimed to investigate the stability of Neuraminidase (NA) and its complexes with CID 70139197 and CID 44428312 through molecular dynamics (MD) simulations. The MD simulations were carried out for 100 ns on a GPU system, and the trajectory data from the production MD phase were analyzed. The root-mean-square deviation (RMSD) was measured in relation to the initial conformations to determine the structural stability of the protein and its complexes. The results indicate that the RMSD of Neuraminidase initially varied briefly, but it was observed to stabilize following 15 ns of simulations. The NA_CID 44428312 complex was shown to be stable throughout the simulation, while the NA_CID 70139197 complex achieved structural stability after 5 ns of simulation. The RMSD plot of Neuraminidase and its complexes with CID 70139197 and CID 44428312 is presented in **Figure III. 7**. The average RMSD of the NA and its complexes with CID 70139197 and CID 44428312 were found to be 0.197, 0.168, and 0.117 nm, respectively. The RMSD analysis clearly demonstrates that the Neuraminidase and its complexes with CID 70139197 and CID 44428312 are stable during the simulation for 100 ns. These findings provide valuable insights into the structural stability of Neuraminidase and its complexes and can be useful for the development of novel inhibitors against influenza virus.

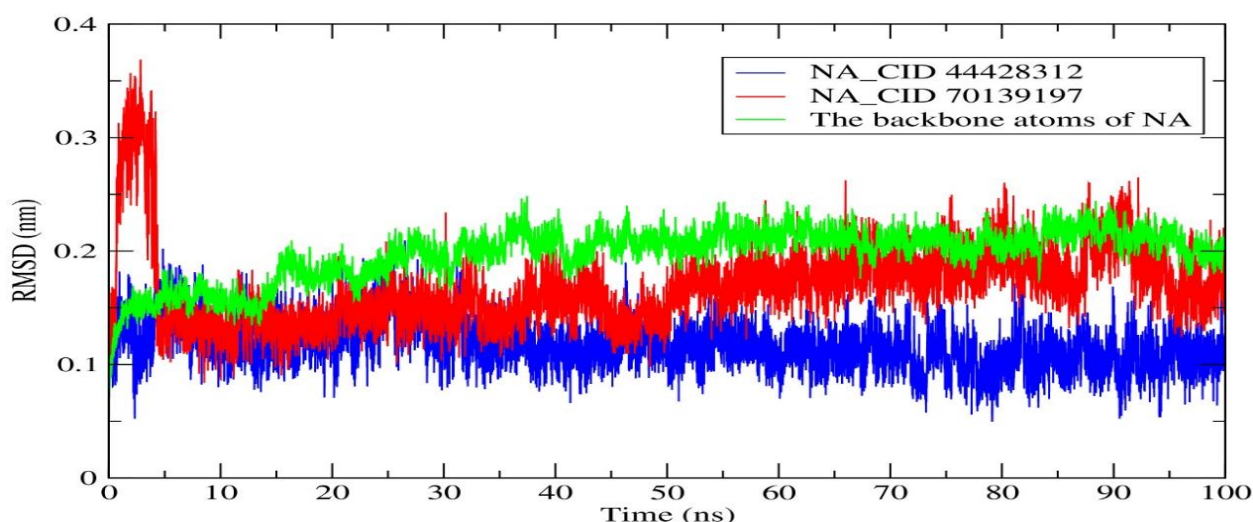


Figure III. 7. Root-mean-square deviation (RMSD) analysis of the backbone atoms of Neuraminidase and its complexes with CID 70139197 and CID 44428312.

In this study, we evaluated the root-mean-square fluctuation (RMSF) of the C-alpha atoms of Neuraminidase (NA) and its complexes with CID 70139197 and CID 44428312, as depicted in **Figure III. 8**. The analysis showed that the RMSF of the C-alpha atoms of most atoms of NA and its complexes was less than 0.25 nm, indicating low atomic mobility and structural stability. Notably, the NA_CID 70139197 complex displayed higher fluctuation at atoms 995 of the NA protein, with an RMSF value of 0.35. This observation suggests that the interaction of the ligand with the protein induced conformational changes and increased the dynamics of the protein at that specific region. The RMSF plot shows the fluctuation of each ligand atom during the simulation period. Both ligands exhibit a similar dynamical shift towards the binding site of Neuraminidase, indicating a stable interaction with the protein.

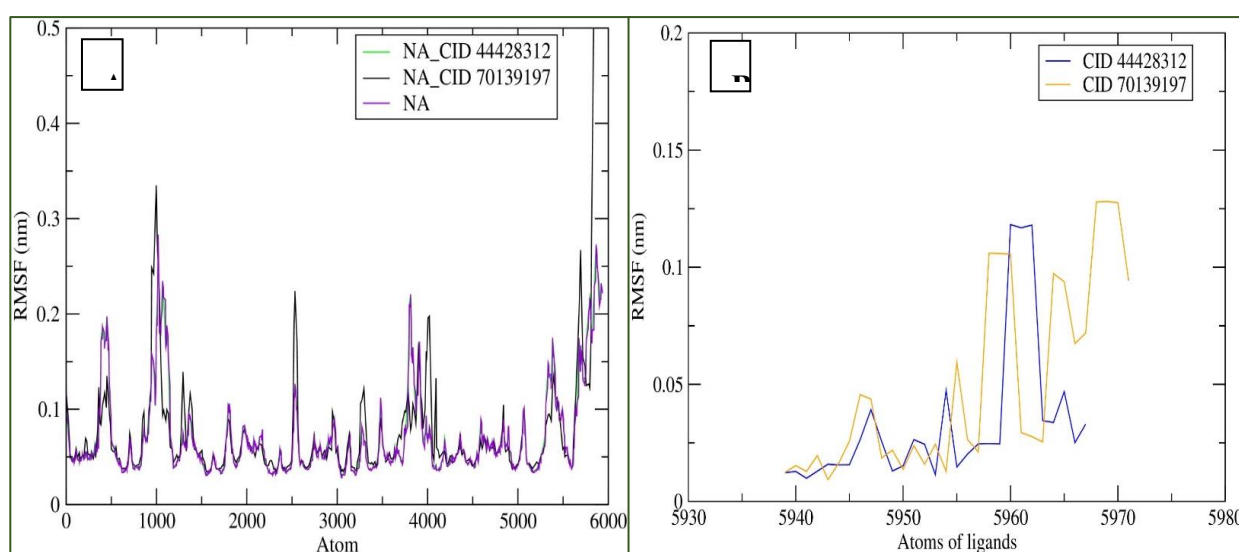


Figure III. 8. Root-mean-square fluctuation (RMSF) of the C-alpha atoms of Neuraminidase (NA) and its complexes with CID 70139197 and CID 44428312. **A.** RMSF of the C-alpha atoms of NA and its complexes. **B.** RMSF of the atoms of CID 44428312 and CID 70139197.

In order to evaluate the stability of Neuraminidase (NA) and its complexes with CID 70139197 and CID 44428312 during the 100 ns simulation period, we calculated the radius of gyration (Rg) of each system. Rg is a measure of the compactness of a molecule and is defined as the root-mean-square distance between each atom in a molecule and its center of mass. A decrease in Rg indicates a more compact structure, while an increase in Rg indicates a more extended structure. In **Figure III. 9**, we present the Rg values for each system plotted over the course of the simulation period.

We observed that the Rg values for NA_CID 44428312 and NA_CID 70139197 remained similar throughout the simulation, indicating a stable interaction between the ligands and the protein. The average Rg values for NA, NA_CID 44428312, and NA_CID 70139197 were 1.967, 0.324, and 0.323 nm, respectively. The average Rg values of the two complexes were less than

0.33 nm, which indicates a stable conformation of the protein-ligand complexes during the simulation period. This observation is consistent with the RMSD and RMSF analyses, which also demonstrated the stability of the complexes. Overall, our results suggest that both CID 70139197 and CID 44428312 form stable complexes with NA and may have potential as lead compounds for drug development targeting Neuraminidase.

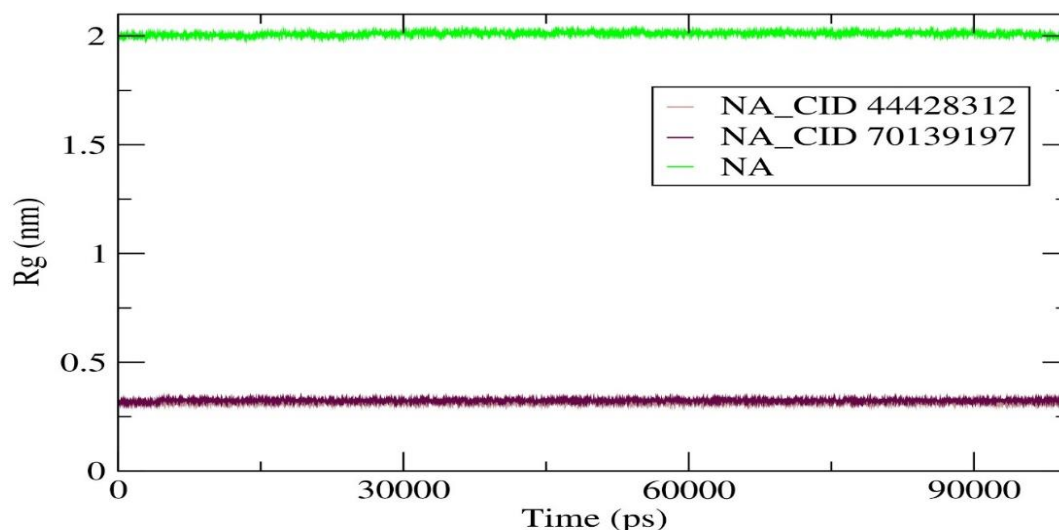


Figure III. 9. Radius of gyration (R_g) of Neuraminidase and its complexes with CID 44428312 and CID 70139197.

To gain insight into the nature of the interaction between the ligands CID 44428312 and CID 70139197 with the Neuraminidase, we analyzed the hydrogen bond profiles of the NA_CID 44428312 and NA_CID 70139197 complexes, as depicted in **Figure III. 10**. Our analysis revealed that the NA_CID 44428312 complex formed an average of 8.4 hydrogen bonds during the simulation, while the NA_CID 70139197 complex formed an average of 5.2 hydrogen bonds.

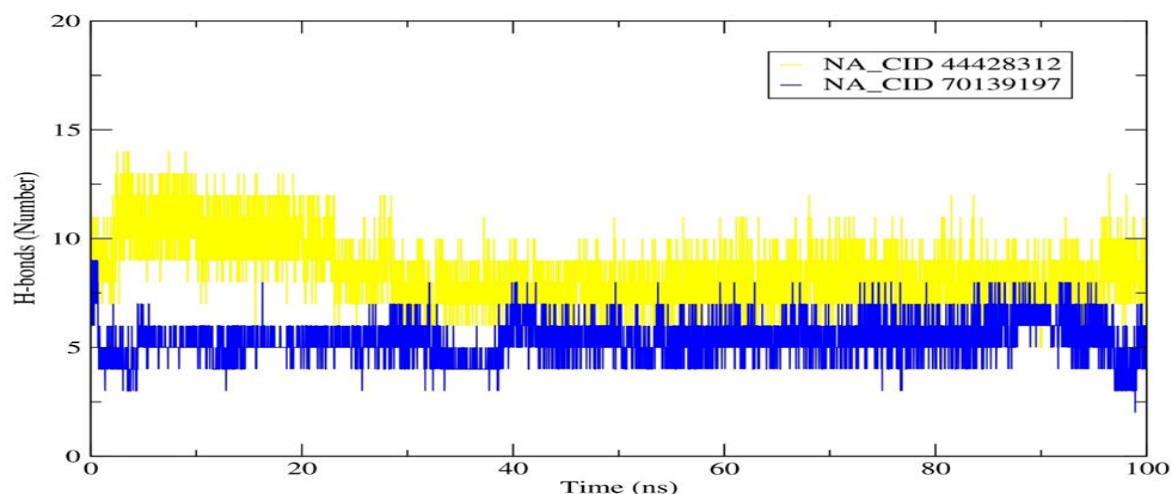


Figure III. 10. Hydrogen bond existence map of Neuraminidase complexes with CID 44428312 and CID 70139197 during 100 ns of simulation.

The higher number of hydrogen bonds in the NA_CID 44428312 complex can be attributed to the presence of more polar functional groups in CID 44428312 as compared to CID 70139197. The polar functional groups in CID 44428312, such as hydroxyl and carbonyl groups, facilitate the formation of hydrogen bonds with the Neuraminidase, leading to a greater number of hydrogen bonds being formed and a stronger binding interaction. In contrast, CID 70139197 has fewer polar functional groups and therefore forms fewer hydrogen bonds with the protein. These results suggest that the hydrogen bonding interaction plays an important role in stabilizing the NA_CID 44428312 complex and underscores the importance of considering the chemical properties of ligands when designing new drugs targeting the Neuraminidase.

3.8 MMPBSA Analysis

3.8.1 Analysis of NA_44428312 Complex

The results of the MMPBSA analysis showed that the total binding free energy of the protein-ligand complex was -56.86 kcal/mol. The energetic contributions of different energy components were calculated (**Figure III. 11**), and it was found that the van der Waals interaction energy (-5.35 kcal/mol) and electrostatic interaction energy (-297.52 kcal/mol) were the major contributors to the binding free energy. The energy contributions from the other energy components, such as bond, angle, dihedral, 1-4 van der Waals, and 1-4 electrostatic interactions, were negligible.

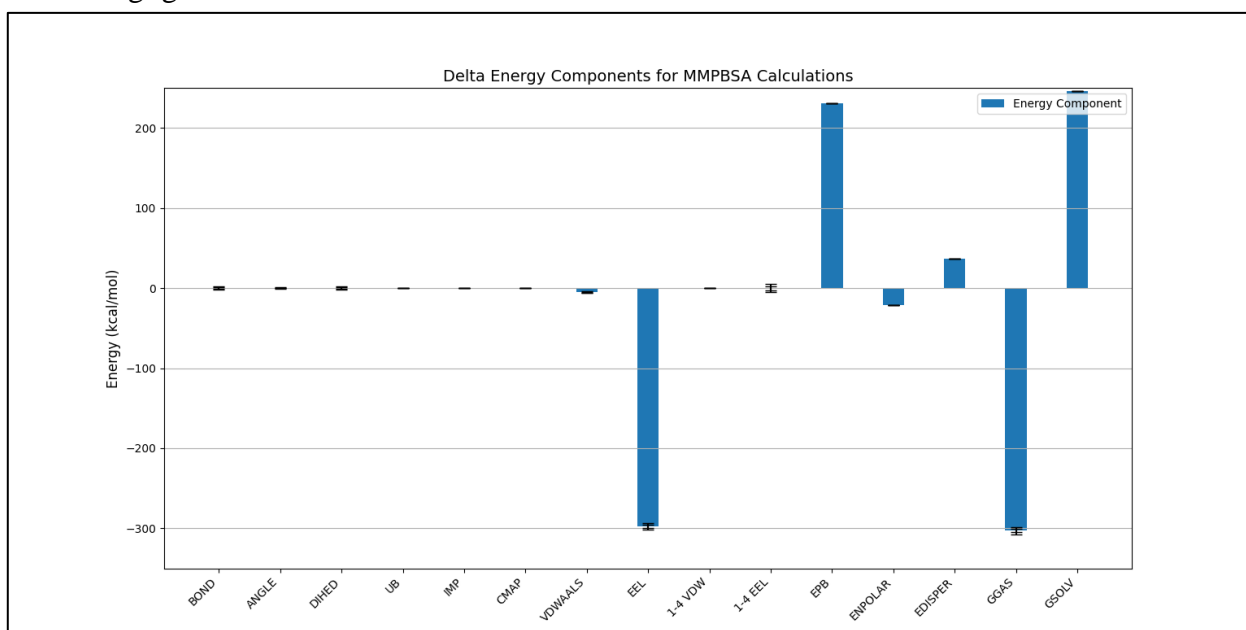


Figure III. 11. Delta energy components for MMPBSA calculations for the complex (NA_44428312), receptor (NA) and ligand (CID 44428312).

3.8.2 Analysis of NA_70139197

The results of the MMPBSA analysis revealed that the total binding free energy of the protein-ligand complex was -12.2 kcal/mol. This value was calculated by summing up the average energy values of all the energy components of the system, which were obtained from the MMPBSA Delta calculation (**Figure III. 12**). Among the energy components, VDWAALS and EEL contributed the most to the total binding free energy, with average energy values of -15.24 kcal/mol and -201.1 kcal/mol, respectively.

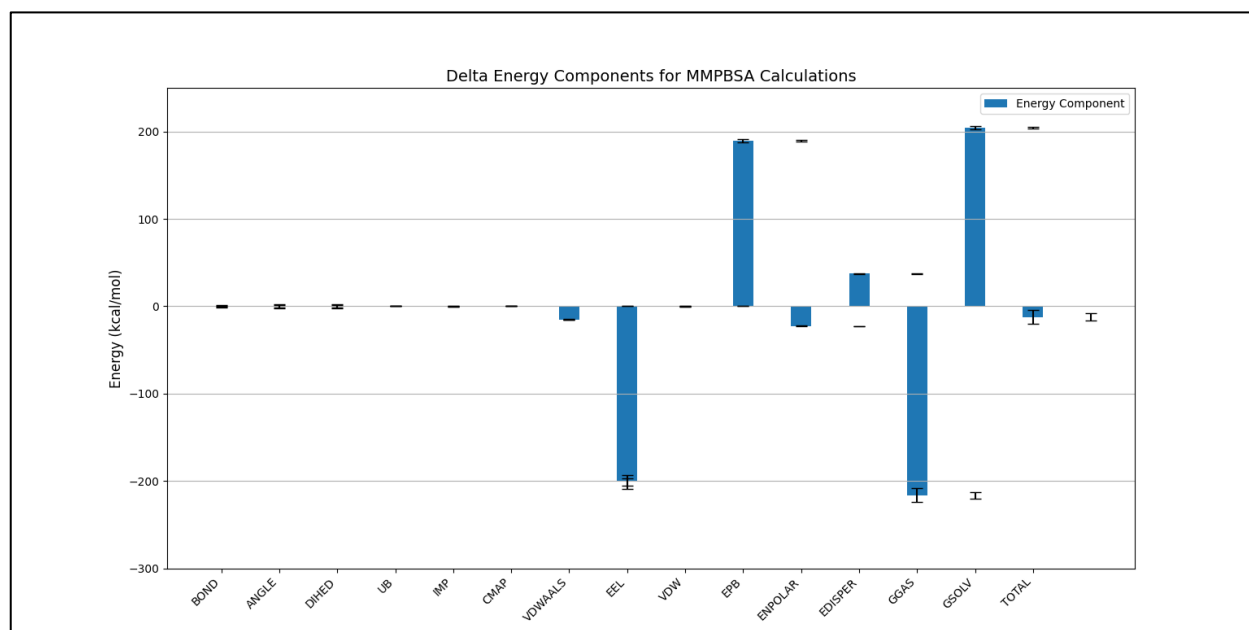


Figure III. 12. Delta energy components for MMPBSA calculations for the complex (NA_70139197), receptor (NA) and ligand (CID 70139197).

The energy components EPB and GSOLV also made significant contributions to the total binding free energy, with average energy values of 189.27 kcal/mol and 204.13 kcal/mol, respectively. On the other hand, the energy components BOND, ANGLE, and DIHED showed negligible contributions to the total binding free energy, with average energy values of 0 kcal/mol for all three components.

The standard deviation of the energy values showed relatively low variability among the energy components, with the exception of EEL, GGAS, and VDWAALS, which had standard deviations of 15.55 kcal/mol, 14.08 kcal/mol, and 1.6 kcal/mol, respectively. The standard error of the mean (SEM) of the energy values was also calculated and showed that the SEM for most energy components was relatively low. However, the SEM values for EEL, GGAS, and VDWAALS were comparatively high, indicating a relatively higher level of uncertainty in these energy components.

In conclusion, the MMPBSA analysis provided insight into the contribution of various energy components to the total binding free energy of the protein-ligand complex. The results suggest that VDWAALS, EEL, EPB, and GSOLV are the key energy components that contribute significantly to the binding of the ligand to the protein. These findings can potentially be used to guide further optimization of ligand binding affinity and drug design.

4. Conclusion

The pharmacophore model (ADDPR 4) for Neuraminidase inhibitors was created in this paper, and then we built a 3D-QSAR model and estimated its predictive power. From the maps, we discussed the different chemical groups that increase the inhibitory activity of Neuraminidase. A virtual screening using the pharmacophore (ADDPR 4) was done to look for new molecules that inhibit Neuraminidase. The results obtained by the docking study demonstrated the significance of hydrogen bonds, hydrophobic, and electrostatic interactions. In addition, the interaction with the Glu279 amino acid of the active site is also highly significant for inhibitory activity. The ADME parameters of the five hits were comparable with those of known biologically active compounds. We also verified the safety of the five hits molecules. Finally, the stability of the best two compounds with Neuraminidase was verified by MD and MM-PBSA calculations and shown to be highly stable complexes throughout the entire simulation time. In conclusion, the hits acquired via virtual database screening have offered new vital points for developing novel Neuraminidase inhibitors.

5. Reference

- [1] Muchtaridi, M., Nuwarda, R. F., Ikram, E. H. K., Abdul Rahim, A. S., Gazzali, A. M., & Wahab, H. A. (2022). Neuraminidase inhibitor of *Garcinia atroviridis* L. fruits and leaves using partial purification and molecular characterization. *Molecules*, 27(3), 949.
- [2] Houser, K., & Subbarao, K. (2015). Influenza vaccines: challenges and solutions. *Cell host & microbe*, 17(3), 295-300.
- [3] Gamblin, S. J., & Skehel, J. J. (2010). Influenza hemagglutinin and neuraminidase membrane glycoproteins. *Journal of biological chemistry*, 285(37), 28403-28409.
- [4] Wagner, R., Matrosovich, M., & Klenk, H. D. (2002). Functional balance between haemagglutinin and neuraminidase in influenza virus infections. *Reviews in medical virology*, 12(3), 159-166.
- [5] Macalino, S. J. Y., Gosu, V., Hong, S., & Choi, S. (2015). Role of computer-aided drug design in modern drug discovery. *Archives of pharmacal research*, 38, 1686-1701.
- [6] Cheng, T., Li, Q., Zhou, Z., Wang, Y., & Bryant, S. H. (2012). Structure-based virtual screening for drug discovery: a problem-centric review. *The AAPS journal*, 14, 133-141.
- [7] Raju, B., Verma, H., Narendra, G., Sapra, B., & Silakari, O. (2022). Multiple machine learning, molecular docking, and ADMET screening approach for identification of selective inhibitors of CYP1B1. *Journal of Biomolecular Structure and Dynamics*, 40(17), 7975-7990.
- [8] Zhang, J., Shan, Y., Pan, X., Wang, C., Xu, W., & He, L. (2011). Molecular docking, 3D-QSAR Studies, and in silico ADME prediction of p-aminosalicylic acid derivatives as neuraminidase inhibitors. *Chemical Biology & Drug Design*, 78(4), 709-717.
- [9] Badhani, B., & Kakkar, R. (2017). In silico studies on potential MCF-7 inhibitors: a combination of pharmacophore and 3D-QSAR modeling, virtual screening, molecular docking, and pharmacokinetic analysis. *Journal of Biomolecular Structure and Dynamics*, 35(9), 1950-1967.
- [10] Pattar, S. V., Adhoni, S. A., Kamanavalli, C. M., & Kumbar, S. S. (2020). In silico molecular docking studies and MM/GBSA analysis of coumarin-carbonodithioate hybrid derivatives divulge the anticancer potential against breast cancer. *Beni-Suef University journal of basic and applied sciences*, 9(1), 1-10.

- [11] Gubareva, L. V., Sleeman, K., Guo, Z., Yang, H., Hodges, E., Davis, C. T., ... & Stevens, J. (2017). Drug susceptibility evaluation of an influenza A (H7N9) virus by analyzing recombinant neuraminidase proteins. *The Journal of infectious diseases*, 216(suppl_4), S566-S574.
- [12] Rohini, K., Roy, R., Ramanathan, K., & Shanthi, V. (2019). E-pharmacophore hypothesis strategy to discover potent inhibitor for influenza treatment. *Journal of Theoretical and Computational Chemistry*, 18(04), 1950021.
- [13] Giordano, D., Biancaniello, C., Argenio, M. A., & Facchiano, A. (2022). Drug design by pharmacophore and virtual screening approach. *Pharmaceuticals*, 15(5), 646.
- [14] Mishra, A., Jha, V., & Rajak, H. (2022). Molecular structural investigations of quinoxaline derivatives through 3D-QSAR, molecular docking, ADME prediction and pharmacophore modeling studies for the search of novel antimalarial agent. *Journal of the Indian Chemical Society*, 99(2), 100343.
- [15] Sharma, V., Kumar, H., & Wakode, S. (2016). Pharmacophore generation and atom based 3D-QSAR of quinoline derivatives as selective phosphodiesterase 4B inhibitors. *RSC advances*, 6(79), 75805-75819.
- [16] Yang, J., Hu, J., Zhang, G., Qin, L., Wen, H., & Tang, Y. (2021). Pharmacophore modeling and 3D-QSAR study for the design of novel α -synuclein aggregation inhibitors. *Journal of Molecular Modeling*, 27(9), 260.
- [17] Bhole, R. P., Bonde, C. G., Bonde, S. C., Chikhale, R. V., & Wavhale, R. D. (2021). Pharmacophore model and atom-based 3D quantitative structure activity relationship (QSAR) of human immunodeficiency virus-1 (HIV-1) capsid assembly inhibitors. *Journal of Biomolecular Structure and Dynamics*, 39(2), 718-727.
- [18] Veerasamy, R., Rajak, H., Jain, A., Sivadasan, S., Varghese, C. P., & Agrawal, R. K. (2011). Validation of QSAR models-strategies and importance. *Int. J. Drug Des. Discov*, 3, 511-519.
- [19] Gubareva, L. V., Sleeman, K., Guo, Z., Yang, H., Hodges, E., Davis, C. T., ... & Stevens, J. (2017). Drug susceptibility evaluation of an influenza A (H7N9) virus by analyzing recombinant neuraminidase proteins. *The Journal of infectious diseases*, 216(suppl_4), S566-S574.
- [20] Sakkiah, S., Thangapandian, S., & Lee, K. W. (2012). Pharmacophore modeling, molecular docking, and molecular dynamics simulation approaches for identifying new lead compounds for inhibiting aldose reductase 2. *Journal of molecular modeling*, 18, 3267-3282.

- [21] Xu, L., Zhao, L., Che, J., Zhang, Q., Cao, R., & Li, X. (2021). Identification of novel influenza polymerase PB2 inhibitors using virtual screening approach and molecular dynamics simulation analysis of active compounds. *Bioorganic & Medicinal Chemistry*, 52, 116515.
- [22] Daina, A., Michielin, O., & Zoete, V. (2017). SwissADME: a free web tool to evaluate pharmacokinetics, drug-likeness and medicinal chemistry friendliness of small molecules. *Scientific reports*, 7(1), 42717.
- [23] Banerjee, P., Eckert, A. O., Schrey, A. K., & Preissner, R. (2018). ProTox-II: a webserver for the prediction of toxicity of chemicals. *Nucleic acids research*, 46(W1), W257-W263.
- [24] Raies, A. B., & Bajic, V. B. (2016). In silico toxicology: computational methods for the prediction of chemical toxicity. *Wiley Interdisciplinary Reviews: Computational Molecular Science*, 6(2), 147-172.
- [25] Van Der Spoel, D., Lindahl, E., Hess, B., Groenhof, G., Mark, A. E., & Berendsen, H. J. (2005). GROMACS: fast, flexible, and free. *Journal of computational chemistry*, 26(16), 1701-1718.
- [26] Halimi, M., & Bararpour, P. (2022). Natural inhibitors of SARS-CoV-2 main protease: structure based pharmacophore modeling, molecular docking and molecular dynamic simulation studies. *Journal of Molecular Modeling*, 28(9), 279.
- [27] Giordano, D., Biancaniello, C., Argenio, M. A., & Facchiano, A. (2022). Drug design by pharmacophore and virtual screening approach. *Pharmaceuticals*, 15(5), 646.
- [28] Wang, B., Wang, K., Meng, P., Hu, Y., Yang, F., Liu, K., ... & Tian, Y. (2018). Design, synthesis, and evaluation of carboxyl-modified oseltamivir derivatives with improved lipophilicity as neuraminidase inhibitors. *Bioorganic & Medicinal Chemistry Letters*, 28(21), 3477-3482.

***Chapter IV: Discovery of Novel Potent Drugs for Influenza by
Inhibiting the Vital Function of Neuraminidase via Fragment-
Based Drug Design (FBDD) and Molecular Dynamics
Simulation Strategies***

1. Introduction

The rapid development of influenza viruses is their most notable feature. Over 500,000 people are expected to perish annually from this influenza epidemics worldwide [1]. Influenza viruses are distinct from other viruses, In terms of immunological variability, seasonality, and effects on the general population. All age groups can experience explosive acute respiratory illness outbreaks, and many people die as a result, especially the elderly and chronically ill [2]. While vaccination is the major way for influenza prevention, there are a number of potential situations in which vaccine is ineffective, and effective antiviral medications are critical [3].

Neuraminidase inhibitors are medications that block the activity of the viral Neuraminidase (NA) protein. The greatest strategy to control and prevent the infection has been to block sialic acid receptors and limit virus-host cell connections. This limits the migration of viruses and the infection of new host cells [4]. Neuraminidase inhibitors have a limited bioavailability and are given by inhalation, which might create complications in people with respiratory illness [5].

Structure activity relationship (SAR) elucidates that ethyl ester prodrug in *Oseltamivir* improves bioavailability. In addition, the presence of the guanidino group in both *Zanamivir* and *Peramivir* analogs enhances the ionic interactions with Neuraminidase enzyme compared to the single amine moiety. On the other hand, phosphonic acid assists as suitable acid bond bioisosteres for the carboxylic acid group with improved selectivity, potency, and bioavailability. A comprehensive summary of the SAR is presented in **Figure IV. 1**.

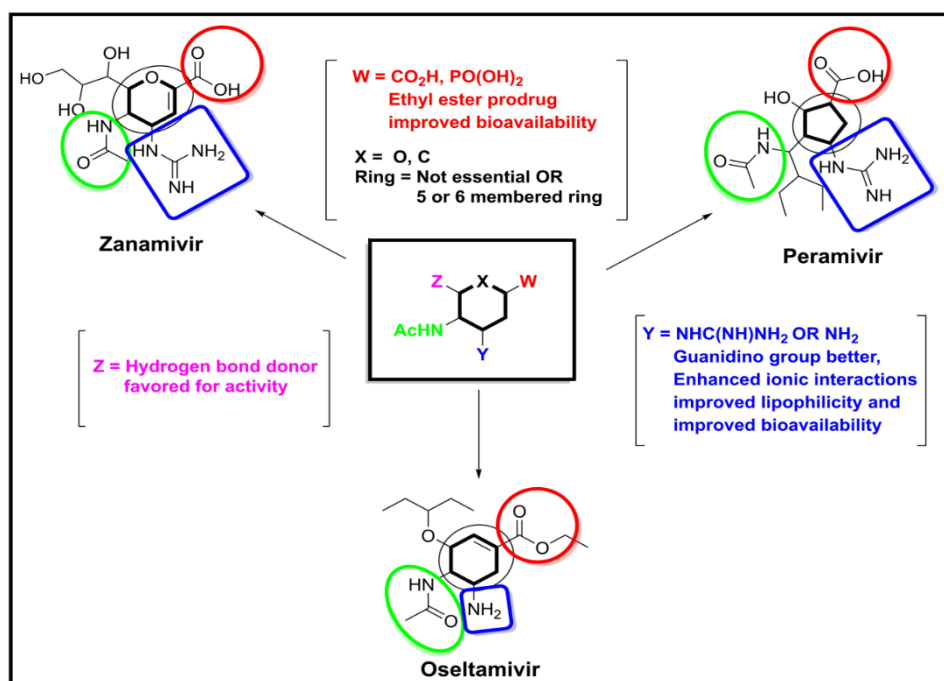


Figure IV. 1. SAR of Zanamivir, Peramivir and Oseltamivir drugs.

Fragment-based drug design (FBDD) is a strategy for creating active molecules from fragments. FBDD frequently creates a molecule from a chemical fragment with a low binding affinity to the target, low chemical structural complexity, and low molecular weight (less than 300 Da) [6]. These benefits have motivated researchers to use this strategy to produce inhibitors for many various types of targets. In addition, with increasing numbers of compounds created using FBDD entering various phases of clinical testing, this approach has gained widespread acceptance in drug discovery [7].

In the present investigation, we used *in silico* methodologies including fragment-based drug design, molecular docking, ADMET, MD simulation, and MM-PBSA calculations to identify effective and potential Neuraminidase inhibitors that could potentially be used to treat influenza infection. A computational study revealed ten compounds that successfully bind to Neuraminidase.

2. Computational Methods

2.1. Protein and fragments preparation

Firstly, the Protein Data Bank was accessed to acquire the crystal structure of Neuraminidase with *Zanamivir*, which has a resolution of 2.40 Å (PDB ID: 5L17) [8]. The Protein Preparation Wizard panel tool of the Schrödinger software suite (Maestro, v 11.8), was executed to prepare the protein structure [9]. Using the OPLS3e force field, the geometry has been optimized and reduced. At pH of 7.0, partial atomic charges were assigned and potential ionization states were created. The structure was then refined via constrained minimization, so that the atom junction had an RMSD default value of 0.3 Å [10]. The obtained structure was subsequently utilized to produce a receptor grid. In the next phase, the *ZINC 20* database was employed to extract 29,791-fragment structures (<https://zinc20.docking.org/tranches/home/>). Furthermore, all saved fragments have a molecular weight of 200 Daltons and a partition coefficient (LogP) within -1 and 1. The LigPrep module of Schrödinger suite v 11.8 optimizes the 3D structures of fragments [11]. Following this step, each fragment can be examined with the Neuraminidase receptor via molecular docking investigation.

2.2. Fragment linking and molecular docking studies

In the last decade, fragment-based drug discovery (FBDD) has emerged as an effective tool for identifying therapeutic leads. The method discovers small molecules that are approximately half the size of traditional medications [12]. SP-docking was applied to dock all 29,791 fragments into the prepared active site of Neuraminidase, whereas all fragments with good docking scores were chosen for fragment linking. **Figure IV. 2** illustrates the fragment-based drug design (FBDD) strategy used in the present study.

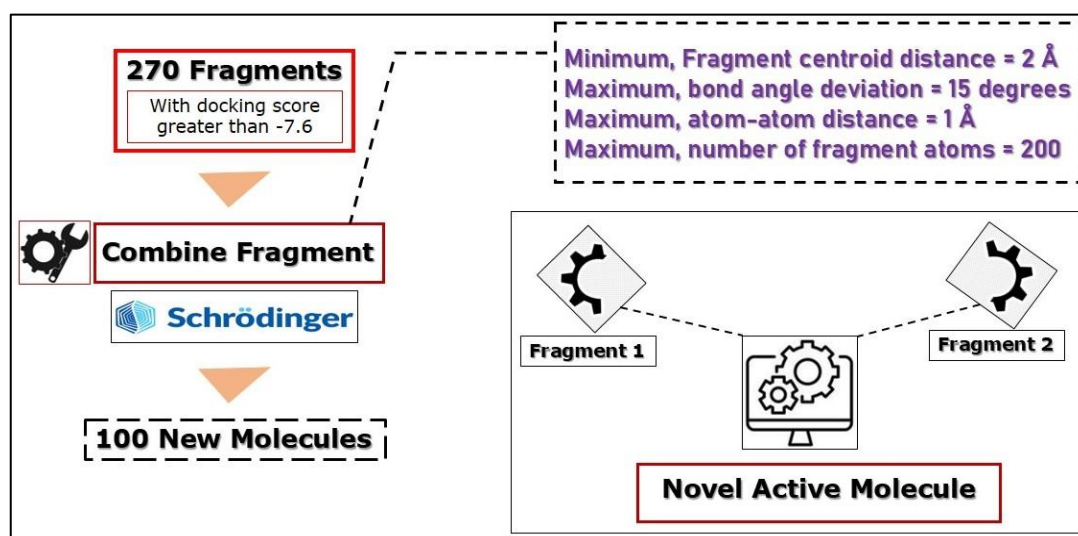


Figure IV. 2. Fragment-based drug design (FBDD) strategy.

The "combine fragments" tool from the Schrodinger module was employed for creating novel molecules by combining the fragments. The combine fragment tool generally combines fragments by identifying the possible connections that could be constructed between them [13]. During direct joining, the minimum bond angle variation was set to 15 degrees, the maximum atom-atom distance between fragments was kept at 1, the minimum fragment centroid distance was kept at 2 Å and the maximum number of fragment atoms was set to 200. In addition, the tool's default parameters were executed, with the maximum output of the newly generated structures being 100. The newly formed molecules, with *Zanamivir* and two neuraminidase clinical inhibitors (*Peramivir* and *Oseltamivir*) were docked within the active site of neuraminidase via the extra precision (XP-docking) function of Maestro's Glide module. The Discovery Studio Visualizer was used to depict the interactions established between the novel compounds and the active sites of Neuraminidase [14].

2.3 ADMET prediction

The objective of this phase was to look at the possibilities afforded by computer-assisted modeling for predicting absorption, distribution, metabolism and elimination of novel molecules. The most important goal of *in silico* ADME estimation is to accurately forecast the *in vivo* pharmacokinetics of a putative therapeutic molecule in man when it exists only as a virtual form [15]. ADME characteristics of each new compound, with a particular focus on solubility and absorbability, were estimated using SwissADME [16]. The ProToxII platform was adopted to evaluate the toxicity of the novel molecules, which estimates the hepatotoxicity, immunotoxicity, carcinogenicity, mutagenicity, cytotoxicity and LD₅₀ values [17]. VEGA-QSAR v 1.2.3 was also used to predict total body elimination half-life and Plasma Protein Binding and other important parameters [18].

2.4 Molecular dynamic simulation

The strategy described in this paper include the specific processes required to conduct molecular dynamics simulations of the top four compounds with Neuraminidase receptor. These four novel compounds were chosen due their exceptionally high binding affinities with active site of Neuraminidase. The Gromacs-2023 was used to run molecular dynamics simulations for 100 ns on Ubuntu operating system (v 24.04). The SwissParam server was implemented to construct the ligand topology files, and the protein topology file was prepared using the CHARMM27 all-atom force field [19, 20]. Each system was then solvated by TIP3P water model and Na⁺ and Cl⁻ ions were added to neutralize the charge. The solvated system was subsequently employed to minimize energy using the steepest descent minimization algorithm until the maximal force was

less than 10.0 kJ/mol. Over the NVT equilibration process, the system was coupled using a v-rescale algorithm at 300 K for 100 ps with a coupling value of 0.1 ps [21]. The NPT was then equilibrated via a Berenson pressure-coupling tool for 100 ps and a coupling constant of 2.0 ps, following the equilibration phases, the production MD simulation with the CHARMM27 force field was run for 100 ns [22].

To understand more about of the formed complexes with Neuraminidase receptor such as the stability, compactness, flexibility and binding affinity, the MD simulation details were analyzed. The RMSD was measured during the simulation to assess the structural stability of the protein-ligand complexes, and RMSF is used to evaluate the flexibility of the protein residues. The R_g was calculated to evaluate the protein-ligand complexes compactness. During 100 ns of simulation, hydrogen bond analysis was executed to look for the hydrogen bonding established between the protein and ligand. In addition, solvent accessible surface area (SASA) were calculated to assess the stability of Neuraminidase and their four complexes. Finally, The Grace software have been utilized for examining the simulation trajectories [23].

2.5 MM-PBSA Calculations

In the current study, we examined the binding energy of the four new compounds and *Zanamivir* within Neuraminidase receptor. The binding free energy (ΔG_{bind}) analysis was performed using the molecular mechanics Poisson-Boltzmann surface area (MM- PBSA) approach included in the gmx_mmpbsa package [24]. The binding-free energy must have been calculated as follows: [25]

$$\Delta G_{\text{bind}} = G_{\text{complex}} - (G_{\text{protein}} + G_{\text{ligand}})$$

Where ΔG_{bind} is the total binding energy of the complex, G_{complex} is the binding energy of native protein, and G_{ligand} is the binding energy of ligand.

2.6 Reaction Based Enumeration

Another Schrödinger process is reaction-based enumeration, which use a retro-synthesis approach to determine the synthetic route of any chemical compounds [26]. The reaction-based enumeration phase requires each of the best four designed Neuraminidase inhibitors as inputs. This generative phase analyzes the input molecules retro-synthetically, followed by combinatorial synthesis of the ensuing reaction pathways [27]. In addition, all routes for each input designed molecule are enumerated using commercially reactant.

3. Results and Discussion

3.1. Fragment-based drug design and molecular docking

In order to generate novel Neuraminidase inhibitors that combine the physicochemical features of various fragments obtained from the ZINC 20 library, fragment-based drug design (FBDD) approach was adopted. Following the preparation of 29,791 fragments via the LigPrep module, the Glide standard precision algorithm (SP-docking) was utilized to dock them within active site of Neuraminidase. Immediately following the SP-docking process, the best 270 fragments attended docking scores greater than -7.6 kcal/mol. In the next phase, these top fragments are joined employing Schrödinger's "combine fragments panel" to generate 100 new compounds. The molecule hits and *Zanamivir*, and two other clinical Neuraminidase inhibitors (*Peramivir* and *Oseltamivir*), were prepared using the LigPrep module with the identical settings to evaluate their inhibitory power via extra precision algorithm (XP-docking) of Glide. **Figure IV. 3** shows the chemical structures of the 10 best-discovered molecules via fragment-based drug design (FBDD) methodology with constituent fragments.

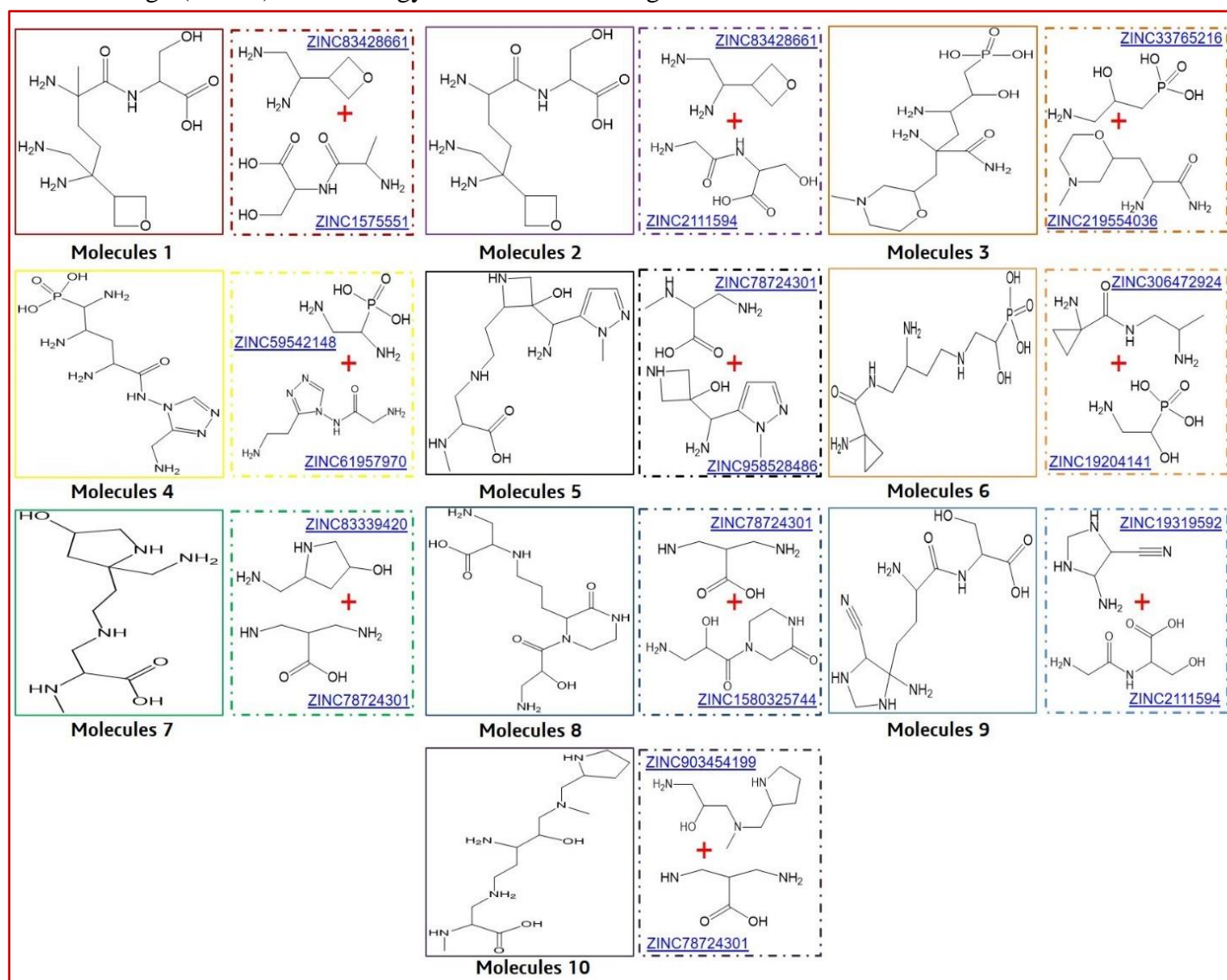


Figure IV. 3. Chemical compositions of the top 10 compounds identified through the fragment-based drug design process and their constituent fragments.

Figure IV. 4 briefly compares the SAR of the best five hybrids with the *Zanamivir* drug and highlights the crucial functional group in the drug-target interactions. Removing or displacing the hydroxyl group in compounds 4 and 5 would diminish the affinity. In addition, compounds 4 and 5 disclosed lower affinity after replacing the amine side chains with triazole and pyrazole, respectively.

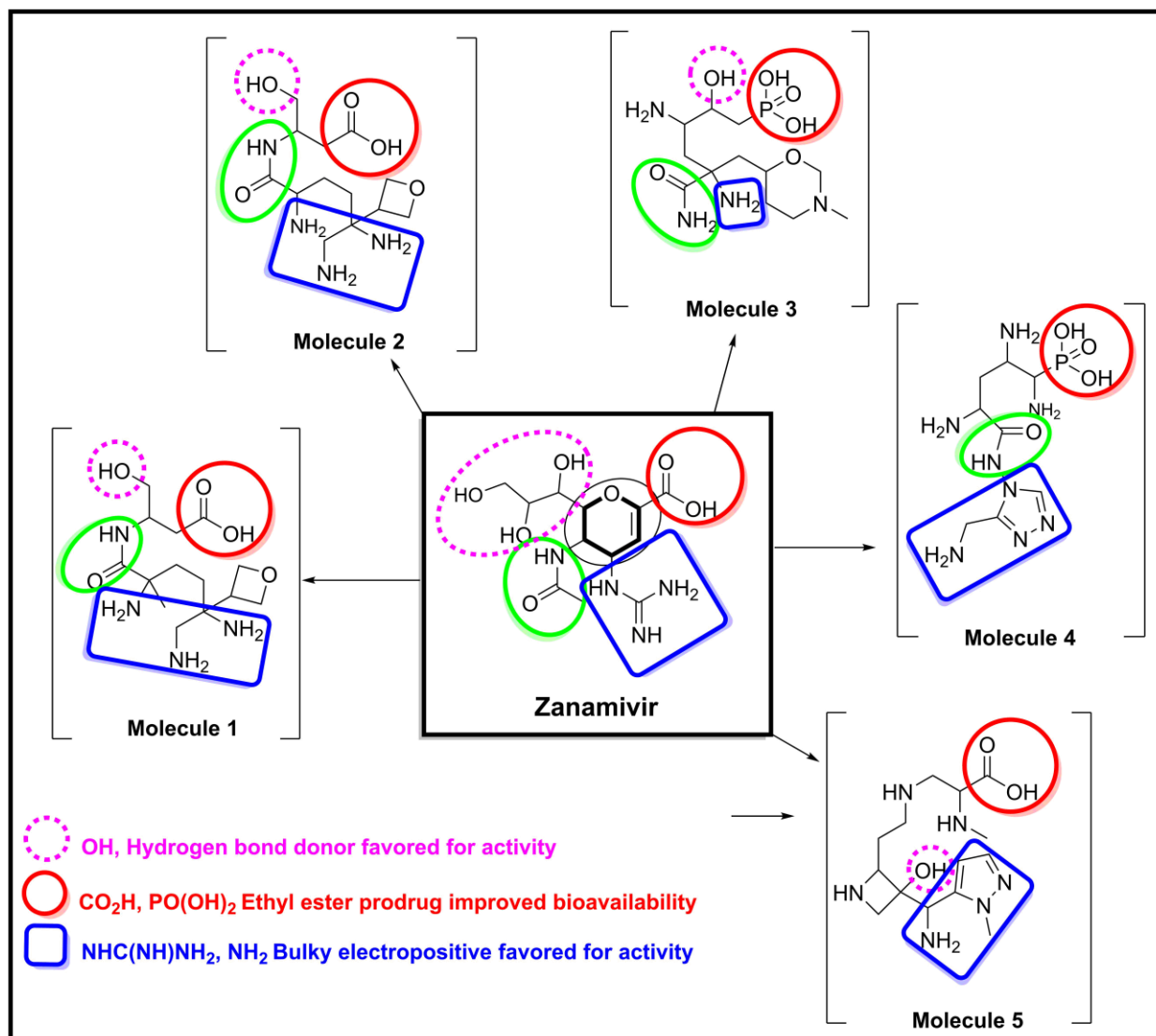


Figure IV. 4. Summary of structure-activity relationships of the best five hit inhibitors.

Peramivir and *Oseltamivir* are currently assess as a combined therapy for severe influenza virus infections in people [28]. The discovered 10 molecules reflect higher docking scores (between -14.626 and -13.813 Kcal/mol) than *Zanamivir*, *Peramivir*, and *Oseltamivir* (-9.848, -8.848, and -6.326 Kcal/mol, respectively). The amino acids Arg119, Glu120, Asp152, Glu278, Arg294, Arg372, and Tyr406 compose the active site of Neuraminidase [29]. The first information acquired by docking investigation, demonstrates that the 10 new compounds have interacted with the active site of Neuraminidase. Furthermore, nine hydrogen bonds are formed by the best molecule (Molecule 01) with the amino acids Arg119, Glu120, Asp152, Trp180, Glu229, Glu278,

Glu279, Arg294 and Arg372 over a distance of 1.54 to 3.03 Å, Which specifies the important role of the hydrogen bond interaction for the inhibitory activity of vital function of Neuraminidase. The second molecule (Molecules 02), established ten hydrogen bond with the amino acids Arg119, Glu120, Asp152, Arg153, Trp180, Glu229, Glu278, Glu279, Arg294 and Arg372 at a distance between 1.59 and 2.99 Å. With two additional amino acids Ans296 and Tyr406, the third molecule (Molecule 03) interacts via the same mode as the second molecule.

The fourth molecule (Molecule 04) specifically interacts with the Neuraminidase receptor by forming eleven hydrogen bonds with the amino acids Arg119, Glu120, Asp152, Arg153, Trp180, Glu229, Glu278, Glu279, Arg294, Arg372, and Tyr406, and by interacting hydrophobically with Arg153 and Arg226 at a distance among 1.58 and 5.02 Å. The rest-generated compounds have the same interactions with the active site of Neuraminidase as the top four molecules. The results of the molecular interactions are summarized in **Table IV. 1**. Our findings on the molecular interactions formed by the ten designed molecules and Neuraminidase receptor are agree with results reported by *Gracy Fathima* and colleagues [31].

Finally, the 10 designed molecules form highly stable complexes with the active site of Neuraminidase compared to *Zanamivir* and the clinical inhibitors (*Peramivir* and *Oseltamivir*). These optimistic findings are beneficial to researchers working on developing new and potent anti-influenza medications. **Figure IV. 5** illustrates the interactions of the ten designed compounds and *Zanamivir* within Neuraminidase receptor. All newly designed compounds were selected for ADMET and molecular dynamics simulation examinations.

Table IV. 1. Docking results of the designed inhibitors and reference ligands.

Molecule	XP Score (Kj/mol)	H-bond	Distance	Hydrophobic	Distance
Molecule 01	-14.626	Arg119, Glu120, Asp152, Trp180, Glu229, Glu278, Glu279, Arg294, Arg372	[1.54 - 3.03]	-	-
Molecule 02	-14.617	Arg119, Glu120, Asp152, Arg153, Trp180, Glu229, Glu278, Glu279, Arg294, Arg372	[1.59 - 2.99]	-	-
Molecule 03	-14.514	Arg119, Glu120, Asp152, Arg153, Trp180, Glu229, Glu278, Glu279, Arg294, Asn296, Arg372, Tyr406	[1.61 - 3.07]	-	-
Molecule 04	-14.341	Arg119, Glu120, Asp152, Arg153, Trp180, Glu229, Glu278, Glu279, Arg294, Arg372, Tyr406	[1.58 - 2.87]	Arg153, Arg226	[2.04 ; 5.02]
Molecule 05	-14.112	Arg119, Glu120, Asp152, Trp180, Glu229, Glu278, Glu279, Arg294, Arg372, Tyr406	[1.66 - 2.87]	-	-
Molecule 06	-13.890	Arg119, Asp152, Trp180, Glu229, Glu278, Glu279, Arg294, Arg372, Tyr406	[1.63 - 1.97]	Arg153	[5.34]
Molecule 07	-13.890	Arg119, Glu120, Asp152, Trp180, Glu229, Glu278, Glu279, Arg294, Arg372, Tyr406	[1.66 - 2.56]	-	-
Molecule 08	-13.865	Arg119, Glu120, Asp152, Arg153, Trp180, Glu229, Glu278, Arg294, Arg372, Tyr406	[1.54 - 2.82]	Arg226	[5.73]
Molecule 09	-13.861	Arg119, Glu120, Asp152, Arg153, Trp180, Glu229, Glu278, Glu279, Arg294, Arg372	[1.54 - 2.82]	-	-
Molecule 10	-13.813	Arg119, Glu120, Asp152, Trp180, Glu229, Glu278, Glu279, Arg294, Arg372, Tyr406	[1.62 - 2.83]	Ala248	[4.10]
<i>Zanamivir</i>	-9.848	Arg119, Asp152, Arg153, Trp180, Glu229, Glu278, Arg294, Arg372,	[1.72 - 2.77]	-	-
<i>Peramivir</i>	-8.848	Arg119, Asp152, Arg153, Trp180, Glu229, Glu279, Arg294, Arg372,	[1.14 - 2.71]	Ile224	[4.39]
<i>Oseltamivir</i>	-6.326	Asp152, Glu278, Glu279, Arg294, Arg372,	[1.79 - 3.17]	-	-

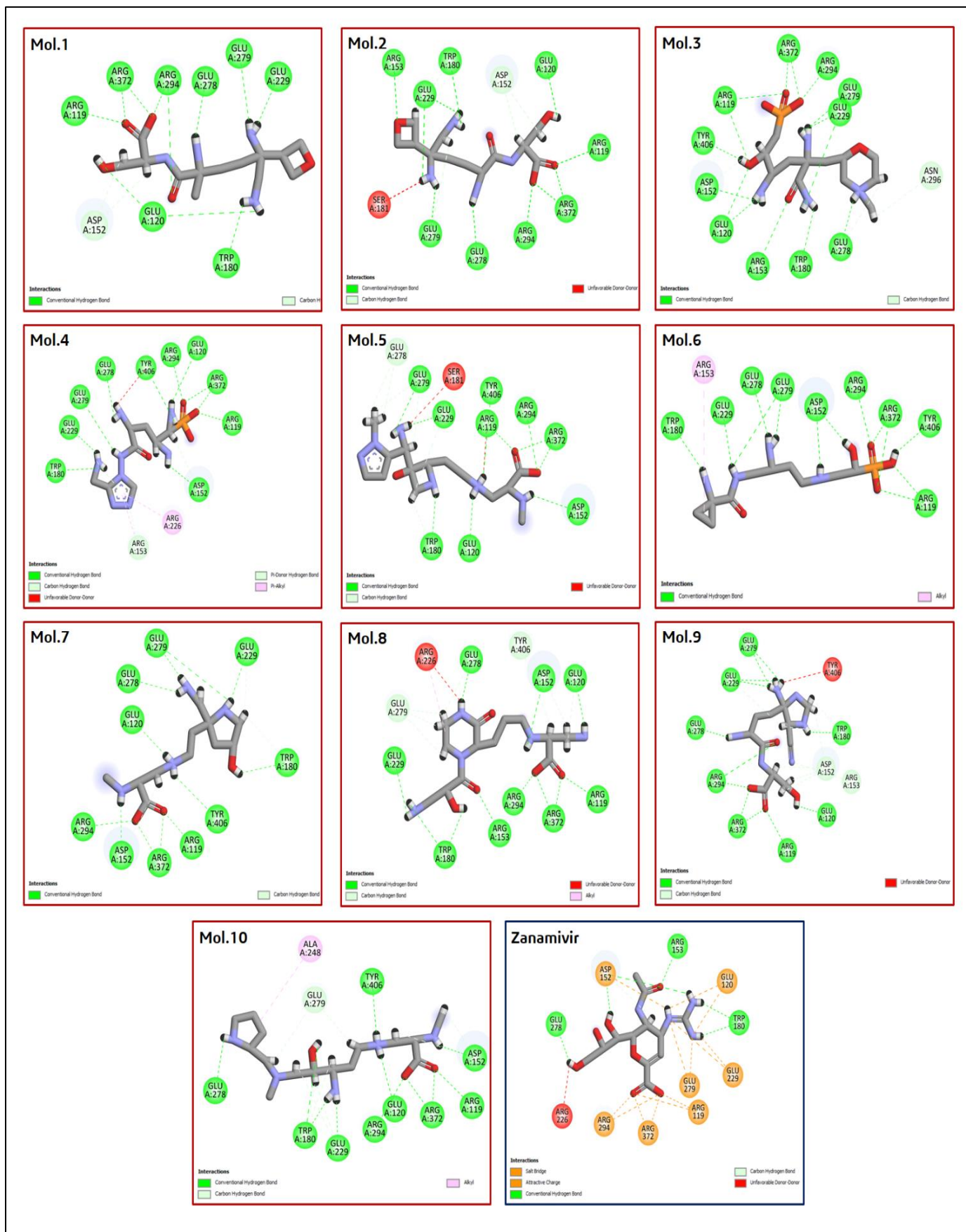


Figure IV. 5. 2D diagram of the designed inhibitors and Zanamivir within Neuraminidase receptor.

3.2. ADMET and bioavailability

The solubility and permeability to biological membranes comprises two of the most essential pharmacokinetic characteristics. For each designed compounds, we calculated the partition coefficient (LogP) and aqueous solubility (LogS). According to the SwissADME details, the hit molecules had LogP values ranging from -4.22 to -1.66, showing the ability of these 10 molecules to permeate the biological membranes (good distribution). In terms of the solubility in water (LogS), the designed compounds are extremely soluble in aqueous milieu, and aiding gastrointestinal absorption (good absorption), with LogS values ranging from 1.58 to 3.42. However, due to this solubility, renal elimination will be simple and quick (elimination efficacy). **Table IV. 2**, combines the pharmacokinetic features computed employing the SwissADME website. The generated compounds had the same bioavailability score (0.55), confirming the favorable pharmacokinetic profiles (good absorption and distribution). The ten compounds permeated the skin, having Logkp values ranging from -13.80 to -11.37 cm/s, indicating tissue affinity for the molecules developed. In addition, with the exception of molecule 4, the molecule hits follow Lipinski's rule. Furthermore, none of the proposed compounds inhibits the activity of liver enzymes (Cytochromes P450). Finally, in order to estimate the inhibitory activity of designed molecules in vitro and in vivo, their synthesis in a chemical laboratory will be very simple (synthetic accessibility values between 3.32 and 4.71).

Table IV. 2. ADME features of newly designed compounds and drug-like characteristics.

Molecule	MW (g/mol)	LogP	LogS (ESOL)	Bioavailability Score	CYP450 inhibitors	LogKp cm/s	Synthetic accessibility	Lipinski
Molecule 01	318.37	-2.30	2.55	0.55	No	-12.42	3.51	Yes
Molecule 02	304.34	-2.60	2.76	0.55	No	-12.47	3.40	Yes
Molecule 03	354.34	-3.28	2.95	0.55	No	-13.48	4.71	Yes
Molecule 04	322.26	-4.22	3.42	0.55	No	-13.80	4.48	No
Molecule 05	326.39	-2.49	1.96	0.55	No	-12.11	3.99	Yes
Molecule 06	310.29	-2.91	3.05	0.55	No	-12.88	3.91	Yes
Molecule 07	260.33	-2.25	2.16	0.55	No	-11.37	3.32	Yes
Molecule 08	331.37	-3.23	2.54	0.55	No	-12.57	3.48	Yes
Molecule 09	300.31	-3.16	2.31	0.55	No	-12.06	3.80	Yes
Molecule 10	331.45	-1.66	1.58	0.55	No	-11.35	3.91	Yes

The ProToxII results (**Table IV. 3**) reveal that all of the compounds generated are safe. The prediction of hepatotoxicity, carcinogenicity, Immunotoxicity, Mutagenicity and Cytotoxicity for the novel designed Neuraminidase inhibitors was inactive, indicating no toxicity for these molecules. The predicted LD₅₀ values vary from 300 to 3000 mg/kg, while the toxicity classes

ranging from 03 to 05. These findings supported the notion that the designed compounds can be promising new Neuraminidase inhibitors candidates.

Table IV. 3. Evaluation of safety profiles and Predicted LD₅₀ of newly designed molecules.

Molecule	Hepatotoxicity	Carcinogenicity	Immunotoxicity	Mutagenicity	Cytotoxicity	LD ₅₀ (mg/kg)	class
Molecule 01	Inactive	Inactive	Inactive	Inactive	Inactive	1800	04
Molecule 02	Inactive	Inactive	Inactive	Inactive	Inactive	1800	04
Molecule 03	Inactive	Inactive	Inactive	Inactive	Inactive	500	04
Molecule 04	Inactive	Inactive	Inactive	Inactive	Inactive	2700	05
Molecule 05	Inactive	Inactive	Inactive	Inactive	Inactive	300	03
Molecule 06	Inactive	Inactive	Inactive	Inactive	Inactive	3000	05
Molecule 07	Inactive	Inactive	Inactive	Inactive	Inactive	2000	04
Molecule 08	Inactive	Inactive	Inactive	Inactive	Inactive	2000	04
Molecule 09	Inactive	Inactive	Inactive	Inactive	Inactive	1500	04
Molecule 10	Inactive	Inactive	Inactive	Inactive	Inactive	2700	05

Using VEGA QSAR, we examined the Developmental Toxicity model, Skin Irritation, Plasma Protein Binding, Hepatic Steatosis, and Total Body Elimination Half-Life to properly assess probable the potential toxicity (**Table IV. 4**). All compounds had plasma protein binding values ranging from -1.288 to 0.401. Furthermore, none of the designed Neuraminidase inhibitors contributes to hepatic steatosis. In addition, because their total body elimination half-life ranges between 0.910 and 2.538 hours, renal elimination of these molecules will be very simple.

Table IV. 4. Evaluation of safety profiles of the designed Neuraminidase inhibitors using VEGA QSAR.

Molecule	Developmental Toxicity model	Skin Irritation	Plasma Protein Binding	Hepatic Steatosis	Total body elimination half-life (hour)
Molecule 01	Non-Toxicant	NON-Sensitizer	-0.9323	Inactive	1.436
Molecule 02	Non-Toxicant	NON-Sensitizer	-1.0059	Inactive	1.209
Molecule 03	Non-Toxicant	NON-Sensitizer	-0.9572	Inactive	2.261
Molecule 04	Non-Toxicant	NON-Sensitizer	-1.0477	Inactive	0.910
Molecule 05	Non-Toxicant	NON-Sensitizer	-1.0705	Inactive	2.538
Molecule 06	Non-Toxicant	NON-Sensitizer	-0.9082	Inactive	1.805
Molecule 07	Non-Toxicant	NON-Sensitizer	-1.288	Inactive	2.484
Molecule 08	Non-Toxicant	NON-Sensitizer	-1.195	Inactive	1.077
Molecule 09	Non-Toxicant	NON-Sensitizer	-1.0392	Inactive	1.100
Molecule 10	Non-Toxicant	NON-Sensitizer	0.401	Inactive	1.100

3.3 Molecular dynamic simulation (MDS)

At this phase, the top four designed Neuraminidase (NA) inhibitors (Molecule 01_04) and *Zanamivir* were selected for molecular dynamics simulation investigation. MD simulation is a crucial tool to examine the dynamic stability, and development of intermolecular interactions of docked protein-ligand complexes in the discipline of drug design via computational strategies (Sanjay et al., 2020). We ran the simulation for 100 ns in order to evaluate the stability of each system, by computing the root mean square deviation (RMSD), root mean square fluctuations (RMSF), radius of gyration (Rg), hydrogen bond (H-bond) formed between the designed molecules with Neuraminidase receptor, and solvent available surface area (SASA).

3.3.1 RMSD and RMSF analysis

The RMSD values of the generated molecules (Molecule 01–04) within the Neuraminidase receptor are an estimation of their stability. This metric indicates the change in atomic locations with respect to their original beginning positions, reflecting the magnitude of molecular configuration modifications during the simulation. The average RMSD values of NA_Molecules 01-04 complexes were determined and compared to NA_ *Zanamivir* complex, and were found to be between 0.116 and 0.254 nm, while the average RMSD of NA_ *Zanamivir* complex is equivalent to 0.174 nm. On the other hand, the average RMSD of Neuraminidase alone was 0.191 nm as shown in **Figure IV. 6**.

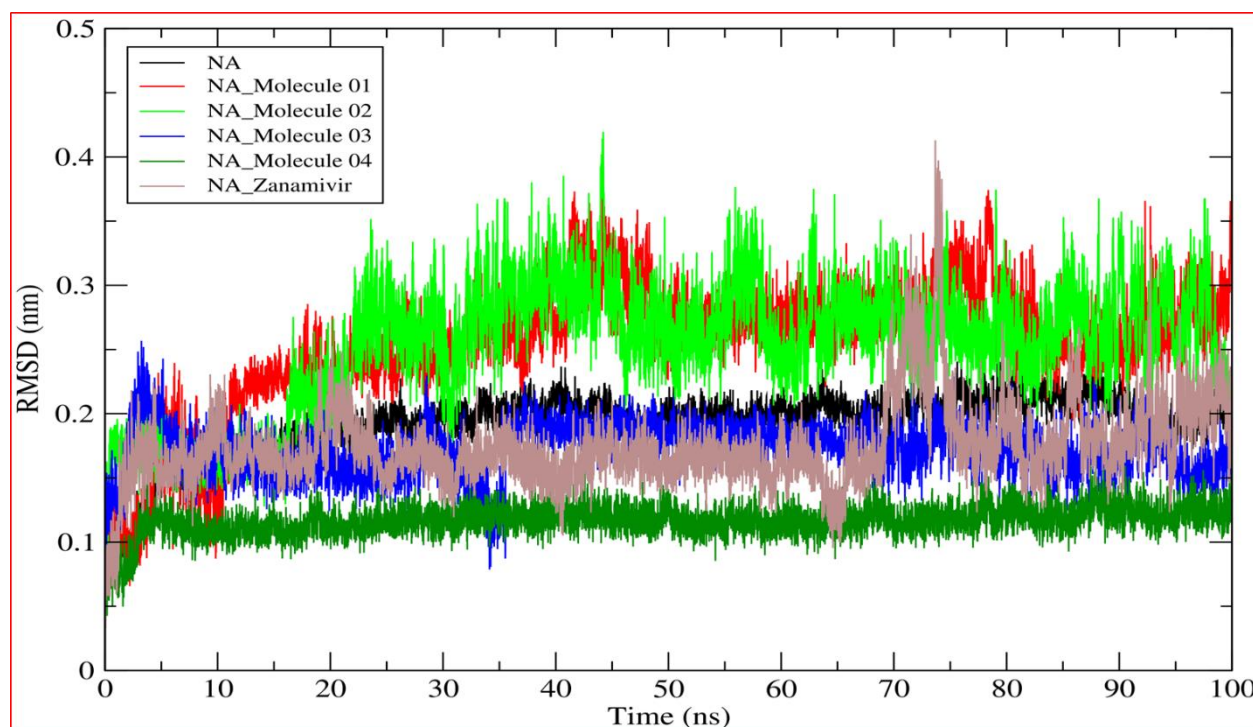


Figure IV. 6. The relative stability of the designed inhibitors with Neuraminidase receptor based on average root-mean-square deviation (RMSD).

The RMSD analysis revealed a small deviation in the NA_Molecule 01 complex that continually grew up to 15 ns, followed by a constant atomic movement until 38 ns, before significantly increasing up to 73 ns and stabilizing after 86 ns. Likewise, for the NA_Molecule 02 complex, a slight deviation is noticed between 0 ns and 30 ns and stays rather stable for the remainder of the simulation time (30 to 100 ns). The average RMSD for backbone atoms of NA_Molecule 03, NA_Molecule 04 complexes had been 0.172 and 0.116 nm, suggesting that the Molecules 03, 04 establish very stable complexes within Neuraminidase receptor during 100 ns of simulation, and they also reflect the aptitude of remaining identified molecules to cause minor conformational changes along the interactions with Neuraminidase receptor during 100 ns of simulation. This shows that the binding of molecules 03 and 04 to the active site of Neuraminidase generated specific modifications in the residues that define the binding site, suggesting relaxation in comparison to the initial X-ray structure utilized in simulations. In addition, the trajectory's visual examination supports the stability of each system. It's worth noting that the RMSD curves for all protein complexes were within the acceptable range. The results of this study provide light on the fundamental stability of Neuraminidase in the presence of the proposed inhibitors and could prove crucial in the generation of new inhibitors against influenza virus.

The root mean square fluctuation (RMSF) is a measure of the residual mobility of amino acids. If the amino acid residues have higher RMSF values, this signifies that the active site is unstable. However, a stable receptor is indicated by low RMSF values of amino acid residues [31]. The average RMSF values of Neuraminidase and its complexes was found to be less than 0.128 nm, demonstrating the small molecular mobility and structural stability. Moreover, they were able to form stable interactions with the Neuraminidase receptor. The overall average RMSF values of Neuraminidase amino acid residues has been calculated for Molecule 01-04 and *Zanamivir* and were 0.110, 0.110, 0.128, 0.102 and 0.136 nm respectively (**Figure IV. 7**).

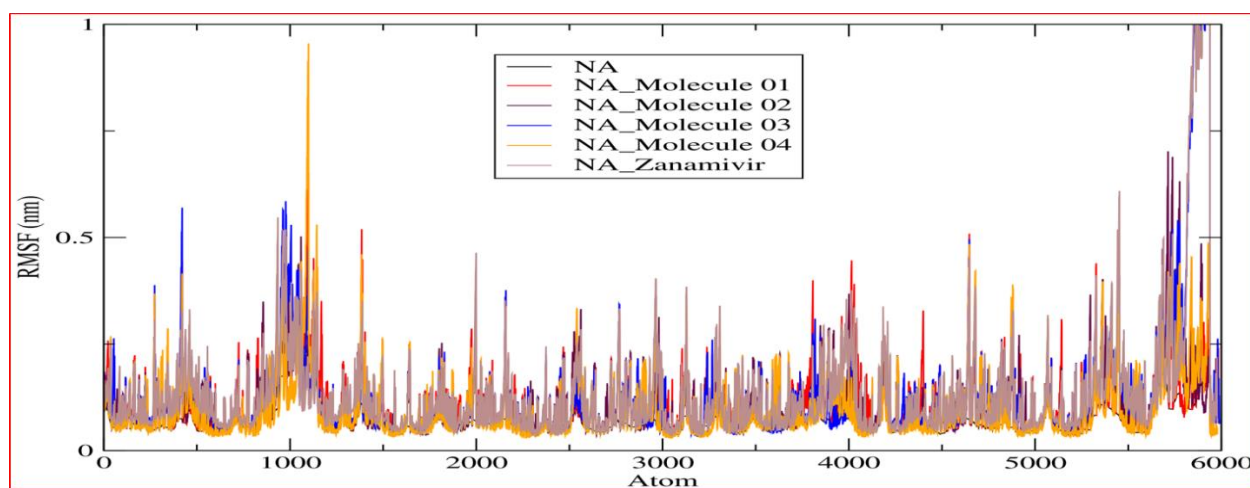


Figure IV. 7. The relative stability of the designed inhibitors with Neuraminidase receptor based on root-mean-square fluctuations (RMSFs).

Particularly, the NA_Molecule 01 and NA_Molecule 04 complexes attended higher fluctuation at atoms 1000 and 5890 of Neuraminidase protein, with an RMSF value of one nm. The RMSF values of each system, including NA, displayed some changes, which indicated a dynamical change from their original configuration. Furthermore, the fluctuation profiles of the every system were identical with that of the Neuraminidase alone, indicating the stability of the four complexes. This finding implies that the interaction of Molecules 01 and 04 with the active site of Neuraminidase caused a structural transformation. Ultimately, the privilege of RMSF study sheds light on the dynamics of the Neuraminidase and its complexes with the proposed compounds, which could potentially be used to the design of possible Neuraminidase inhibitors.

3.3.2 Radius of Gyration (Rg) Analysis

Radius of gyration is a measure of structural compactness and stability. The average radius of gyration values of the Neuraminidase complexed with *Zanamivir* and the designed compounds (Molecule 01-04) are 1.980, 2.020, 2.020, 1.999, 1.997 and 1.980 nm respectively. In addition, the similarity of these values indicates the stability of each designed molecule within Neuraminidase receptor with the absence of the structural change. Consequently, the majority of proposed compounds formed compact and stable complexes with the Neuraminidase receptor when compared to the therapeutic inhibitor of Neuraminidase (*Zanamivir*). The current finding is compatible with the RMSD and RMSF investigations, which also revealed the stability of these systems. We provided the Rg values for each system plotted over 100 ns of simulation in **Figure IV. 8.**

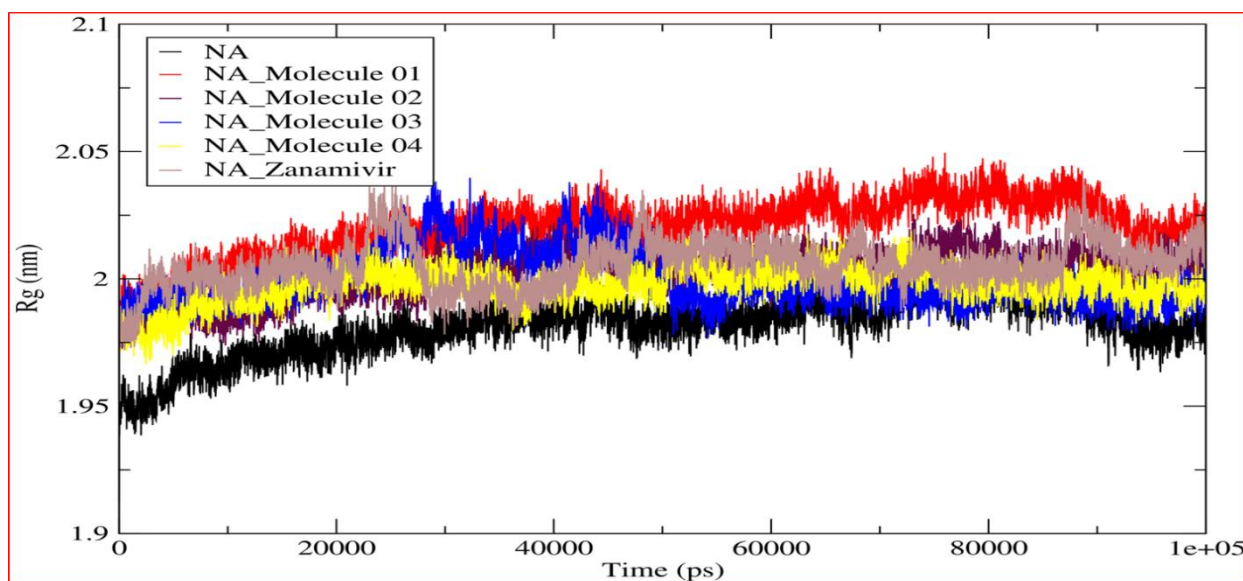


Figure IV. 8. Radius of gyration (Rg) of Neuraminidase and its complexes with Molecule 01-10, including Zanamivir.

3.3.3 Hydrogen Bonds Analysis

In this stage, hydrogen bonds constructed between Neuraminidase receptor and the designed molecules (01-04) can be used for evaluating the stability of the formed complexes. The number of hydrogen bonds during 100 ns was computed and plotted in **Figure IV. 9**.

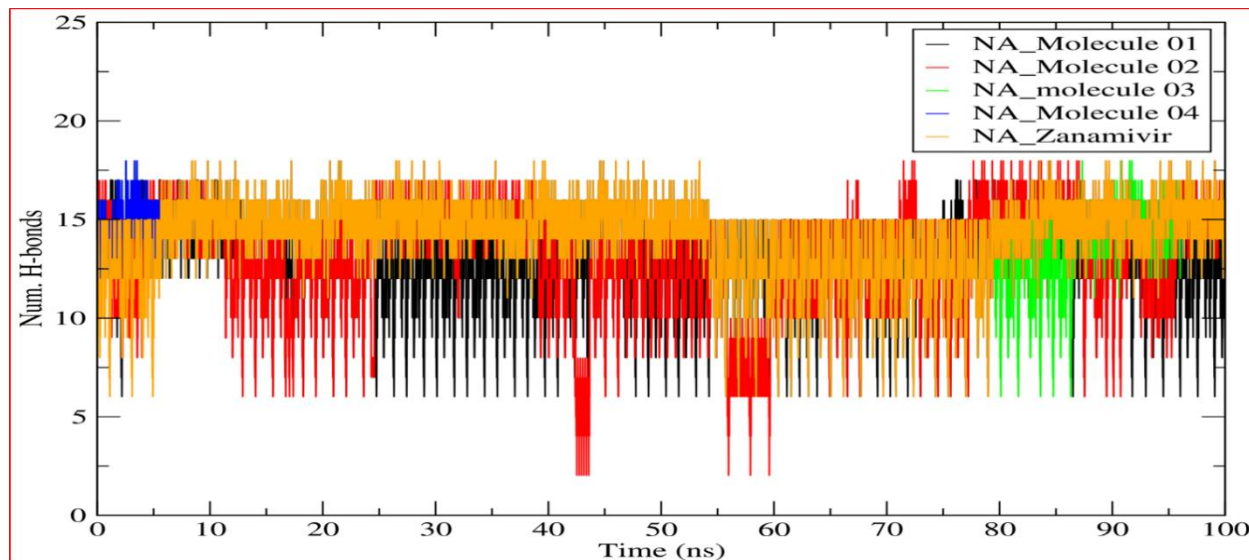


Figure IV. 9. Number of hydrogen bonds formed during 100 ns of simulation between NA, designed molecules and Zanamivir.

Throughout 100 ns of simulation, the NA_Molecule 04 complex had an average hydrogen bond number of 14.24, following that, the NA_Zanamivir complex attended an average hydrogen bonds of 14.09. NA_Molecule 01-03 complexes showed average H-bonds of 12.71, 13.05, and 14.03, respectively. This finding suggests that the hydrogen bonds generated between the active site of Neuraminidase and the developed molecules were dynamic in composition. The lack of a hydrogen bond between Neuraminidase receptor and the two molecules (Molecule 01 and 02) may be due to the interaction of solvent molecules with the binding sites, which weakens the hydrogen bond. The H-bonds analysis reflects the stability of designed molecules with the active site of Neuraminidase, and a bigger number of hydrogen bonds is seen in the Molecule 04.

3.3.4 Solvent accessible surface area (SASA) analysis

Solvent Accessible Surface Area predicts the dynamics changes that take place over the time of the interactions. The average SASA value for NA_Zanamivir complex was 162.38 nm² (**Figure IV. 10**). While the average SASA values of NA_Molecule 01-04 complexes were 163.22, 158.57, 160.45 and 159.42 nm² respectively. These computations identified that the NA_Molecule 02 complex was the least impacted by the water solvent throughout the molecular dynamic simulations, followed by the NA_Molecule 04 complex, indicating that these complexes are considerably more stable in nature than the remainder of the investigated complexes.

Finally, this similarity helps to explain the behavior of designed Neuraminidase inhibitors within the active site of Neuraminidase as well as the creation of a stable binding during interactions. **Table IV. 5** illustrates the average values collected via MDS study for all formed complexes.

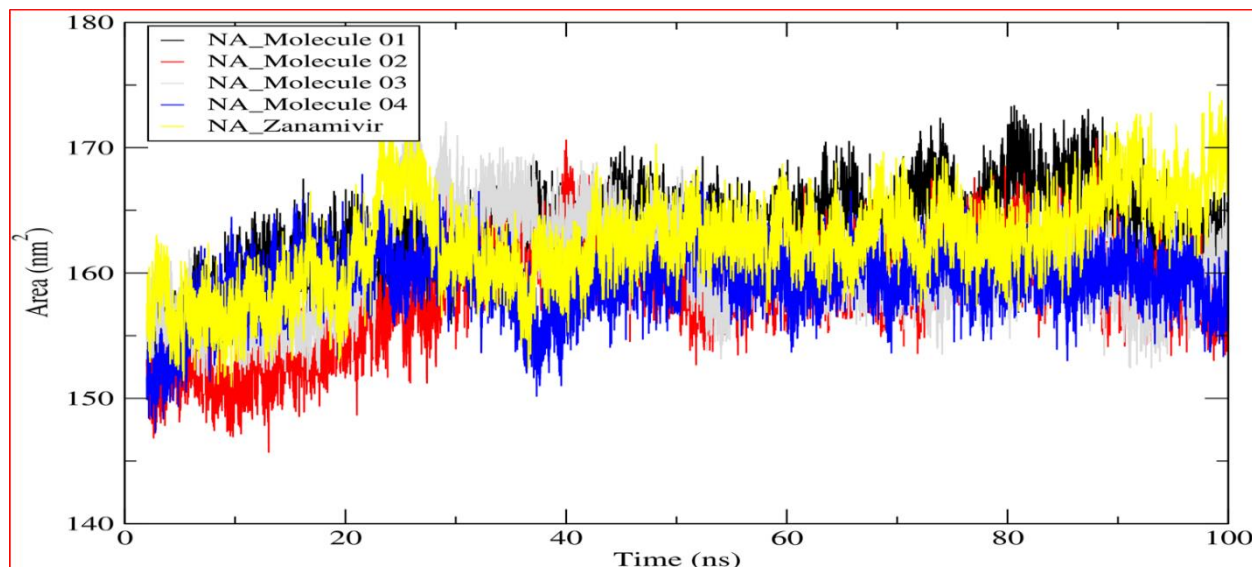


Figure IV. 10. Solvent accessible surface area (SASA) for all complexes during 100 ns of simulation.

Table IV. 5. The average values collected via MDS, including RMSD, RMSF, Rg, H-bonds and SASA.

Complex	Average RMSD (nm)	Average RMSF (nm)	Average Rg (nm)	Average H-bonds (nm)	SASA (nm ²)
NA_Molecule 01	0.254	0.110	2.020	12.71	163.22
NA_Molecule 02	0.252	0.110	2.002	13.06	158.57
NA_Molecule 03	0.172	0.128	1.999	14.03	160.45
NA_Molecule 04	0.166	0.102	1.997	14.24	159.42
NA_Zanamivir	0.174	0.136	2.005	14.09	162.38
NA	0.191	0.071	1.980	-	202.32

3.4. MM-PBSA analysis

The binding free energy of NA_Zanamivir complex and the four complexes (Neuraminidase Molecule 01-04) were calculated via Gromacs software using molecular dynamics trajectories and the MM-PBSA method. The calculated total binding free energy comprises the van der Waals interactions (ΔE_{VDW}), electrostatic interactions (ΔE_{EEL}), non-polar interactions in a solvated system (ΔE_{PB}), non-polar contribution of repulsive solute-solvent interactions to the solvation

energy (ΔE_{NPOLAR}), total gas phase molecular mechanics energy (ΔG_{GAS}), and total solvation energy (ΔG_{SOLV}). The purpose of this investigation was to confirm the affinity of the designed compounds for the Neuraminidase receptor. Furthermore, a higher affinity for Neuraminidase produces a higher negative binding energy. All the generated compounds form more stable complexes with the active site of Neuraminidase than the clinical inhibitor *Zanamivir*. The total binding energies of the four complexes were found between -107.85 and -83.50 KJ/mol (**Table IV. 6**), whereas the NA_*Zanamivir* complex has a binding free energy of -65.63 KJ/mol.

Table IV. 6. Table representing the ΔE_{VDW} , ΔE_{EEL} , ΔE_{PB} , ΔE_{NPOLAR} , ΔG_{GAS} , ΔG_{SOLV} and binding energy for Neuraminidase_Molecule 01-04 and Zanamivir complexes.

Protein-Ligand Complexes	ΔE_{VDW} (KJ/mol)	ΔE_{EEL} (KJ/mol)	ΔE_{PB} (KJ/mol)	ΔE_{NPOLAR} (KJ/mol)	ΔG_{GAS} (KJ/mol)	ΔG_{SOLV} (KJ/mol)	Δ_{TOTAL} (KJ/mol)
NA_Molecule 01	-4.21	-607.36	531.53	-3.46	-611.57	528.07	-83.50
NA_Molecule 02	-2.35	-646.29	544.45	-3.31	-648.64	541.14	-107.50
NA_Molecule 03	-2.58	-547.85	460.35	-3.64	-550.43	456.71	-93.71
NA_Molecule 04	-1.06	-570.97	467.41	-3.22	-572.04	464.19	-107.85
NA_ <i>Zanamivir</i>	-17.04	-306.72	261.63	-3.49	-323.76	258.13	-65.63

Finally, in this phase the electrostatic interactions are the most important contributors to binding energy. The graphic representation of each calculated total binding energy is shown in **Figure IV. 11**.

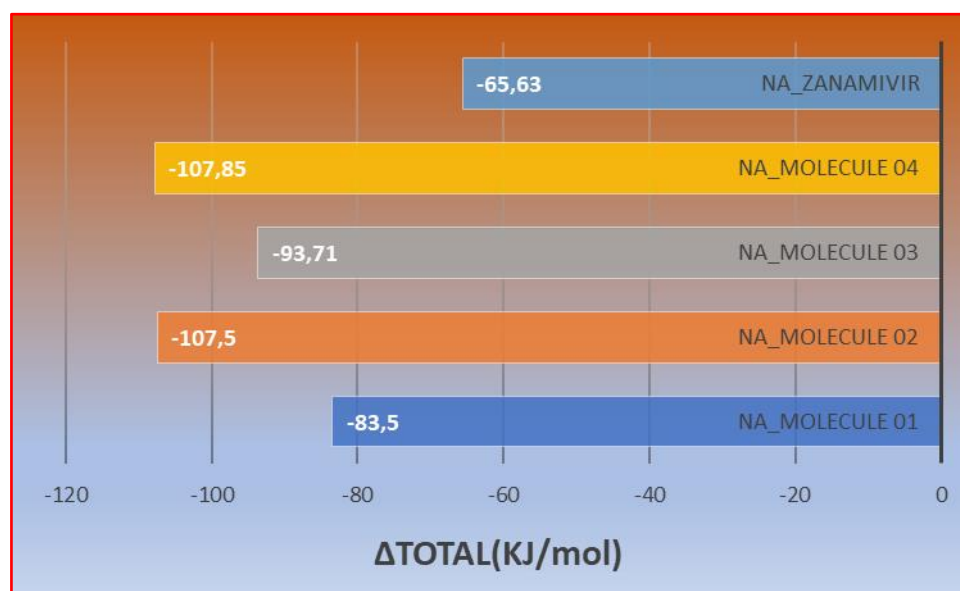


Figure IV. 11. Graphic representation of total binding energies of the five systems.

All of these outcomes are in line with previous investigations, particularly the docking study, since the proposed compounds form exceptionally stable complexes with Neuraminidase and are capable of inhibiting its vital function. Additionally, snapshots of all four complexes were

collected every 30 ns (30 ns, 60 ns, 100 ns). The binding poses of every complex prove their stability over 100 ns of simulation (**Figure IV. 12**).

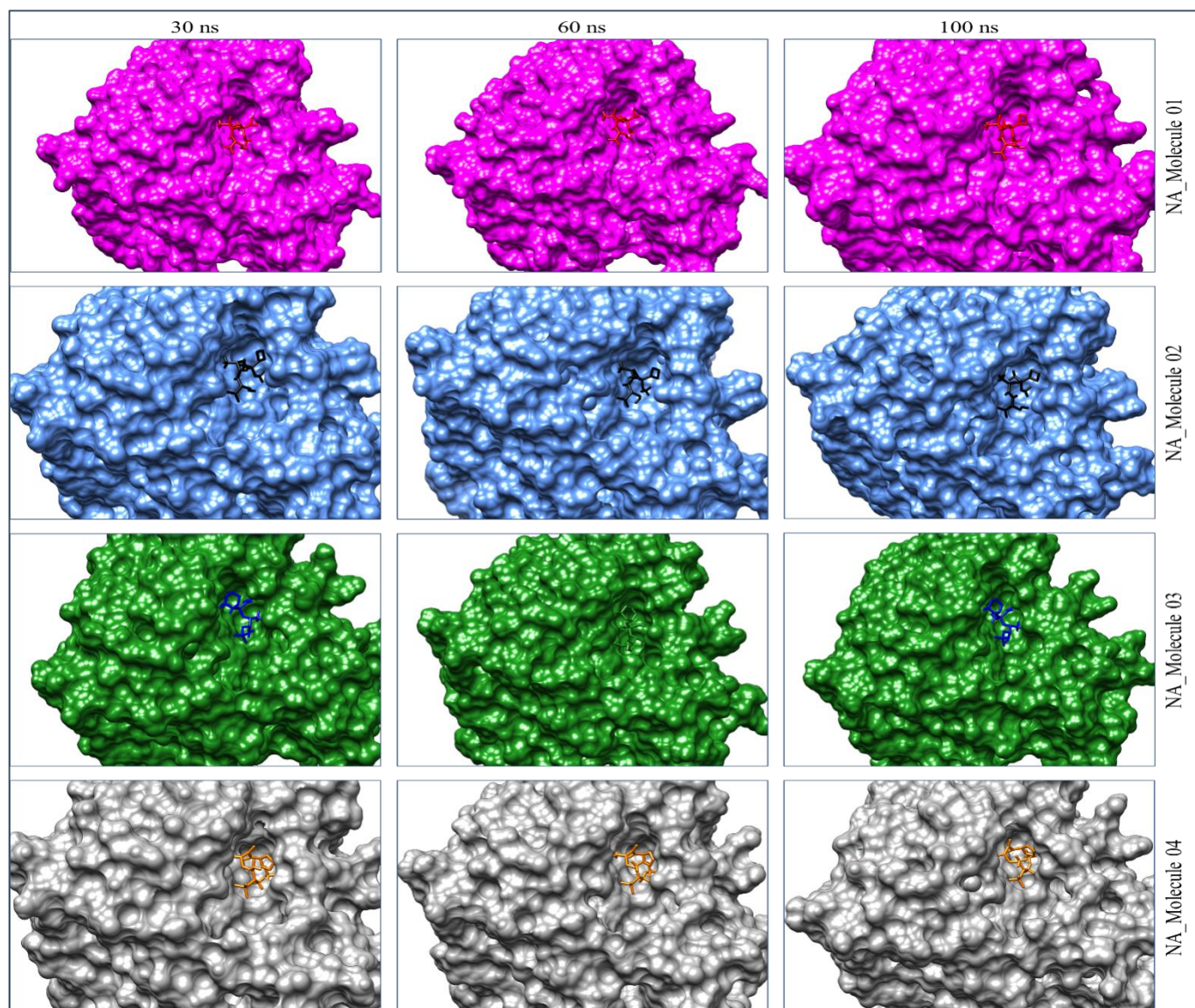


Figure IV. 12. Binding poses of the four complexes (NA_Molecule 01-04) over 100 ns of simulation.

3.5 Reaction Based Enumeration

At this point, we predicted the synthetic route of the proposed Neuraminidase inhibitors (Molecule 01-04) via reaction-based enumeration. The reaction enumeration tool revealed that the amide coupling and alkylation reactions were possible to be used to synthesize the four generated compounds. **Figure IV. 13**, depicts the synthetic route of the proposed compounds (Molecule 01-04) obtained through reaction-based enumeration process.

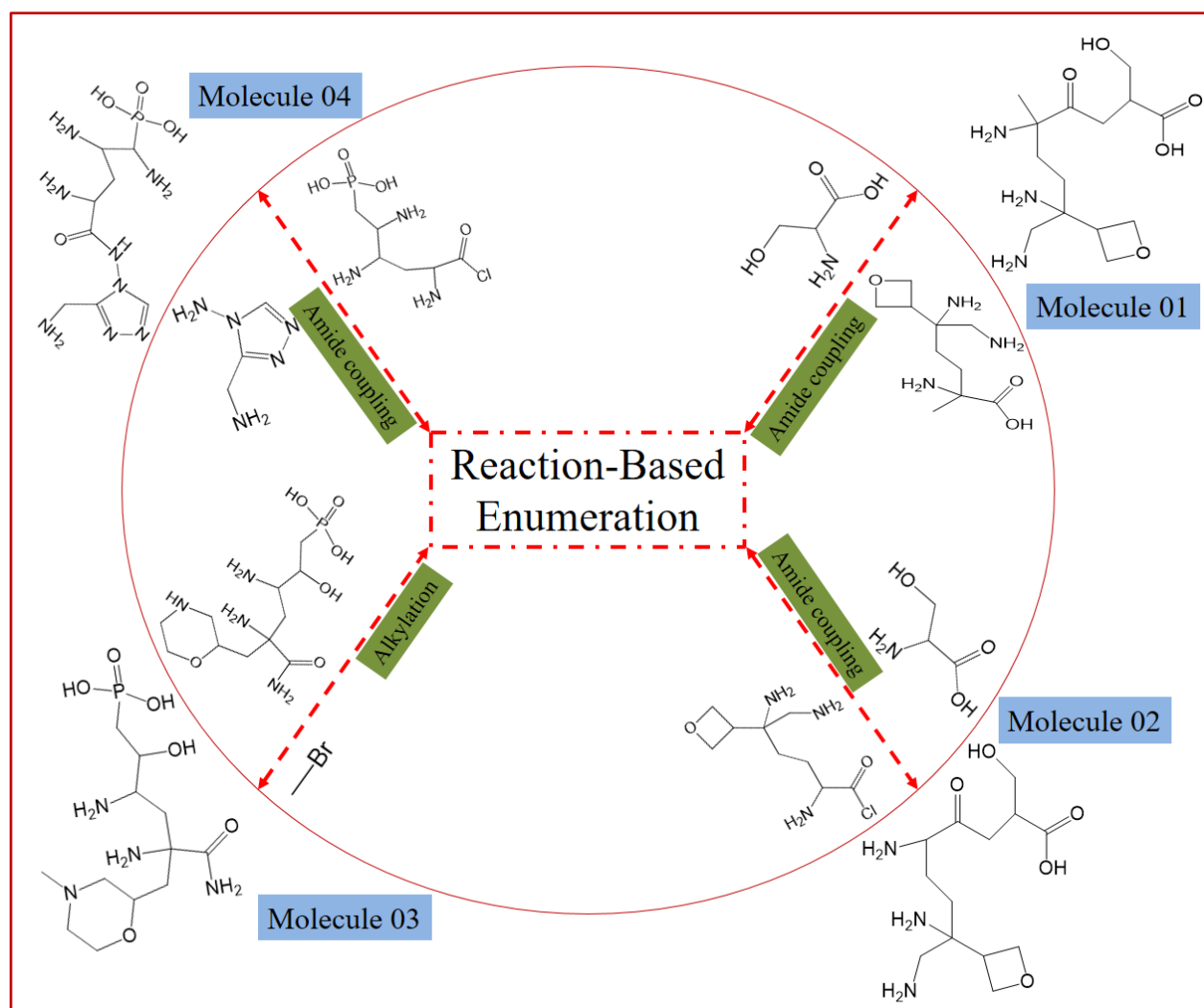


Figure IV. 13. Predicted synthetic pathway of the four designed Neuraminidase inhibitors (Molecule 01-04).

4. Conclusion

The present research employed a fragment-based drug design (FBDD) process to develop effective drugs for influenza by inhibiting the biological function of Neuraminidase. The highest-scoring fragments were selected for fragment linking for generating novel Neuraminidase inhibitors. We were able to acquire ten new neuraminidase inhibitors at the conclusion of the design process. The docking outcomes proved that the ten proposed compounds form extremely stable complexes with the neuraminidase receptor when compared to the clinical Neuraminidase inhibitors (*Zanamivir*, *Peramivir*, and *Oseltamivir*). The analysis of pharmacokinetics and potential toxicity reveals that the ten compounds have favorable pharmacokinetic profiles. The molecular dynamics simulation for 100 ns demonstrated that the top four molecules (Molecule 01-04) were highly stable within Neuraminidase receptor. Furthermore, MM-PBSA calculations

displayed that these complexes were more stable throughout the simulation time compared to the NA_*Zanamivir* complex. All of these findings verified the strong affinity between the proposed compounds and the active site of Neuraminidase. This finding will aid in the creation of effective Neuraminidase inhibitor medications for the treatment of influenza, and it may provide researchers with an opportunity to investigate these compounds for the treatment of influenza infection.

5. Reference

- [1] Gurung, A. B., Ali, M. A., Lee, J., Farah, M. A., & Al-Anazi, K. M. (2021). An updated review of computer-aided drug design and its application to COVID-19. *BioMed research international*, 2021.
- [2] van Riel, D., Munster, V. J., de Wit, E., Rimmelzwaan, G. F., Fouchier, R. A., Osterhaus, A. D., & Kuiken, T. (2007). Human and avian influenza viruses target different cells in the lower respiratory tract of humans and other mammals. *The American journal of pathology*, 171(4), 1215-1223.
- [3] Moscona, A. (2005). Neuraminidase inhibitors for influenza. *New England Journal of Medicine*, 353(13), 1363-1373.
- [4] Wang, C. Z., Han, H. H., Tang, X. Y., Zhou, D. M., Wu, C., Chen, G. R., ... & Tian, H. (2017). Sialylglycan-assembled supra-dots for ratiometric probing and blocking of human-infecting influenza viruses. *ACS applied materials & interfaces*, 9(30), 25164-25170.
- [5] Farina, V., & Brown, J. D. (2006). Tamiflu: the supply problem. *Angewandte Chemie International Edition*, 45(44), 7330-7334.
- [6] Doak, B. C., Norton, R. S., & Scanlon, M. J. (2016). The ways and means of fragment-based drug design. *Pharmacology & therapeutics*, 167, 28-37.
- [7] Li, Q. (2020). Application of fragment-based drug discovery to versatile targets. *Frontiers in molecular biosciences*, 7, 180.
- [8] Gubareva, L. V., Sleeman, K., Guo, Z., Yang, H., Hodges, E., Davis, C. T., ... & Stevens, J. (2017). Drug susceptibility evaluation of an influenza A (H7N9) virus by analyzing recombinant neuraminidase proteins. *The Journal of infectious diseases*, 216(suppl_4), S566-S574.
- [9] Pınar, N. M. Molecular Docking Studies of Coumarins Isolated from Extracts and Essential Oils of *Zosima absinthifolia* Link as Potential Inhibitors for Alzheimer's Disease.
- [10] Rohini, K., Roy, R., Ramanathan, K., & Shanthi, V. (2019). E-pharmacophore hypothesis strategy to discover potent inhibitor for influenza treatment. *Journal of Theoretical and Computational Chemistry*, 18(04), 1950021.
- [11] Vora, J., Patel, S., Athar, M., Sinha, S., Chhabria, M. T., Jha, P. C., & Shrivastava, N. (2019). Pharmacophore modeling, molecular docking and molecular dynamics simulation for screening and identifying anti-dengue phytochemicals. *Journal of Biomolecular Structure and Dynamics*.

- [12] Gurung, A. B., Ali, M. A., Lee, J., Farah, M. A., & Al-Anazi, K. M. (2021). An updated review of computer-aided drug design and its application to COVID-19. *BioMed research international*, 2021.
- [13] Teli, D. M., Patel, B., & Chhabria, M. T. (2022). Fragment-based design of SARS-CoV-2 Mpro inhibitors. *Structural Chemistry*, 33(6), 2155-2168.
- [14] Shamsi, A., Shahwan, M., Khan, M. S., Husain, F. M., Alhumaydhi, F. A., Aljohani, A. S., ... & Islam, A. (2021). Elucidating the interaction of human ferritin with quercetin and naringenin: Implication of natural products in neurodegenerative diseases: Molecular docking and dynamics simulation insight. *ACS omega*, 6(11), 7922-7930.
- [15] Issa, T. N., Wathieu, H., Ojo, A., W Byers, S., & Dakshanamurthy, S. (2017). Drug metabolism in preclinical drug development: a survey of the discovery process, toxicology, and computational tools. *Current drug metabolism*, 18(6), 556-565.
- [16] Daina, A., Michielin, O., & Zoete, V. (2017). SwissADME: a free web tool to evaluate pharmacokinetics, drug-likeness and medicinal chemistry friendliness of small molecules. *Scientific reports*, 7(1), 42717.
- [17] Banerjee, P., Eckert, A. O., Schrey, A. K., & Preissner, R. (2018). ProTox-II: a webserver for the prediction of toxicity of chemicals. *Nucleic acids research*, 46(W1), W257-W263.
- [18] Guevara-Olaya, L., Chimal-Vega, B., Castañeda-Sánchez, C. Y., López-Cossio, L. Y., Pulido-Capiz, A., Galindo-Hernández, O., ... & García-González, V. (2022). LDL Promotes Disorders in β -Cell Cholesterol Metabolism, Implications on Insulin Cellular Communication Mediated by EVs. *Metabolites*, 12(8), 754.
- [19] Van Der Spoel, D., Lindahl, E., Hess, B., Groenhof, G., Mark, A. E., & Berendsen, H. J. (2005). GROMACS: fast, flexible, and free. *Journal of computational chemistry*, 26(16), 1701-1718.
- [20] Zoete, V., Cuendet, M. A., Grosdidier, A., & Michielin, O. (2011). SwissParam: a fast force field generation tool for small organic molecules. *Journal of computational chemistry*, 32(11), 2359-2368.
- [21] Vora, J., Patel, S., Athar, M., Sinha, S., Chhabria, M. T., Jha, P. C., & Shrivastava, N. (2019). Pharmacophore modeling, molecular docking and molecular dynamics simulation for screening and identifying anti-dengue phytochemicals. *Journal of Biomolecular Structure and Dynamics*.

- [22] Halimi, M., & Bararpour, P. (2022). Natural inhibitors of SARS-CoV-2 main protease: structure based pharmacophore modeling, molecular docking and molecular dynamic simulation studies. *Journal of Molecular Modeling*, 28(9), 279.
- [23] Miryala, S. K., Basu, S., Naha, A., Debroy, R., Ramaiah, S., Anbarasu, A., & Natarajan, S. (2022). Datasets comprising the quality validations of simulated protein-ligand complexes and SYBYL docking scores of bioactive natural compounds as inhibitors of Mycobacterium tuberculosis protein-targets. *Data in brief*, 42, 108146.
- [24] Kuzmanic, A., & Zagrovic, B. (2010). Determination of ensemble-average pairwise root mean-square deviation from experimental B-factors. *Biophysical journal*, 98(5), 861-871.
- [25] Poli, G., Granchi, C., Rizzolio, F., & Tuccinardi, T. (2020). Application of MM-PBSA methods in virtual screening. *Molecules*, 25(8), 1971.
- [26] Konze, K. D., Bos, P. H., Dahlgren, M. K., Leswing, K., Tubert-Brohman, I., Bortolato, A., ... & Bhat, S. (2019). Reaction-based enumeration, active learning, and free energy calculations to rapidly explore synthetically tractable chemical space and optimize potency of cyclin-dependent kinase 2 inhibitors. *Journal of chemical information and modeling*, 59(9), 3782-3793.
- [27] Bos, P. H., Houang, E. M., Ranalli, F., Leffler, A. E., Boyles, N. A., Eyrich, V. A., ... & Bhat, S. (2022). AutoDesigner, a de novo design algorithm for rapidly exploring large chemical space for lead optimization: Application to the design and synthesis of d-amino acid oxidase inhibitors. *Journal of Chemical Information and Modeling*, 62(8), 1905-1915.
- [28] Smee, D. F., Hurst, B. L., Wong, M. H., Tarbet, E. B., Babu, Y. S., Klumpp, K., & Morrey, J. D. (2010). Combinations of oseltamivir and peramivir for the treatment of influenza A (H1N1) virus infections in cell culture and in mice. *Antiviral research*, 88(1), 38-44.
- [29] Kati, W. M., Montgomery, D., Maring, C., Stoll, V. S., Giranda, V., Chen, X., ... & Norbeck, D. W. (2001). Novel α - and β -amino acid inhibitors of influenza virus neuraminidase. *Antimicrobial agents and chemotherapy*, 45(9), 2563-2570.
- [30] Selvaraj, G. F., Piramanayagam, S., Devadasan, V., Hassan, S., Krishnasamy, K., & Srinivasan, S. (2020). Computational analysis of drug like candidates against Neuraminidase of Human Influenza A virus subtypes. *Informatics in Medicine Unlocked*, 18, 100284.

***Chapter V: Pharmacoinformatics and Breed-Based De Novo
Hybridization Studies to Develop New Neuraminidase
Inhibitors as Potential Anti-Influenza Agents***

1. Introduction

Influenza virus infection, an acute respiratory ailment. It frequently manifests in global outbreaks and epidemics, primarily coinciding with the winter season. Substantial quantities of influenza viral particles are discernible within the respiratory excretions of afflicted individuals [1, 2]. Managing influenza continues to pose challenges, demanding a comprehensive understanding of available pharmaceuticals and the viability of combination treatments. Effective drug selection hinges on factors including patient age, overall health, and heightened susceptibility to potential complications [3]. Currently, the FDA has approved just two classes of medications for the treatment of different influenza strains and subtypes: matrix-2 (M2) protein ion channel blockers (such as *Amantadine* and *Rimantadine*) and Neuraminidase (NA) inhibitors (such as *Zanamivir* and *Oseltamivir*) [4].

Neuraminidase (NA) is a glycoprotein present on the surface of influenza viruses, particularly those of the A and B types. It plays a critical role in the viral life cycle and contributes to the virus's ability to infect and spread within a host organism. One of the key functions of Neuraminidase is related to the virus's escape from infected cells and its spread to new cells. This is particularly evident during the late stages of viral replication and is related to its enzymatic activity [5]. NAIs are now the most frequently recommended anti-influenza drugs. They have been demonstrated to be effective in accelerating virus clearance, shortening clinical illness period, and reducing hospital stay and death [6, 7].

In this manuscript, we conducted an *in silico* study using a BREED-based de novo hybridization strategy to generate novel Neuraminidase inhibitors. Using structural information and the known positions of two ligands, the BREED *De Novo* method reconstructs fragments from each ligand to create a new ligand [8]. Via a bond-matching and fragment-swapping system similar to Ho and Marshall [9].

The current study aimed to estimate the pharmacokinetic properties, the potential toxicity, and we investigate the stability of complexes by dynamics simulation and MM-PBSA calculation for newly breed Neuraminidase inhibitors molecules.

2. Materials and Methods

2.1 Breed De Novo Hybridization Approach

In this step, we used Maestro software (Maestro, version 11.8, 2018, Schrödinger, New York, NY, USA). In breed-based de novo drug design, co-crystallized compounds from diverse PDB structures or well-known inhibitors against a particular target must be used [8]. Numerous Neuraminidase inhibitors from the literature were gathered for this investigation (**Figure V. 1**) [10]. The LigPrep module, which created the low-energy ligand conformer using the OPLS3e force field [11], optimized the 3D structures of 30 compounds. Diverse fragments were produced from these structures using the `run.\fragment_molecule.py` program at the Schrödinger PowerShell command line with the appropriate input and output folders.

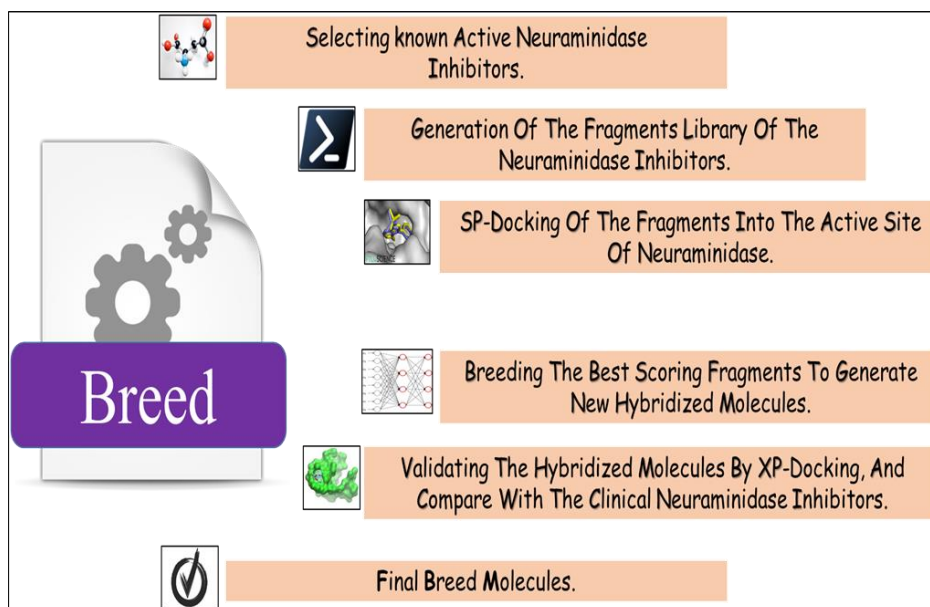


Figure V. 1. Breed-based de novo hybridization strategy.

The fragments were docked into the active site of the receptor using SP docking, and the best-scoring fragments were combined using the Breed Ligand Creation Panel [8]. A breed panel, utilizing three different settings, hybridized the molecule. It should be recalled that two bonds must be of the same order to start and maintain the hybridization (geometry) of the bonded atoms in the new molecule. Additionally, the atoms at the bond ends need to be close to one Å of another [8]. According to Pierce et al. [8], the angle between the bond vectors of two bonds cannot be greater than 15°. The first half of molecule one and the second half of molecule two combine to form a new molecule if the initial molecules are divided in half at the matching bond. The other new molecule is created by joining the first half of molecule two and the second half of molecule one. The atom types, sites, and bonds of the new molecules are identical to those of the corresponding

atoms [9]. The procedure for drug discovery, in general, is a difficult challenge for organic chemists due to the complexity of the pharmacophore feature that increases the properties and efficiency of a drug [12]. Chemists commonly use their specialized knowledge and carry out compound tweaking by hand by adding and removing functional groups. Nevertheless, chemists must carry out each alteration step by hand even if they use methods that forecast the ideal chemical attributes. Every iteration of this process might take many hours, and there might still be no promising candidate medication [8]. The breed-based de novo hybridization approach used in this investigation is shown in **Figure V. 2**.

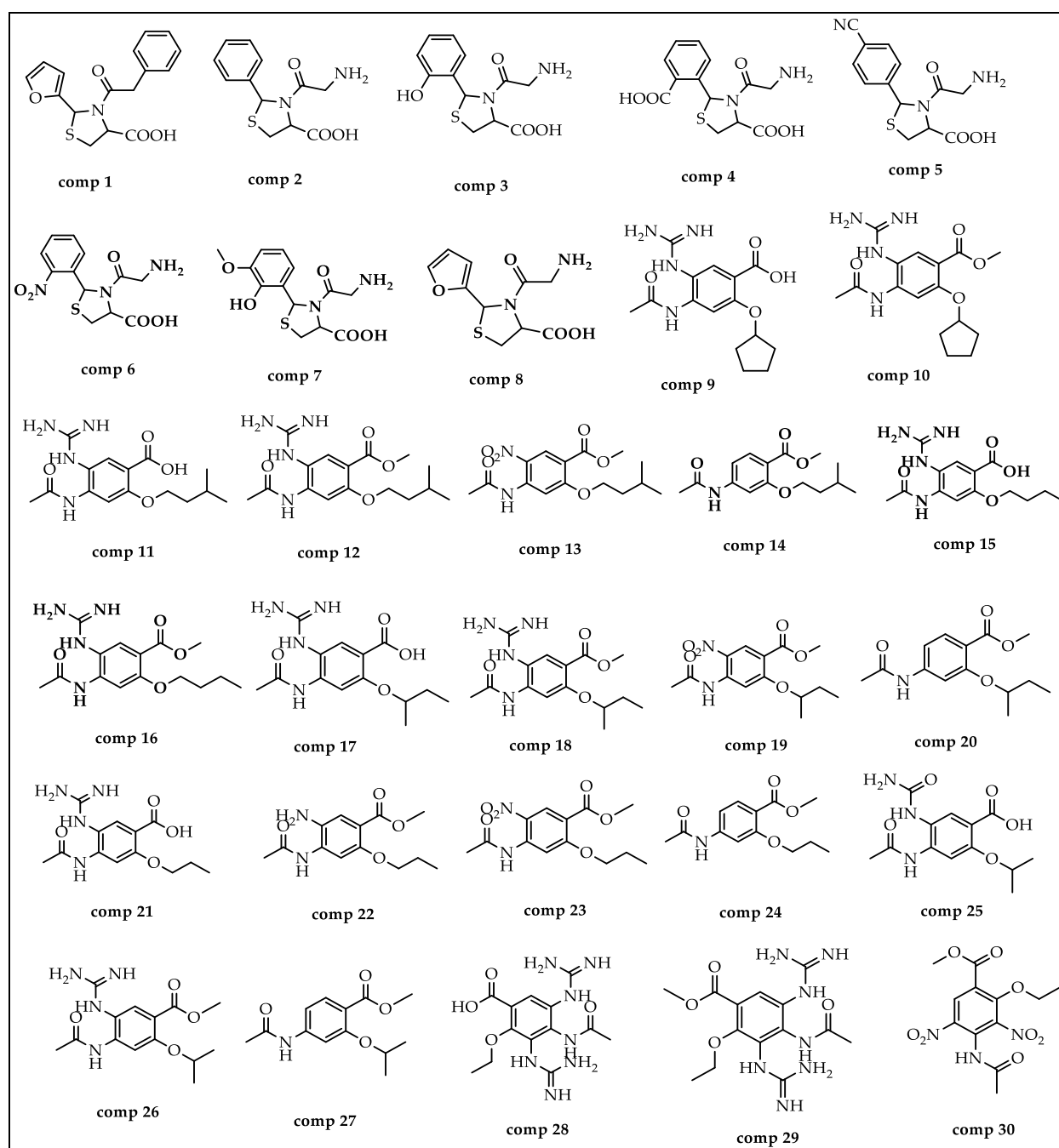


Figure V. 2. The structures of compounds utilized in this research.

2.2 Molecular Docking Study

The crystal structure of Neuraminidase with *Zanamivir* was downloaded from the Protein Data Bank (PDB ID: 5L17) with a resolution of 2.40 Å and zero mutations [13]. The “protein preparation wizard” in Maestro 11.8 was used to prepare proteins. Hydrogen was added following verification of the chemical accuracy.

The process of energy minimization was used to create a protein with a lower energy state with the help of the OPLS3e force field (optimized potential for liquid simulation) [14]. The grid was constructed using the default box dimension in the SP-docking study. For extensive analysis and validation of the de novo drug design results, XP docking was employed to study the interactions of the new breed of molecules and the active site of Neuraminidase.

Finally, we docked two clinical Neuraminidase inhibitors (*Peramivir* and *Oseltamivir*) as supplementary reference ligands in the active site of Neuraminidase to estimate the inhibitory activity of the breed molecules.

2.3 ADMET Prediction

ADMET properties are a very helpful drug discovery approach [15]. The experimental determination of drug candidate pharmacokinetic properties is time-consuming. We investigated the ADMET properties of each breed of molecule, focusing on solubility and permeability to biological membranes, which are two of the most important factors influencing the activity using SwissADME [16]. The ProTox-II platform was used to evaluate the potential toxicity [17]. To study hepatotoxicity, immunotoxicity, and cytotoxicity, the lethal dosage (LD₅₀) was determined for both active and inactive cell types [18].

2.4 Molecular Dynamic Simulation

In this phase, we conducted molecular dynamic (MD) simulations for all breed molecules. The first process consisted of identifying compounds with high binding affinities for Neuraminidase and good ADMET properties. The Gromacs-2022.4 package and the CHARMM27 force field were used to execute the production MD simulation for 100 ns [19]. The SwissParam server was employed for generation of the ligand topology files [20]. Each system was then solvated with the TIP3P water model, and Na⁺ and Cl⁻ ions were introduced to neutralize the charge [19]. Using the steepest descent-minimization technique, the solvated system was then utilized to minimize energy until the maximal force was less than 10.0 kJ/mol. The equilibration process was then divided into two phases: NVT and NPT equilibrations. The system was coupled with a v-rescale algorithm at 300 K for 100 ps with a

coupling value of 0.1 ps during the NVT equilibration phase. The NPT was then equilibrated for 100 ps using a Berenson pressure-coupling strategy with a coupling constant of 2.0 ps [21].

The commands `gmx rms`, `gmx rmsf`, `gmx gyrate`, `gmx hbond`, and `gmx sasa` were used to determine the various parameters for each system. The root-mean-square deviation (RMSD) was used to quantify the structural stability of the protein–ligand complex, and the flexibility of the protein residues was assessed using the root-mean-square fluctuation (RMSF) [22]. During 100 ns of simulation, the radius of gyration (Rg) was calculated to assess the compactness of the protein–ligand complex, hydrogen bond analysis was performed to determine the protein–ligand hydrogen bonding interactions, and the solvent-accessible surface (SASA) area was computed to assess the overall stability of each system. In addition, we conducted free-energy landscape analysis, which involves calculating and diagonalizing the covariance matrix [23]. Grace software was employed to visualize the simulation trajectories [24].

2.5 Binding Free Energy

For the molecular mechanics Poisson–Boltzmann surface area (MM-PBSA), the protocol implemented in the `g_mmpbsa` package was used to perform the analysis of the binding free energy (ΔG_{bind}) [25]. The MM-PBSA calculation provides a quantitative prediction of the interactions between proteins and ligand compounds. The binding free energy was calculated as follows:

$$\Delta G_{\text{bind}} = G_{\text{complex}} - (G_{\text{protein}} + G_{\text{ligand}})$$

Where ΔG_{bind} is the total binding energy of the complex, G_{complex} is the binding energy of the native protein, and G_{ligand} is the binding energy of the ligand.

2.6 Reaction-Based Enumeration

Reaction-based enumeration is another Schrödinger tool that predicts the synthetic pathway of any compound using a retro-synthetic approach [26]. The current study used reaction-based enumeration to establish the synthetic route of the final breed compounds.

3. Results

3.1 Breed-Based De novo and Molecular Docking Approaches

A breed-based de novo strategy was employed in the current investigation to develop new Neuraminidase inhibitors. A total of 282 different fragments were generated from thirty potent Neuraminidase inhibitors using the Schrödinger PowerShell command “run.\fragment_molecule.py”. We initially docked all the generated fragments (282) in the active site of Neuraminidase using SP docking. **Figures V. 3** and **V. 4** show all fragments with docking scores greater than -6 Kcal/mol, while **Table V. 1** reveals the SP docking scores of the top fragments. Compounds 28, 17, 11, 9, 21, 4, 5, 3, and 29 produced high-scoring fragments (between -7.002 and -8.700 Kcal/mol) with the Neuraminidase receptor. The breed de novo hybridization approach has now progressed toward fully automating the design process, which could significantly accelerate the procedure and produce better results [27]. The top fragments (with docking scores greater than -6.0) were selected for the breed de novo hybridization process. Subsequently, all 67 novel breed compounds, including *Zanamivir* and clinical Neuraminidase inhibitors (*Oseltamivir* and *Peramivir*), were selected for SP rather than the process of XP docking into the active site of Neuraminidase. The best breed molecules, with breed scores between 7.886 and 15.623, were as follows: Breed 1 was obtained through hybridization of comp17 (frag5) and comp4 (frag13); Breed 2 was obtained through hybridization of comp28 (frag3) and comp17 (frag7); Breed 3 was obtained through hybridization of comp28 (frag3) and comp17 (frag12); Breed 4 was obtained through hybridization of comp28 (frag3) and comp9 (frag1); Breed 5 was obtained through hybridization of comp28 (frag3) and comp11 (frag13); Breed 6 was obtained through hybridization of comp28 (frag3) and comp11 (frag17); and Breed 7 was obtained through hybridization of comp28 (frag3) and comp11 (frag16), as illustrated in **Figure V. 5**.

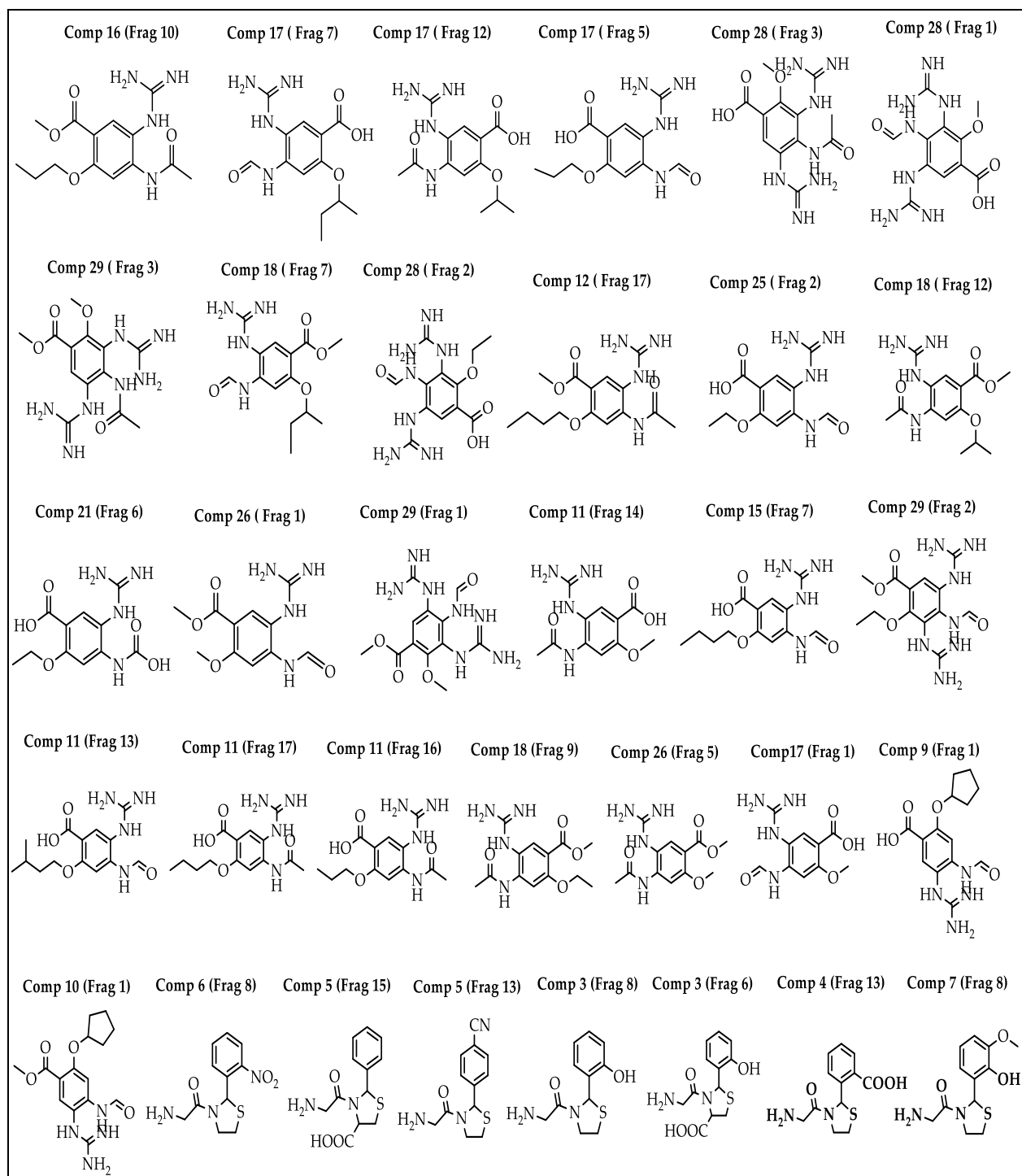


Figure V. 3. Structures of the best fragments.

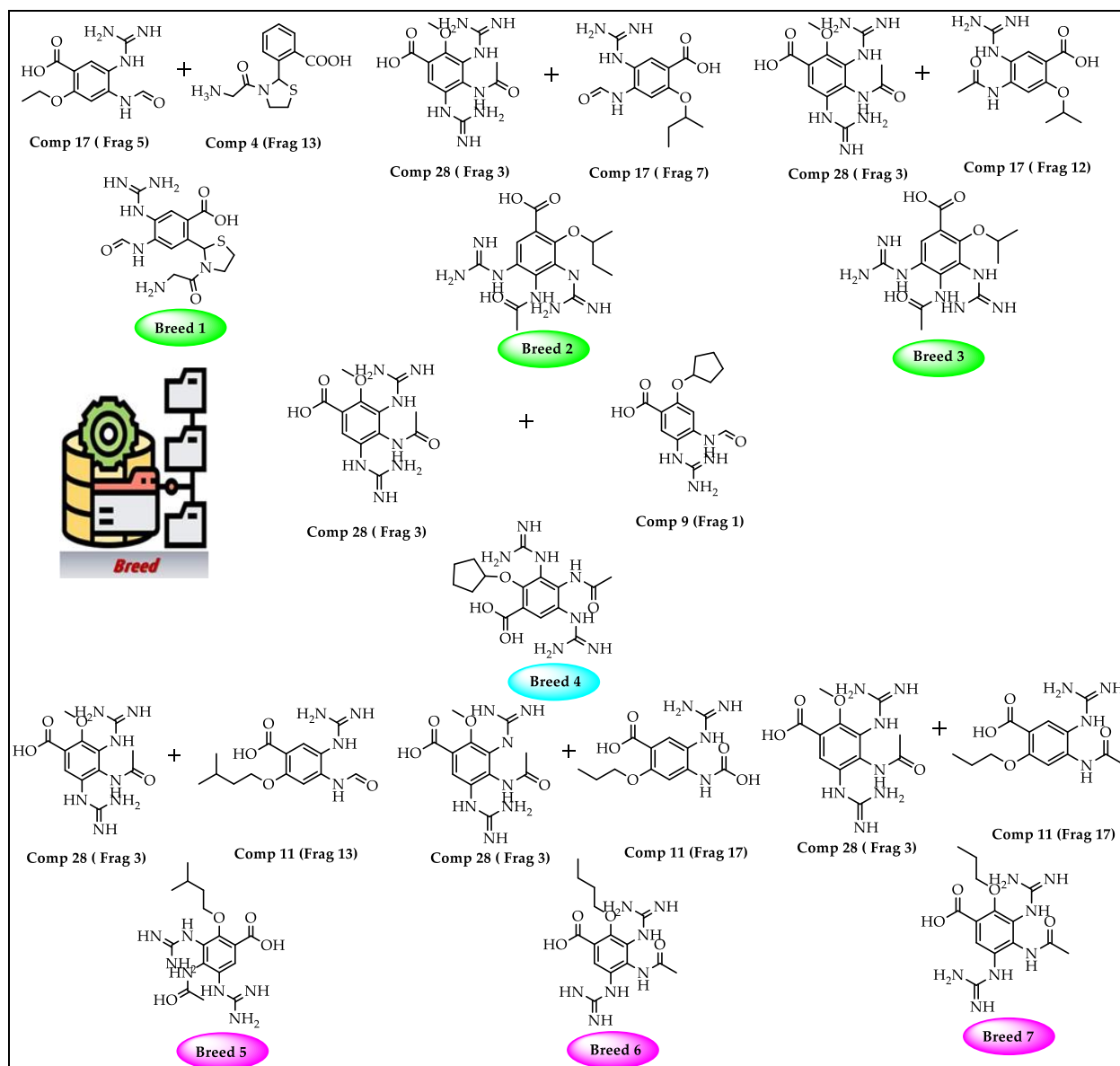


Figure V. 4. Breed generation of top-scoring compounds from different fragments.

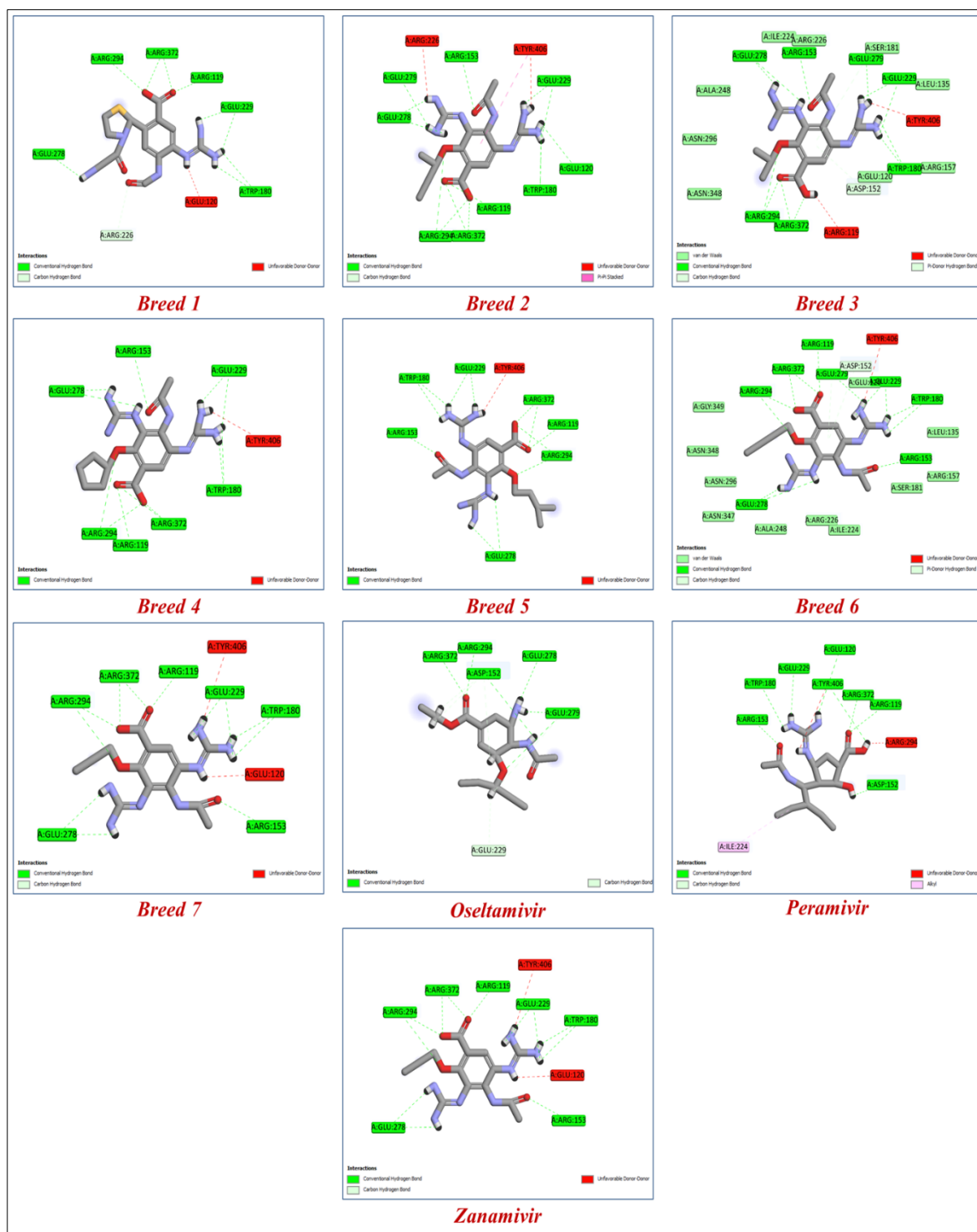


Figure V. 5. The binding interactions of the seven new breed molecules, Zanamivir, Peramivir, and Oseltamivir within the active site of Neuraminidase.

Table V. 1. SP docking results for the best fragments.

Fragment	SP-Score (kcal/mol)	Fragment	SP-Score (kcal/mol)	Fragment	SP-Score (kcal/mol)
Comp28 (Frag3)	-8.700	Comp5 (Frag15)	-7.085	Comp26 (Frag5)	-6.425
Comp28 (Frag1)	-8.425	Comp17 (Frag1)	-7.055	Comp6 (Frag8)	-6.370
Comp17 (Frag12)	-8.030	Comp17 (Frag7)	-7.048	Comp18 (Frag9)	-6.264
Comp11 (Frag16)	-7.897	Comp3 (Frag8)	-7.030	Comp16 (Frag10)	-6.117
Comp9 (Frag1)	-7.679	Comp29 (Frag1)	-7.002	Comp18 (Frag12)	-6.166
Comp17 (Frag5)	-7.661	Comp25 (Frag2)	-6.960	Comp12 (Frag17)	-6.144
Comp28 (Frag2)	-7.654	Comp29 (Frag3)	-6.883	Comp26 (Frag1)	-6.135
Comp11 (Frag14)	-7.409	Comp11 (Frag13)	-6.883	Comp5 (Frag13)	-6.073
Comp11 (Frag17)	-7.296	Comp29 (Frag2)	-6.743	Comp15 (Frag7)	-6.042
Comp21 (Frag6)	-7.287	Comp7 (Frag8)	-6.518	Comp10 (Frag1)	-6.031
Comp4 (Frag13)	-7.263	Comp18 (Frag7)	-6.464	Comp3 (Frag6)	-6.012

Antivirals are essential to the control and prevention of influenza. *Oseltamivir* and *Zanamivir* are the only Neuraminidase inhibitor medications that are now licensed globally. Recently, *laninamivir* and *Peramivir* gained permission in Japan [28]. To know more about how breed molecules inhibit the vital function of the Neuraminidase of influenza virus, we docked *Oseltamivir* and *Peramivir* into the Neuraminidase receptor. The results obtained indicate that the seven new breed compounds had binding affinity values between -10.529 and -11.867 kcal/mol, and the binding affinity value of reference molecules (*Zanamivir*) was -9.848 kcal/mol, while the clinical inhibitors *Peramivir* and *Oseltamivir* had binding affinity values of -8.844 and -6.326 kcal/mol, respectively. These results demonstrate that the seven breed molecules formed very stable complexes with the active site of Neuraminidase. The docking modeling results and the breed score are presented in **Table V. 2**. The important information we obtained from this study is that hydrogen-bonding interactions are responsible for inhibitory activity. The amino acids in the active site of Neuraminidase that interacted with the seven types of molecules via hydrogen bonds were Arg119, Trp180, and Glu278. The best molecule (Breed 1) interacted with the amino acids Asp152, Arg226, and Glu226 at a distance between 1.61 and 3.33 Å; on the other hand, the reference molecule (*Zanamivir*) interacted with the amino acids Asp152, Glu229, Glu278, Glu279, and Arg372 at a distance between 1.50 and 4.15 Å. This result indicates that the interaction with the amino acids Arg226 and Glu226 plays a very important role in inhibiting the vital function of Neuraminidase. Similar to hydrogen bonds formed between molecules (Breed 2–Breed 7) with amino acids Arg119, Trp180, and Glu278, other hydrogen bonds with amino acids Glu120, Arg153, Arg194, Glu229, Glu279, and Arg372, with distances ranging from 1.22 to 5.98 Å, formed stable complexes with the Neuraminidase receptor compared to Neuraminidase with *Zanamivir*, *Peramivir*, and *Oseltamivir* complexes. Figure 4 shows the binding interactions of the seven tested molecules, *Zanamivir*, *Peramivir*, and *Oseltamivir*, with Neuraminidase inhibitors.

Table V. 2. Docking results of the breed molecules and Zanamivir, Peramivir, and Oseltamivir with the Neuraminidase receptor.

Molecules	Breed Score	SP-Score	XP-Score	H-Bond Interactions	Distance
Breed 1	15.623	-8.799	-11.867	Arg119, Asp152, Trp180, Arg226, Glu226, Glu278, Arg294, Arg372.	1.61–3.33
Breed 2	11.080	-8.372	-10.804	Arg119, Glu120, Arg153, Trp180, Glu229, Glu278, Glu279, Arg294, Arg372.	1.57–5.98
Breed 3	9.952	-8.316	-10.791	Arg119, Asp152, Arg153, Trp180, Glu229, Glu278, Glu279, Arg294, Arg372.	1.48–3.99
Breed 4	13.604	-8.278	-10.765	Arg119, Asp152, Arg153, Trp180, Glu229, Glu278, Glu279, Arg294, Arg372.	1.50–4.91
Breed 5	7.886	-8.457	-10.706	Arg119, Asp152, Arg153, Trp180, Arg194, Glu229, Glu278, Glu279, Arg372.	1.22–3.81
Breed 6	8.298	-7.949	-10.628	Arg119, Asp152, Arg153, Trp180, Glu229, Glu278, Glu279, Arg294, Arg372.	1.48–3.99
Breed 7	10.740	-7.890	-10.529	Arg119, Arg152, Arg153, Trp180, Glu229, Glu278, Arg294, Arg372.	1.57–4.15
Zanamivir	-	-7.610	-9.848	Arg119, Arg152, Arg153, Trp180, Glu229, Glu278, Glu279, Arg294, Arg372.	1.50–4.15
Peramivir	-	-7.370	-8.844	Arg119, Glu120, Asp152, Arg153, Trp180, Glu229, Glu279, Arg294, Arg372.	1.55–4.39
Oseltamivir	-	-5.588	-6.326	Asp152, Glu229, Glu278, Glu279, Arg294, Arg372.	1.50–4.15

3.2 ADMET Prediction

The physicochemical characteristics of a compound have a major effect on its pharmacokinetics in the body, and a firm understanding and accurate prediction of these properties are critical for successful drug discovery [28, 29]. We estimated the pharmacokinetic properties for the seven breed molecules (**Table V. 3**), in particular, the most important parameters, such as LogP, solubility, permeability, and bioavailability, to ensure that the seven breed molecules would reach the biological target (Neuraminidase).

Table V. 3. Pharmacokinetic and physicochemical parameters for the seven breed molecules.

Molecules	MW (g/mol)	Log S (ESOL)	Consensus Log P	Cytochrome P450 Inhibitors	Bioavailability Score	Log Kp cm/s	Synthetic Accessibility
Breed 1	366.40	0.77	-1.55	No	0.55	-11.38	3.60
Breed 2	365.39	-1.18	-0.40	No	0.17	-9.02	3.79
Breed 3	351.36	-0.83	-0.74	No	0.17	-9.31	3.19
Breed 4	409.48	-2.28	0.24	No	0.17	-8.41	3.78
Breed 5	379.41	-1.42	-0.13	No	0.17	-8.85	3.46
Breed 6	365.39	-1.07	-0.43	No	0.17	-9.08	3.35
Breed 7	351.36	-0.83	-0.59	No	0.17	-9.24	3.24

The seven breed molecules had molecular masses below 410 g/mol, which facilitated the intestinal absorption of these molecules by oral administration. Second, the partition coefficients (LogP) of the breed molecules were between -2.28 and 0.77. These results clearly show the affinity of these molecules toward biological membranes and confirm the good distribution of these substances in the body. For aqueous solubility, all the breed molecules were soluble in aqueous media (including the intracellular medium), and the LogS (ESOL) values were between

−0.74 and 0.24. Because of this aqueous solubility, the breed molecules would be easily eliminated through the kidneys. The bioavailability score for Breed 1 was 0.55, while the rest of the breed molecules had the same bioavailability score (0.17). The seven breed molecules did not inhibit the vital function of hepatic enzymes (cytochrome P450), such as CYP 1A2, CYP 2C19, CYP 2C9, CYP 2D6, and CYP 3A4, and they also had Log Kp (skin permeation) values between −8.41 and −11.38. Ultimately, the synthesis of these seven breed molecules in the chemical laboratory is quite simple for in vitro and in vivo research.

The results obtained by ProToxII (**Table V. 4**) show that all the breed molecules were safe. The predicted LD₅₀ for the top molecules (Breed 1) was 1098 mg/kg and the toxicity class was 4, while the rest of the breed molecules (Breeds 2–7) had LD₅₀ values between 3200 and 4000 mg/kg and the same toxicity class (class 5). According to the results obtained by the molecular docking and the ADMET study, seven breed molecules (Breeds 1–7) were selected for simulation investigation of their molecular dynamics [28,30].

Table V. 4. Toxicity prediction of breed molecules.

Molecules	Cytotoxicity	Carcinogenicity	Mutagenicity	Immunotoxicity	Toxicity Class	LD50 (mg/kg)
Breed 1	Inactive	Inactive	Inactive	Inactive	4	1098
Breed 2	Inactive	Inactive	Inactive	Inactive	5	3200
Breed 3	Inactive	Inactive	Inactive	Inactive	5	3200
Breed 4	Inactive	Inactive	Inactive	Inactive	5	4000
Breed 5	Inactive	Inactive	Inactive	Inactive	5	3200
Breed 6	Inactive	Inactive	Inactive	Inactive	5	3200
Breed 7	Inactive	Inactive	Inactive	Inactive	5	3200

3.3 Study of Molecular Dynamics

Molecular dynamic simulation (MDS) [28] was employed to examine the physical movements of the Neuraminidase (NA) and its complexes (Breeds 1–7) during 100 ns of simulations. The root-mean-square deviation (RMSD), root-mean-square fluctuation (RMSF), radius of gyration (Rg), hydrogen bonds (H-bonds), and solvent-accessible surface area (SASA) were calculated to assess the stability of the Neuraminidase and its seven complexes (Breeds 1–7).

3.3.1 RMSD and RMSF Analysis

The RMSD is a factor used to determine the equilibration, protein flexibility, and average distance between backbone atoms of a protein [28]. The RMSD plot for the backbone atoms of the Neuraminidase (NA) and its complexes with Breeds 1–7 is displayed in **Figure V. 6**. The results indicated that the RMSD of the Neuraminidase was stable during 100 ns of simulation, while the NA_Breed 7 complex attained structural stability after 15 ns of simulation.

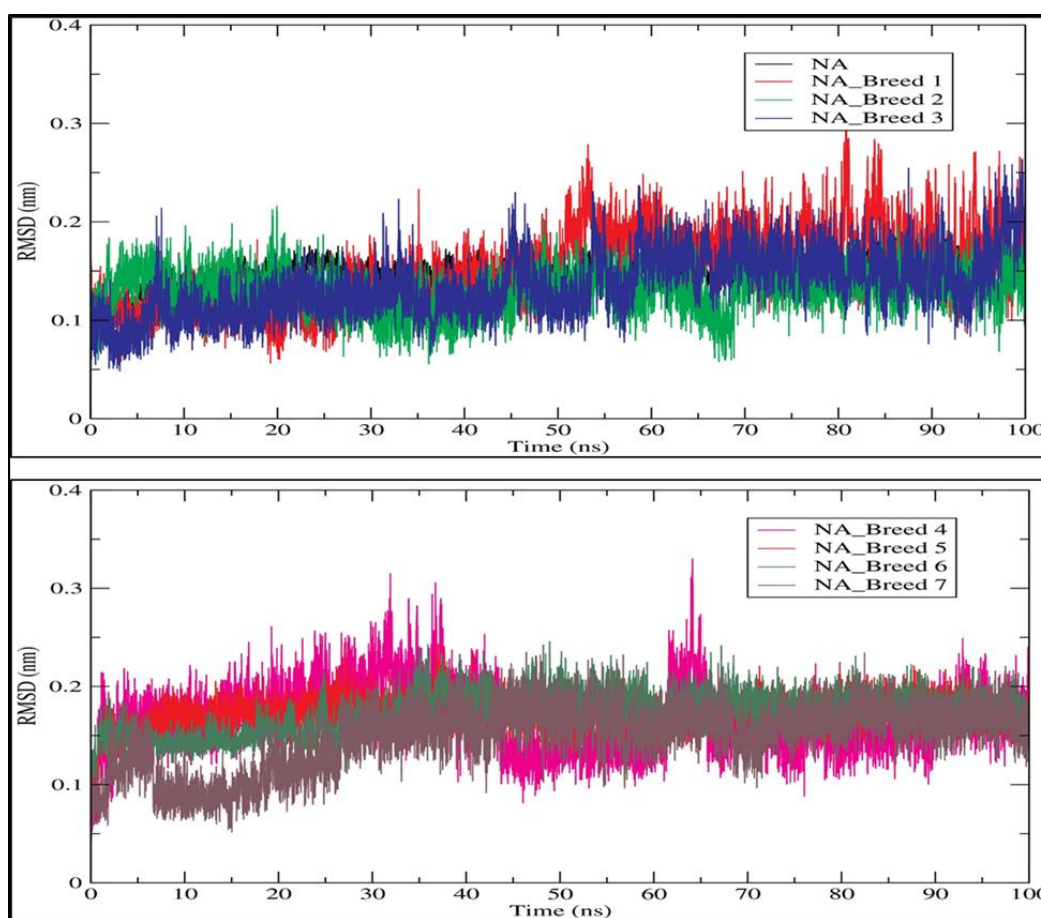


Figure V. 6. Root-mean-square deviation (RMSD) profile of the backbone atoms of Neuraminidase and its complexes with Breeds 1–7.

The rest of the complexes were very stable during the simulation period. The average RMSD values for the NA and its complexes with Breed 1, Breed 2, Breed 3, Breed 4, Breed 5, Breed 6, and Breed 7 were 0.148, 0.149, 0.131, 0.135, 0.166, 0.172, 0.172, and 0.148 nm, respectively. Finally, the RMSD analysis indicated that the MD trajectories were generally stable during the 100 ns of simulation and were able to help in the development of new influenza virus inhibitors. In this research, we calculated the root-mean-square fluctuation (RMSF) of the Neuraminidase (NA) and its complexes with Breeds 1–7, as shown in **Figure V. 7**. This study showed that more flexibility during the molecular dynamic simulation was shown by higher RMSF values, whereas good stability of the complex was reflected by lower RMSF values. The analysis revealed that the average RMSF for the Neuraminidase and its complexes was less than 0.123 nm. The average RMSD for the Neuraminidase was 0.106 nm, while Neuraminidase complexes (NA Breeds 1–7) had average RMSF values that ranged from 0.100 to 0.123 nm, demonstrating the structural stability and little atomic movement of the Neuraminidase and its complexes. On the other hand, the NA Breed 1–7 complexes had higher fluctuations at atoms 450, 1000, 5400, and 5800 of the

Neuraminidase protein, with RMSF values ranging between 0.4 and 0.6 nm. These findings indicate that the interactions of the breed molecules with the Neuraminidase caused conformational changes and increased the protein dynamics in those particular regions. The results obtained (**Table V. 5**) indicate that these breed molecules (Breeds 1–7) with the active site of the Neuraminidase form good, stable complexes [23].

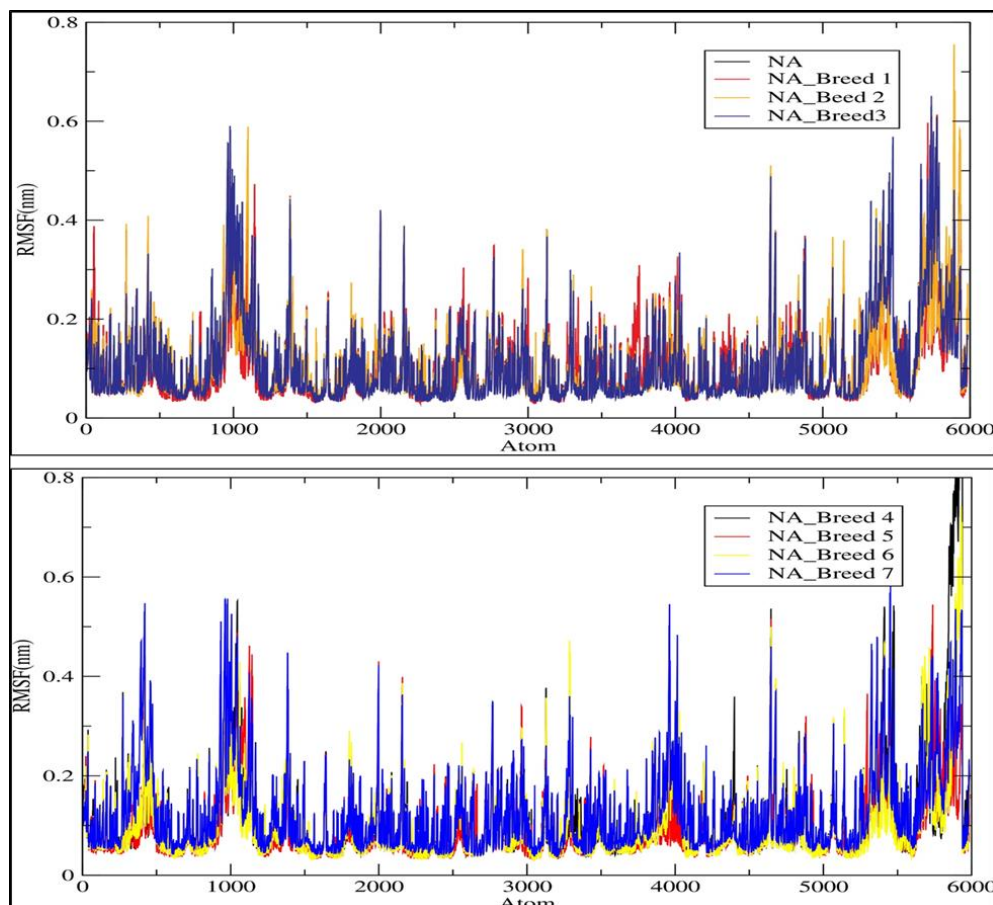


Figure V. 7. Root-mean-square fluctuation (RMSF) of the C-alpha atoms of Neuraminidase (NA) and its complexes with Breeds 1–7.

Table V. 5. The average values of various parameters, including RMSD, RMSF, Rg, and H-bonds.

Complex	Average RMSD (nm)	Average RMSF (nm)	Average Rg (nm)	Average HB (nm)	SASA (nm ²)
NA_Breed 1	0.149	0.105	1.998	9.428	158.812
NA_Breed 2	0.131	0.109	2.009	12.444	158.835
NA_Breed 3	0.135	0.110	2.000	9.196	157.379
NA_Breed 4	0.166	0.115	1.991	9.018	156.121
NA_Breed 5	0.172	0.100	2.003	11.057	157.397
NA_Breed 6	0.172	0.106	1.998	9.964	156.429
NA_Breed 7	0.148	0.123	2.002	12.064	159.806
NA	0.148	0.106	2.003	-	160.245

3.3.2 Radius of Gyration (Rg)

We estimated the radius of gyration (Rg) of each system to assess the stability of the Neuraminidase and its complexes (NA_Breed 1–7) during the 100 ns simulation (**Figure V. 8**). In general, the greater the Rg was, the less compact the Neuraminidase_Breed 1–7 complexes were. During the MD simulation, Rg was employed to determine whether the complexes were stably folded or unfolded. The average Rg value of the Neuraminidase was determined to be in the range of 2.003 nm. Moreover, the average Rg values of NA_Breed 1, NA_Breed 2, NA_Breed 3, NA_Breed 4, NA_Breed 5, NA_Breed 6, and NA_Breed 7 complexes were 1.998, 2.009, 2.000, 1.991, 2.003, 1.998, and 2.002 nm, respectively. As previously stated, if a protein maintained a relatively constant value of Rg throughout the MD simulation, it was considered to be stably folded; if its Rg changed over time, it was considered to be unfolded [31, 32]. Overall, our results suggest that all the tested molecules formed stable complexes with NA and were able to inhibit the vital function of the Neuraminidase.

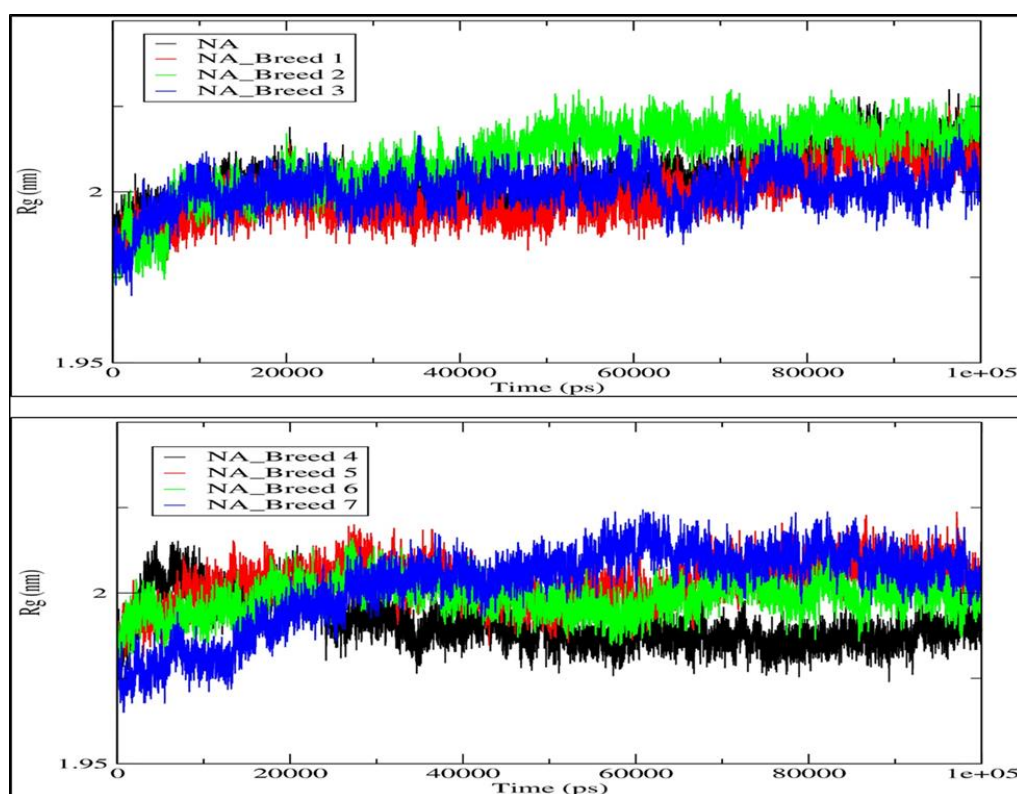


Figure V. 8. Radius of gyration (Rg) of Neuraminidase and its complexes with Breeds 1–7.

3.3.3 Hydrogen Bonding Analysis

We analyzed the hydrogen bond profiles of the seven complexes to obtain a better understanding of the interaction between the breed molecules and Neuraminidase, as shown in **Figure V. 9**. The formation of hydrogen bonds between a ligand and a receptor is necessary for

the ligand–protein complex to be stable [33]. Our analysis revealed that the NA_Breed 2 and NA_Breed 7 complexes formed averages of 12.444 and 12.064 hydrogen bonds during the simulation. The rest of the complexes formed average hydrogen bonds of between 9 and 11. The existence of more polar groups in the breed molecules (Breed 2 and Breed 7) made it possible to form more hydrogen bonds with the active site of the Neuraminidase, in addition to having a strong binding interaction. The rest of the complexes, on the other hand, had some less polar groups and, thus, formed fewer hydrogen bonds with the Neuraminidase receptor. This research indicates that hydrogen-bonding interaction is essential in the stabilization of the breed molecule with Neuraminidase.

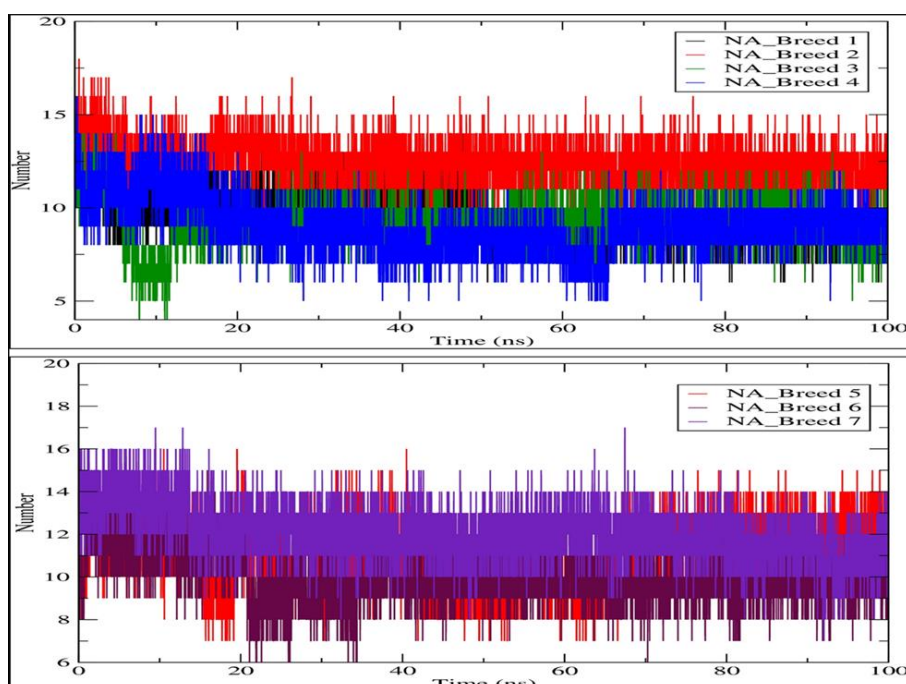


Figure V. 9. Map of hydrogen bond existence of Neuraminidase complexes with Breeds 1–7.

3.3.4 Solvent-Accessible Surface Area (SASA)

A greater SASA value shows that the protein volume is expanding, and a low fluctuation is observed over the simulation duration [29]. The average SASA values of all systems were 158.812, 158.835, 157.379, 156.121, 157.397, 156.429, and 159.806 nm² for NA_Breed 1, NA_Breed 2, NA_Breed 3, NA_Breed 4, NA_Breed 5, NA_Breed 6, and NA_Breed 7, respectively, and 160.245 nm² for the Neuraminidase (**Figure V. 10**). All of these findings suggest that the seven complexes were stable over 100 ns of simulation [28].

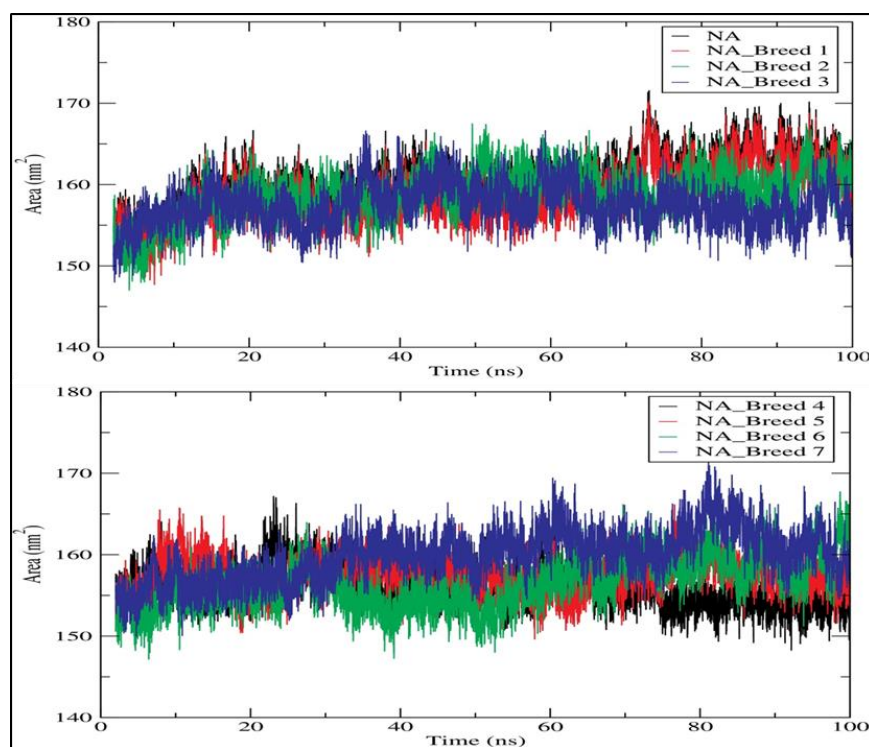


Figure V. 10. Solvent-accessible surface area (SASA) for Neuraminidase and its complexes during 100 ns of simulation.

3.4 MM-PBSA Analysis

The binding free energy of the seven complexes (Neuraminidase_Breed 1–7) was estimated using the MM-PBSA approach applied in Gromacs using MD trajectories. The van der Waals interactions (ΔE_{VDW}), electrostatic interactions (ΔE_{EEL}), nonpolar interactions in a solvated system (ΔE_{PB}), nonpolar contribution of repulsive solute–solvent interactions to the solvation energy (ΔE_{NPOLAR}), nonpolar contribution of attractive solute–solvent interactions to the solvation energy (ΔE_{DISPER}), total gas-phase molecular mechanics energy (ΔG_{GAS}), and total solvation energy (ΔG_{SOLV}) are all included in the total binding free energy. The total binding energies of the seven complexes were found to be within an acceptable range of between -76.06 and -34.96 KJ/mol. **Table V. 6** shows the MM-PBSA results. With reference to binding affinity with Neuraminidase, the NA_Breed 7 complex showed the lowest binding free energy and the highest binding affinity (-76.06 KJ/mol). The binding free energies for NA_Breed 1, NA_Breed 2, NA_Breed 3, NA_Breed 4, NA_Breed 5, and NA_Breed 6 were -55.00 , -74.55 , -47.61 , -44.89 , -34.96 , and -42.48 KJ/mol, respectively. These free energy calculations confirmed the molecular docking result, demonstrating that these breed molecules interacted with the active site of Neuraminidase positively and could be used for the development of new Neuraminidase inhibitors.

Table V. 6. Table representing the ΔE_{VDW} , ΔE_{EEL} , ΔE_{PB} , ΔE_{NPOLAR} , ΔE_{DISPER} , ΔG_{GAS} , ΔG_{SOLV} , and binding energy for Neuraminidase_Breed 1–7 complexes.

Protein–Ligand Complexes	ΔE_{VDW} (KJ/mol)	ΔE_{EEL} (KJ/mol)	ΔE_{PB} (KJ/mol)	ΔE_{NPOLAR} (KJ/mol)	ΔE_{DISPER} (KJ/mol)	ΔG_{GAS} (KJ/mol)	ΔG_{SOLV} (KJ/mol)	Δ_{TOTAL} (KJ/mol)
NA_Breed 1	-11.61	-385.46	319.53	-25.45	47.99	-397.07	342.07	-55.00
NA_Breed 2	-15.34	-400.88	320.91	-29.39	50.15	-416.22	341.67	-74.55
NA_Breed 3	-12.39	-363.90	306.55	-27.48	49.61	-376.28	328.67	-47.61
NA_Breed 4	-17.29	-347.68	297.99	-29.23	51.32	-364.97	320.08	-44.89
NA_Breed 5	-19.90	-328.15	290.05	-29.25	52.29	-348.05	313.10	-34.96
NA_Breed 6	-24.00	-338.25	297.31	-28.89	51.35	-362.25	319.77	-42.48
NA_Breed 7	-10.87	-407.23	321.76	-28.41	48.69	-418.10	342.04	-76.06

Gibbs free-energy landscapes were also produced using the first two PCs to differentiate the conformational modes of the Neuraminidase and its complexes (NA Breeds 1–7). The Gibbs free-energy landscapes examined the orientation of the backbone atom fluctuation in Neuraminidase and Neuraminidase complexes (NA Breeds 7–1) from the MD trajectory. The Gibbs energy landscape plot following 100 ns of simulation, with the extracted structures from low-energy regions for each system, is shown in **Figure V. 11**. The results demonstrate that the NA had a Gibbs free energy of 0–14.4 KJ/mol, while the NA_Breed 1–7 complexes had Gibbs free energies of 0–14.2, 0–14.4, 0–14, 0–15.6, 0–12.9, 0–15, and 0–14.1 KJ/mol, respectively.

The blue, cyan, and green areas of the plot represent low-energy states with extremely stable protein conformations, whereas the red area represents a high-energy conformation. The energy landscape had numerous distinct minima that represented metastable structural states separated by a modest energy barrier. The binding of all breed molecules produced the most metastable conformational designs, with regional minima dispersed to approximately two to three areas of the energy landscape. In comparison to Neuraminidase alone, the smaller and more concentrated blue minimal-energy regions in NA_Breed 1, NA_Breed 2, and NA_Breed 3 imply extremely stable complexes. Furthermore, the structures (Neuraminidase conformations) were found to be similar for all systems. The results demonstrate that the seven types of molecules formed very stable complexes with Neuraminidase.

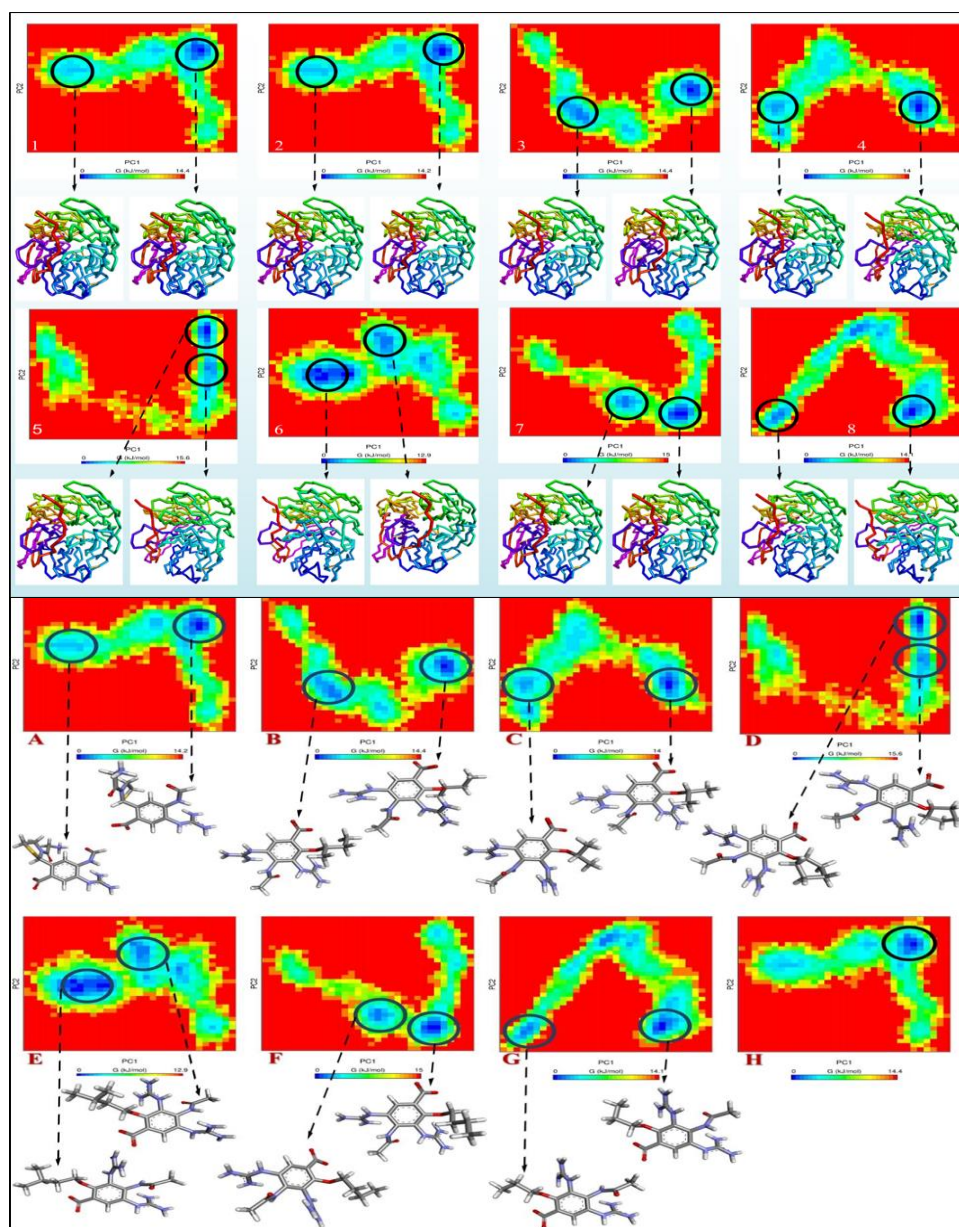
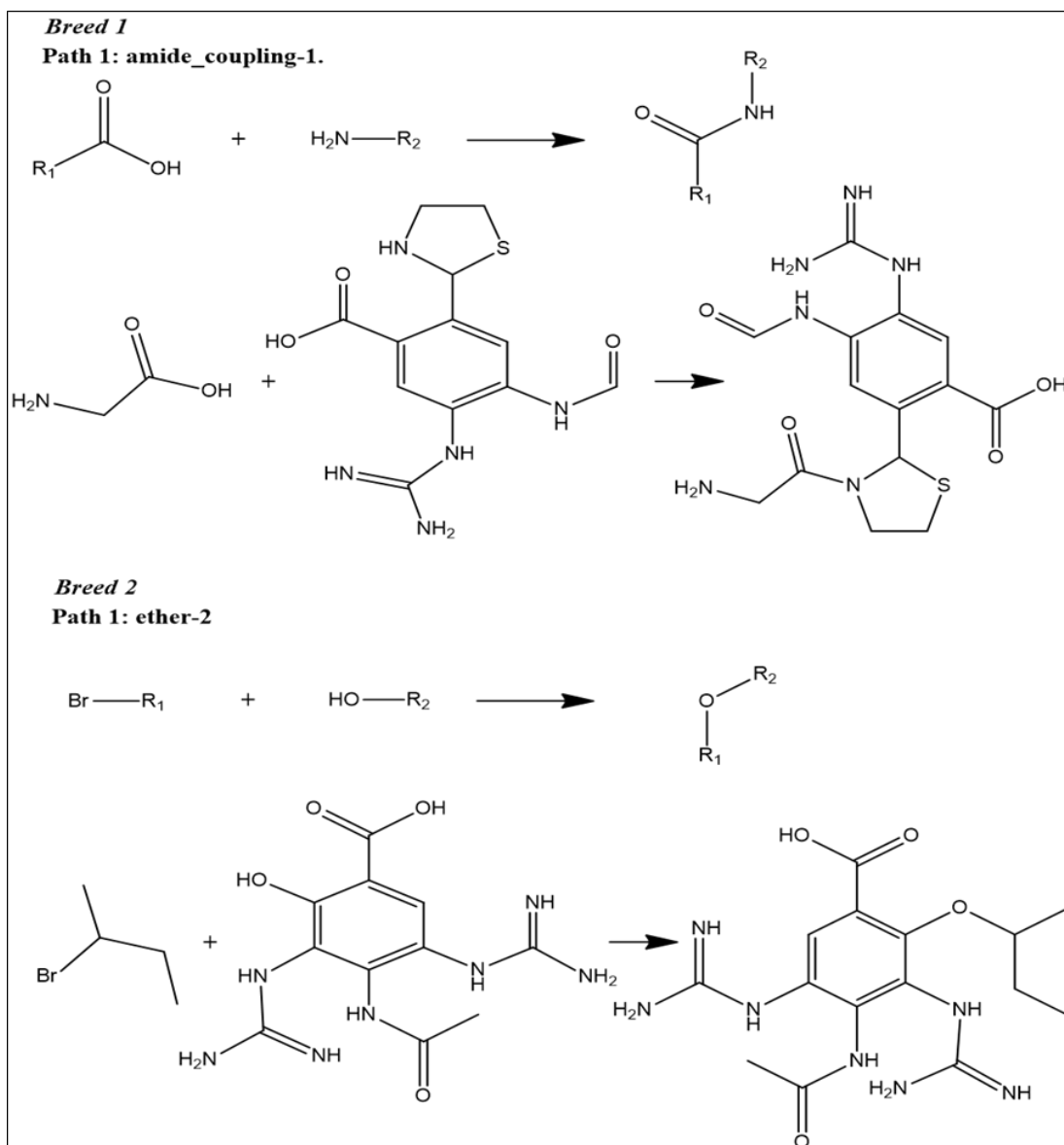


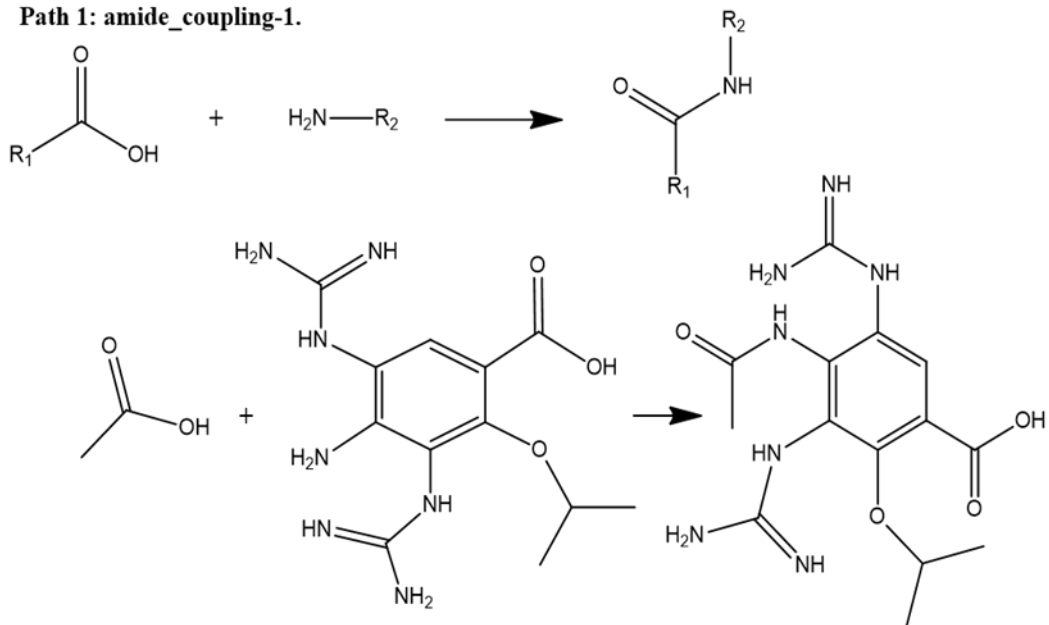
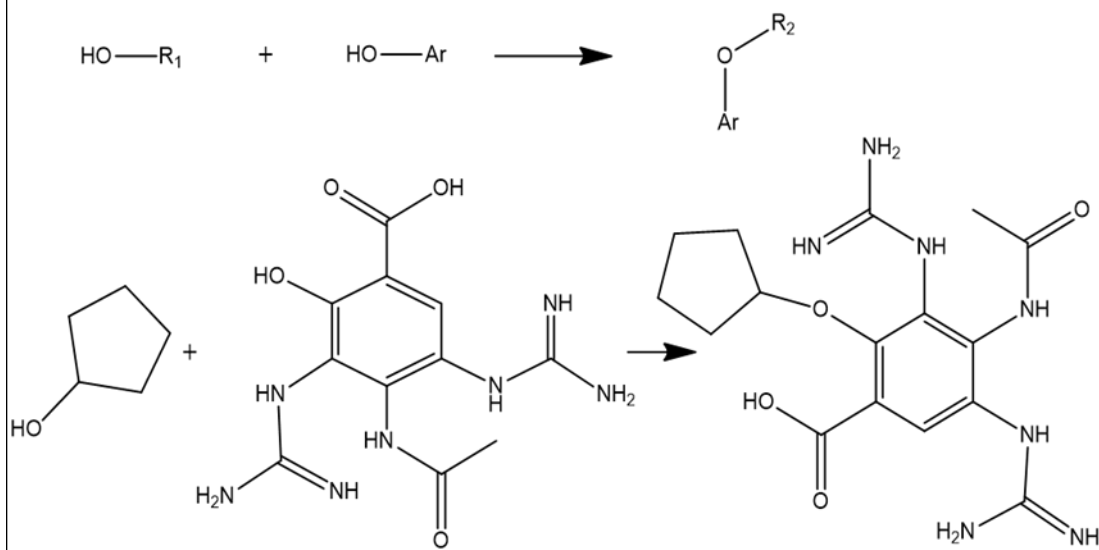
Figure V. 11. The Gibbs energy landscape maps over 100 ns of simulations for (A) NA, (B) NA_Breed 1, (C) NA_Breed 2, (D) NA_Breed 3, (E) NA_Breed 4, (F) NA_Breed 5, (G) NA_Breed 6, and (H) NA_Breed 7, with the extracted structures from the low-energy areas (in blue).

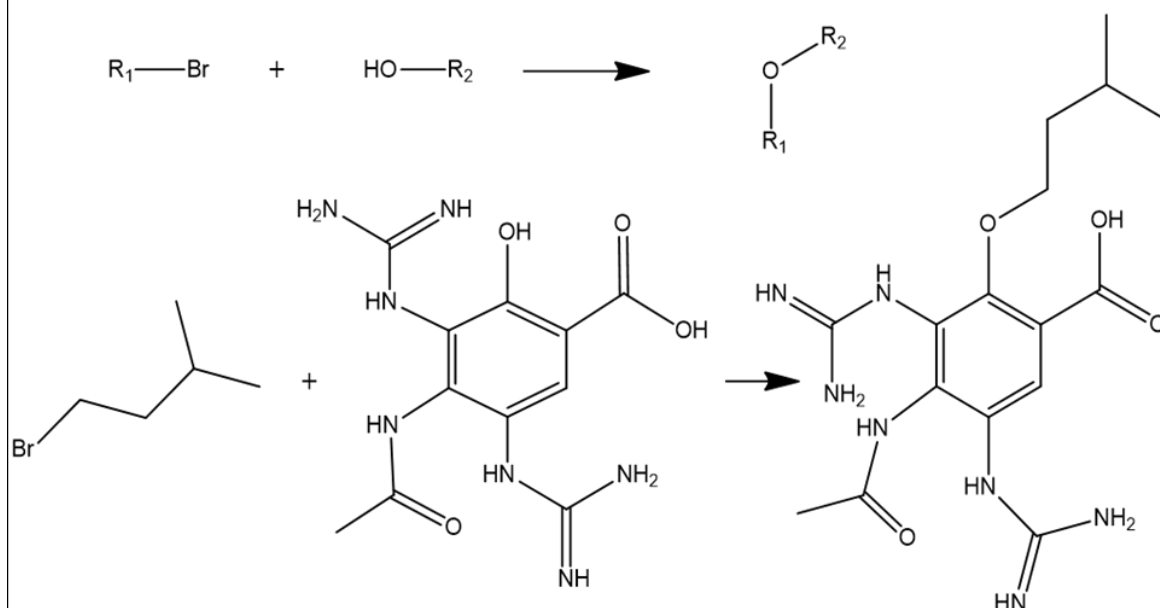
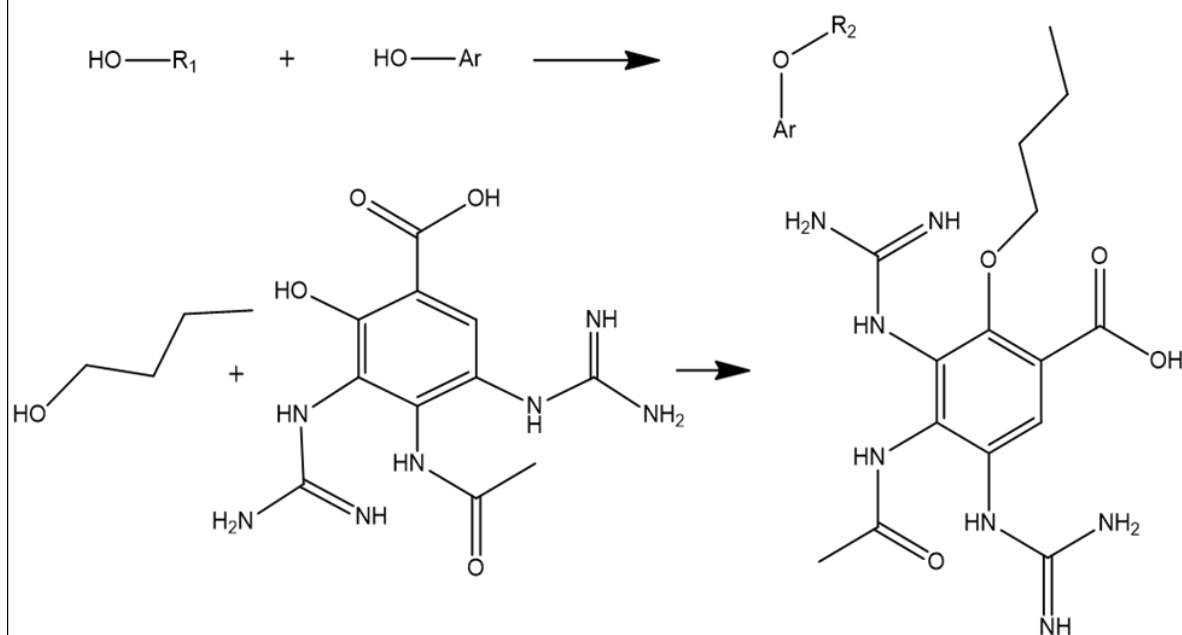
3.5 Reaction-Based Enumeration

At this step, we used reaction-based enumeration to predict the synthetic pathways of the breed molecules (Breeds 1–7). It is another Schrödinger tool for predicting the synthetic pathway of every molecule using a retro-synthetic methodology. The reaction enumeration tool showed that

the amide coupling, ether, and Mitsunobu reactions could be utilized to synthesize all of the breed molecules, as described in **Figure V. 12**.



Breed 3**Path 1: amide_coupling-1.****Breed 4****Path 1: Mitsunobu-1**

Breed 5**Path 1: ether-2****Breed 6****Path 1: Mitsunobu-1**

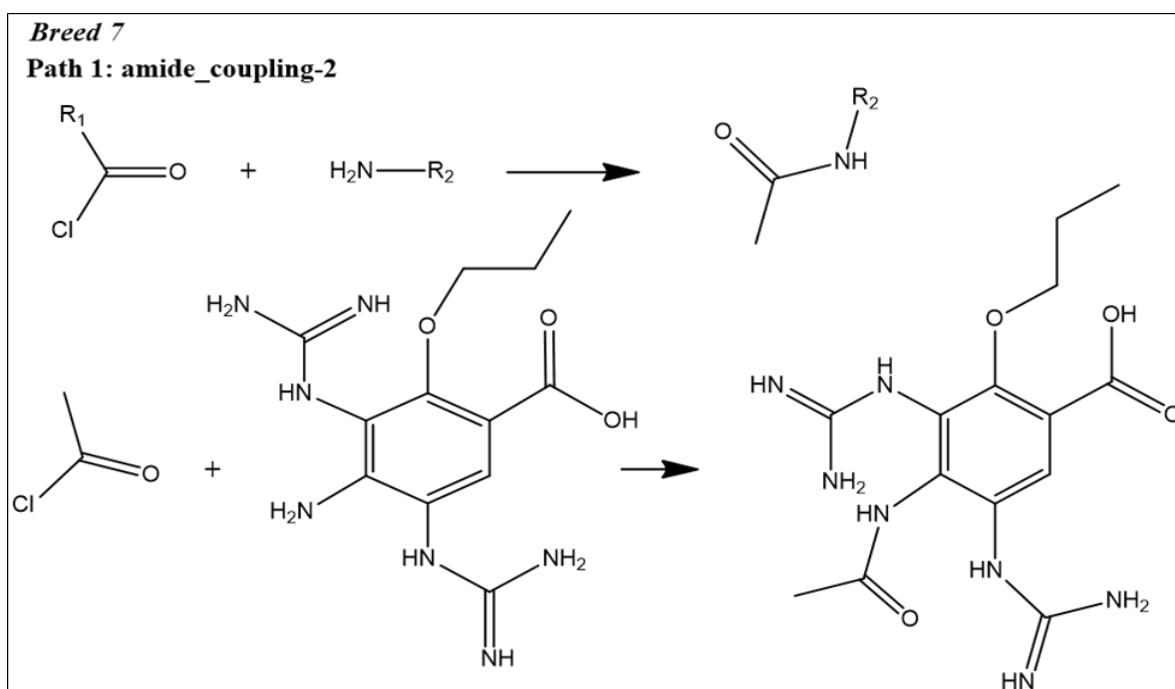


Figure V. 12. Predicted synthetic pathways of all the breed molecules (Breeds 1–7).

4. Discussion

Neuraminidase is a key target in virology and the development of potent anti-influenza medicines. By inhibiting the biological activity of Neuraminidase, the influenza virus is prevented from moving to further uninfected host cells and is eliminated. The primary objective was to create prospective novel compounds with anti-influenza activity that is more effective than existing anti-influenza drugs (*Zanamivir*, *Oseltamivir*, and *Peramivir*). Compared with the inhibitory power of clinical Neuraminidase inhibitors, all seven designed molecules bound effectively to the Neuraminidase receptor, where the proposed molecules attached to other amino acids forming the active site, such as Asp152 and Arg372, which explains the good inhibitory activity of the proposed molecules. The contribution of 2-amino-1-(2-methylthiazolidin-3-yl) ethanone, 2-methoxybutane, 2-methoxypropane, methoxycyclopentane, 1-methoxy-3-methylbutane, 1-methoxybutane, and 1-methoxypropane groups via the interaction of hydrogen bonds can again explain the good inhibitory activity of the developed molecules against Neuraminidase. However, these chemical groups had different functions, and they interacted effectively with the essential amino acids that composed the active site, showing that the suggested compounds had a high affinity for the Neuraminidase receptor. As pharmacokinetic profiles, the proposed molecules had good permeability toward the membrane bilayer (LogP between -1.55 and 0.24) and good aqueous solubility, which allowed the solubilization of these molecules in the intracellular medium. The hepatic metabolism of the designed compounds was quick and did not produce toxic substances, and no inhibition of cytochrome P450, such as CYP 3A4, was observed. Because of their high

water solubility (LogS between -2.28 and 0.77), all of the designed compounds would be quickly removed by the kidneys at the nephron level. In terms of potential toxicity, we found no evidence of any toxicity produced by any of the proposed compounds. All of the aforementioned results indicate that their pharmacokinetic profile is optimal. When we examined the stability of the designed molecules within the Neuraminidase receptor using molecular dynamics simulations, we clearly saw insignificant atomic mobility and the continuation of structural stability. During 100 ns of simulation, the seven proposed compounds had average RMSD values ranging from 0.131 to 0.172 nm. In addition, the average RMDF was between 0.1 and 0.123 nm. For the validation of the molecular docking results, the MM-PBSA calculations were in line with the molecular docking study, indicating that all of the molecules proposed formed more stable complexes with the Neuraminidase active site, with binding free energies between -76.06 and -34.96 KJ/mol. At the molecular level, Gibbs free-energy landscapes again showed the small dynamic shift of the Neuraminidase and its complexes, which confirms the extent of structural stability and the preservation of the initial configuration of all these complexes. Through the experimental examination, our outcomes indicate that the proposed compounds can be synthesized in a chemical laboratory, and it is worth noting that all of the proposed molecules are simple to manufacture using traditional mechanisms. This will make it easier to evaluate and estimate the effectiveness of the designed compounds to inhibit the biological function of Neuraminidase in vitro and in vivo. The results of this study will possibly help researchers in the development of anti-influenza medications and virology.

5. Conclusions

Developing new Neuraminidase inhibitors is vital for combating evolving flu strains, enhancing treatment options, reducing resistance, and safeguarding global public health against influenza outbreaks. The objective of this research was to identify novel inhibitor molecules against the Neuraminidase of influenza. To develop novel Neuraminidase inhibitors, we used a breed-based de novo approach. According to the docking studies, seven breed molecules (Breeds 1–7) demonstrated high stability within the Neuraminidase receptor compared to the clinical Neuraminidase inhibitors (*Zanamivir*, *Oseltamivir* and *Peramivir*). On the other hand, to reach the pharmacological target, the pharmacokinetics of the seven breed compounds were investigated, and the results show that they have excellent pharmacokinetic profiles, such as bioavailability and permeability toward biological membranes. The molecular dynamics simulations for 100 ns revealed that the seven breed molecules (Breeds 1–7) were particularly stable in the active site of Neuraminidase. In addition, MM-PBSA computations demonstrated that the complexes were very stable throughout the duration of the simulation. This research can contribute to the development

of novel and potent Neuraminidase inhibitor drugs for the treatment of influenza and could give researchers the opportunity to examine these breed molecules for the treatment of influenza and its symptoms. Finally, the future of Neuraminidase inhibitors for the flu involves improved efficacy, reduced resistance, and personalized treatments, aiding in better management and prevention of influenza outbreaks.

6. References

- [1] Kalil, A. C., & Thomas, P. G. (2019). Influenza virus-related critical illness: *pathophysiology and epidemiology*. *Critical care*, 23, 1-7.
- [2] Moghadami, M. (2017). A narrative review of influenza: a seasonal and pandemic disease. *Iranian journal of medical sciences*, 42(1), 2.
- [3] Świerczyńska, M., Mirowska-Guzel, D. M., & Pindelska, E. (2022). Antiviral drugs in influenza. *International journal of environmental research and public health*, 19(5), 3018.
- [4] Ghaffari, H., Tavakoli, A., Moradi, A., Tabarraei, A., Bokharaei-Salim, F., Zahmatkeshan, M., ... & Ataei-Pirkooh, A. (2019). Inhibition of H1N1 influenza virus infection by zinc oxide nanoparticles: another emerging application of nanomedicine. *Journal of biomedical science*, 26(1), 1-10.
- [5] Matrosovich, M. N., Matrosovich, T. Y., Gray, T., Roberts, N. A., & Klenk, H. D. (2004). Neuraminidase is important for the initiation of influenza virus infection in human airway epithelium. *Journal of virology*, 78(22), 12665-12667.
- [6] Jefferson, T., Demicheli, V., Di Pietrantonj, C., Rivetti, D., & Cochrane Acute Respiratory Infections Group. (1996). Amantadine and rimantadine for influenza A in adults. *Cochrane Database of Systematic Reviews*, 2012(7).
- [7] Kaiser, L., Wat, C., Mills, T., Mahoney, P., Ward, P., & Hayden, F. (2003). Impact of oseltamivir treatment on influenza-related lower respiratory tract complications and hospitalizations. *Archives of internal medicine*, 163(14), 1667-1672.
- [8] Pierce, A. C., Rao, G., & Bemis, G. W. (2004). BREED: Generating novel inhibitors through hybridization of known ligands. Application to CDK2, p38, and HIV protease. *Journal of medicinal chemistry*, 47(11), 2768-2775.
- [9] Ho, C.M.; Marshall, G.R. SPLICE: A program to assemble partial query solutions from three-dimensional database searches into novel ligands. *J. Comput.-Aided Mol. Des.* 1993, 7, 623–647
- [10] Kaczor, A. A., Targowska-Duda, K. M., Patel, J. Z., Laitinen, T., Parkkari, T., Adams, Y., ... & Poso, A. (2015). Comparative molecular field analysis and molecular dynamics studies of α/β hydrolase domain containing 6 (ABHD6) inhibitors. *Journal of molecular modeling*, 21, 1-16.
- [11] Opoku, F., Govender, P. P., Pooe, O. J., & Simelane, M. B. (2019). Evaluating iso-mukaadial acetate and ursolic acid acetate as plasmodium falciparum hypoxanthine-guanine-xanthine phosphoribosyltransferase inhibitors. *Biomolecules*, 9(12), 861.

- [12] Usha, T., Shanmugarajan, D., Goyal, A. K., Kumar, C. S., & Middha, S. K. (2017). Recent updates on computer-aided drug discovery: time for a paradigm shift. *Current topics in medicinal chemistry*, 17(30), 3296-3307.
- [13] Gubareva, L. V., Sleeman, K., Guo, Z., Yang, H., Hodges, E., Davis, C. T., ... & Stevens, J. (2017). Drug susceptibility evaluation of an influenza A (H7N9) virus by analyzing recombinant neuraminidase proteins. *The Journal of infectious diseases*, 216(suppl_4), S566-S574.
- [14] Roos, K.; Wu, C.; Damm, W.; Reboul, M.; Stevenson, J.M.; Lu, C.; Dahlgren, M.K.; Mondal, S.; Chen, W.; Wang, L. OPLS3e: Extending force field coverage for drug-like small molecules. *J. Chem. Theory Comput.* 2019, 15, 1863–1874
- [15] Daina, A., Michielin, O., & Zoete, V. (2017). SwissADME: a free web tool to evaluate pharmacokinetics, drug-likeness and medicinal chemistry friendliness of small molecules. *Scientific reports*, 7(1), 42717.
- [16] Banerjee, P., Eckert, A. O., Schrey, A. K., & Preissner, R. (2018). ProTox-II: a webserver for the prediction of toxicity of chemicals. *Nucleic acids research*, 46(W1), W257-W263.
- [17] Raies, A. B., & Bajic, V. B. (2016). In silico toxicology: computational methods for the prediction of chemical toxicity. *Wiley Interdisciplinary Reviews: Computational Molecular Science*, 6(2), 147-172.
- [18] Van Der Spoel, D., Lindahl, E., Hess, B., Groenhof, G., Mark, A. E., & Berendsen, H. J. (2005). GROMACS: fast, flexible, and free. *Journal of computational chemistry*, 26(16), 1701-1718.
- [19] Zoete, V., Cuendet, M. A., Grosdidier, A., & Michielin, O. (2011). SwissParam: a fast force field generation tool for small organic molecules. *Journal of computational chemistry*, 32(11), 2359-2368.
- [20] Ahmad, S. S., Sinha, M., Ahmad, K., Khalid, M., & Choi, I. (2020). Study of Caspase 8 inhibition for the management of Alzheimer's disease: a molecular docking and dynamics simulation. *Molecules*, 25(9), 2071.
- [21] Rawat, R., Kant, K., Kumar, A., Bhati, K., & Verma, S. M. (2021). HeroMDAnalysis: an automagical tool for GROMACS-based molecular dynamics simulation analysis. *Future Medicinal Chemistry*, 13(05), 447-456.
- [22] Kumari, M., Singh, R., & Subbarao, N. (2022). Exploring the interaction mechanism between potential inhibitor and multi-target Mur enzymes of mycobacterium tuberculosis using molecular

docking, molecular dynamics simulation, principal component analysis, free energy landscape, dynamic cross-correlation matrices, vector movements, and binding free energy calculation. *Journal of Biomolecular Structure and Dynamics*, 40(24), 13497-13526.

[23] Singh, N., & Siddiqi, M. I. (2017). Computational evaluation of glutamine synthetase as drug target against infectious diseases: molecular modeling, substrate-binding analysis, and molecular dynamics simulation studies. *Medicinal Chemistry Research*, 26, 450-460.

[24] Kuzmanic, A., & Zagrovic, B. (2010). Determination of ensemble-average pairwise root mean-square deviation from experimental B-factors. *Biophysical journal*, 98(5), 861-871.

[25] Konze, K. D., Bos, P. H., Dahlgren, M. K., Leswing, K., Tubert-Brohman, I., Bortolato, A., ... & Bhat, S. (2019). Reaction-based enumeration, active learning, and free energy calculations to rapidly explore synthetically tractable chemical space and optimize potency of cyclin-dependent kinase 2 inhibitors. *Journal of chemical information and modeling*, 59(9), 3782-3793.

[26] Patel, H. M., Shaikh, M., Ahmad, I., Lokwani, D., & Surana, S. J. (2021). BREED based de novo hybridization approach: generating novel T790M/C797S-EGFR tyrosine kinase inhibitors to overcome the problem of mutation and resistance in non small cell lung cancer (NSCLC). *Journal of Biomolecular Structure and Dynamics*, 39(8), 2838-2856.

[27] Alqahtani, S. (2017). In silico ADME-Tox modeling: progress and prospects. *Expert opinion on drug metabolism & toxicology*, 13(11), 1147-1158.

[28] Maowa, J., Hosen, M. A., Alam, A., Rana, K. M., Fujii, Y., Ozeki, Y., & Kawsar, S. M. A. (2021). Pharmacokinetics and molecular docking studies of uridine derivatives as SARS-COV-2 Mpro inhibitors. *Physical Chemistry Research*, 9(3), 385-412.

[29] Rana, K. M., Maowa, J., Alam, A., Dey, S., Hosen, A., Hasan, I., ... & Kawsar, S. M. (2021). In silico DFT study, molecular docking, and ADMET predictions of cytidine analogs with antimicrobial and anticancer properties. *In Silico Pharmacology*, 9, 1-24.

[30] Ghasemi, F., Zomorodipour, A., Karkhane, A. A., & Khorramizadeh, M. R. (2016). In silico designing of hyper-glycosylated analogs for the human coagulation factor IX. *Journal of Molecular Graphics and Modelling*, 68, 39-47.

[31] Kawsar, S. M., Kumer, A., Munia, N. S., Hosen, M. A., Chakma, U., & Akash, S. (2022). Chemical descriptors, PASS, molecular docking, molecular dynamics and ADMET predictions of glucopyranoside derivatives as inhibitors to bacteria and fungi growth. *Organic Communications*, 15(2), 203.

[32] Chen, D., Oezguen, N., Urvil, P., Ferguson, C., Dann, S. M., & Savidge, T. C. (2016). Regulation of protein-ligand binding affinity by hydrogen bond pairing. *Science advances*, 2(3), e1501240.

[33] Islam, R.; Parves, M.R.; Paul, A.S.; Uddin, N.; Rahman, M.S.; Mamun, A.A.; Hossain, M.N.; Ali, M.A.; Halim, M.A. A molecular modeling approach to identify effective antiviral phytochemicals against the main protease of SARS-CoV-2. *J. Biomol. Struct. Dyn.* 2021, 39, 3213–3224.

***Chapter VI: Comparative Molecular Field Analysis (CoMFA),
Molecular Docking and ADMET Study on Thiazolidine-4-
carboxylic acid Derivatives as New Neuraminidase Inhibitors***

1. Introduction

Influenza is a respiratory disease caused by the *Orthomyxoviridae* virus family. Every year, influenza viruses generate seasonal epidemics that mostly affect the adult population. 10-30% of sick people are hospitalized, and 3-15% die [1]. Influenza symptoms include a sudden onset of high temperature, aching muscles, headache, severe exhaustion, a nonproductive cough, a sore throat, and a runny nose [2]. The variation of influenza viruses can develop in a pandemic, posing a major danger to public health [3]. Neuraminidase (NA) is a glycoprotein located in the envelope of the influenza virus that plays a critical role in the process of infecting and spreading amongst human host cells [4]. Neuraminidase is an important target of drug design for the treatment of influenza infections because to its involvement in viral propagation and its largely preserved active site [5]. Neuraminidase inhibitors (NAI) represent the only extensively approved class of antiviral medications used for the treatment and prevention of seasonal influenza [6]. *Oseltamivir* is widely utilized, whereas *Zanamivir*, *Peramivir*, and *Laninamivir* are used in fewer nations concurrently [7]. NAIs are the most often given anti-influenza medications nowadays, they have been shown to be beneficial in speeding viral clearance, lowering clinical disease duration, and decreasing hospital stay and death [8].

Computer-Aided Drug Design (CADD) is the process of using computer methods and resources to design and identify novel potential pharmaceutical drugs [9]. A QSAR is simply a mathematical equation that is derived from a set of molecules with a known activity using computational techniques. A variety of statistical approaches and computed molecular descriptors may be employed to identify the exact form of the relationship between structure and activity, and this relationship is subsequently employed to predict the activity of new compounds [10, 11]. QSAR investigations are based on the notion that changes in bioactivity are related with structural and molecular variation in a group of molecules [12]. The three-dimensional quantitative structure-activity relationship is one of the most successful and valuable strategies for the development and design of potent medications (3D-QSAR) [13].

The goal of this study was to design new Neuraminidase inhibitors for the treatment of influenza. The goals of this research are to develop new Neuraminidase inhibitors for the treatment of influenza. In a 3D-QSAR study based on a series of biologically active thiazolidine-4-carboxylic acid derivatives, we used comparative molecular field analysis (CoMFA) to find a statistically significant relationship between the three-dimensional structure of the molecules and their biological activity. After designing these molecules, we performed a docking study to arrange them in the active site of Neuraminidase based on their stability. To identify the molecules with

the best pharmacological properties, the compounds identified were also subjected to in silico absorption, distribution, metabolism, elimination, and toxicity (ADMET) property testing. We used ProToxII to assess the potential toxicity of all proposed molecules. Finally, we provided a reaction mechanism for the synthesis of each of these proposed compounds for future research into Neuraminidase inhibitors.

2. Materials and Methods

2.1 Experimental Databases

A set of twenty-five thiazolidine-4-carboxylic acid derivatives reported by *Asadollah, M et al and Yu. L et al* were chosen for molecular modelling studies [13, 15]. Thiazolidine-4-carboxylic acid is a cyclic sulphur amino acid with a molecular structure similar to proline, hence the name thioproline. The thiazolidine-4-carboxylic acid sulfhydryl group is essential in metabolism as an antioxidant protector and in detoxification processes [16]. Inhibitory activity was provided as IC₅₀ values, which were then converted to pIC₅₀ values [$pIC_{50} = -\log (IC_{50})$] and used in 3D-QSAR experiments. All experimental data were divided into two categories. a training set for model generation and a test set for external evaluation of model accuracy; the training set contains twenty molecules and the test set contains five molecules. The variability of bioactivity rates and biological properties was also taken into account when randomly partitioning the training and test sets [17]. (**Table VI. 1**).

2.2 Structure Preparation and Alignment

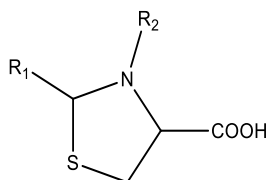
The SYBYL-X 2.0 software suite (Certara Enhances SYBYL-X Drug Design and Discovery Software Suite) was used to construct and optimise the structures of the twenty-five compounds with energy minimization [18]. The tripos standard force field was used, and a condition of 0.01 kcal/(mol) in Gasteiger-Hückel charge atomic partial was established. The tripos standard force field was used, and a condition of 0.01 kcal/(mol) in Gasteiger-Hückel charge atomic partial was established [19, 20]. Molecular alignment is the most sensitive component, and it has a significant impact on 3D-QSAR models [21]. The structures that have been minimised and aligned are used to create the 3D-QSAR model.

2.3 Generation of 3D-QSAR by CoMFA

Our goal was to develop a predictive 3D-QSAR model using comparative molecular field analysis (CoMFA). The CoMFA method is a useful 3D-QSAR tool that has been used successfully in several medicinal chemistry studies. One of the significant advantages of this approach is its immediate application in the examination of any structure-dependent biological characteristics [21]. The CoMFA theory states that differences in a target property between chemicals are frequently associated with changes in the noncovalent fields that surround those structures. These fields, which are the electrostatic (Coulombic) and steric (Lennard-Jones) fields, are computed at regular intervals within a predetermined area [23]. Steric and electrostatic descriptors were

generated using a tripos force field and an ordered divergence grid of 2 Å with a cutoff energy value of 30 kcal/mol [24]. All other parameters have been reset to their default settings.

Table VI. 1. A Tabular analysis of relationship between structures of compounds and experimental Activity.



Compound	R ₁	R ₂	pIC ₅₀
01	C ₆ H ₅ –	H	4.672
02	(2-OH)C ₆ H ₅ –	H	4.695
03	(2-COOH)C ₆ H ₅ –	H	4.742
04	(4-CN)C ₆ H ₅ –	H	4.631
05	(2-NO ₂)C ₆ H ₅ –	H	4.648
06	(2-OH, 3-CH ₃ O)C ₆ H ₅ –	H	4.91
07	C ₄ H ₃ O–	H	4.366
08	C ₆ H ₅ –	ClCH ₂ CO–	5.123
09	(2-OH)C ₆ H ₅ –	ClCH ₂ CO–	5.234
10	(2-COOH)C ₆ H ₅ –	ClCH ₂ CO–	4.971
11	(4-CN)C ₆ H ₅ –	ClCH ₂ CO–	5.063
12	(2-NO ₂)C ₆ H ₅ –	ClCH ₂ CO–	5.116
13	(2-OH, 3-CH ₃ O)C ₆ H ₅ –	ClCH ₂ CO–	5.101
14	C ₄ H ₃ O–	ClCH ₂ CO–	4.889
15	C ₆ H ₅ –	PhCH ₂ CO–	5.917
16	(2-OH)C ₆ H ₅ –	PhCH ₂ CO–	6.187
17	(2-COOH)C ₆ H ₅ –	PhCH ₂ CO–	5.717
18	(4-CN)C ₆ H ₅ –	PhCH ₂ CO–	5.607
19	(2-OH, 3-CH ₃ O)C ₆ H ₅ –	PhCH ₂ CO–	5.79
20	C ₄ H ₃ O–	PhCH ₂ CO–	5.539
21	C ₆ H ₅ –	NH ₂ CH ₂ CO–	6.276
22	(2-OH)C ₆ H ₅ –	NH ₂ CH ₂ CO–	6.678
23	(2-COOH)C ₆ H ₅ –	NH ₂ CH ₂ CO–	6.553
24	(2-OH, 3-CH ₃ O)C ₆ H ₅ –	NH ₂ CH ₂ CO–	6.854
25	C ₄ H ₃ O–	NH ₂ CH ₂ CO–	6.009

2.4 PLS analysis and Validations

PLS regression is a well-established multivariate method that has been widely used in a variety of chemical fields [25]. A PLS model was built for the training set, and the model was validated using the remaining test set. To be trustworthy and predictive, 3D-QSAR models should be validated by producing correct predictions for external data sets that were not used in the

model's development [10]. PLS can assess complex structure-activity data more realistically and efficiently determine how molecular structure affects biological activity [26]. As a result, we estimate the model's predictive power using external validation. A QSAR model is predictive, according to Golbraikh and Tropsha, if the following conditions are met [27].

$$R^2_{\text{pred}} > 0.6, \quad [r^2 - r^2_0] / r^2 < 0.1, \quad [r^2 - r'^2_0] / r^2 < 0, \quad \text{and} \quad 0.85 < k < 1.15 \text{ or } 0.85 < k' < 1.15$$

Roy and Paul developed the term r^2_m to verify the external predictability of the chosen model [27]. An r^2_m value greater than 0.5 may be interpreted as indicating good external predictability.

The 3D-QSAR model was also validated using a Y-randomization test, which eliminates chance correlations between dependent and independent variables [28]. If the randomised models' correlation coefficient values R^2 and Q^2 are less than the original non-randomized model's R^2 and Q^2 , we can be confident that the QSAR models are robust and not the result of random correlation [29].

2.5 Molecular Docking

Molecular docking is a computational tool for determining the structure of a protein-ligand interaction automatically [30]. The true docking process, on the other hand, is so adaptable that receptors and ligands must adjust their conformation to match each other well [31]. This technique has been widely used in the drug design research sector in recent years, and it also significantly increases efficiency and lowers research costs [32]. One of the most famous molecular docking software packages, AutoDock Vina, combines a fast stochastic conformational search method with accurate and well-rated force-field-based and empirical scoring systems [33, 34]. The structure of Neuraminidase was obtained from the RCSB database (PDB Id: 4ks2) Influenza Neuraminidase in complex with an antiviral compound (1SJ) [35] as shown in the **Figure VI. 1**. In 1999, the Food and Drug Administration (FDA) approved *Oseltamivir* as a Neuraminidase inhibitor [36]. As a second reference ligand, we docked *Oseltamivir* into the Neuraminidase protein pocket. The receptors were then processed with UCSF Chimera 1.16 to remove non-standard residues before being docked using AutoDock Vina 1.1.2 [37]. The AUTOGUID system, which calculates ligand binding energy with their receptor, was used to define the three-dimensional grid [38]. The active site is located at coordinates ($x = -23.4893 \text{ \AA}$, $y = 20.7720 \text{ \AA}$, and $z = -9.6124 \text{ \AA}$), and the grid size is $x = 26.4819$, $y = 25.6602$, and $z = 24.2547$. The docking results were visualised using the Biovia discovery studio visualizer [39].

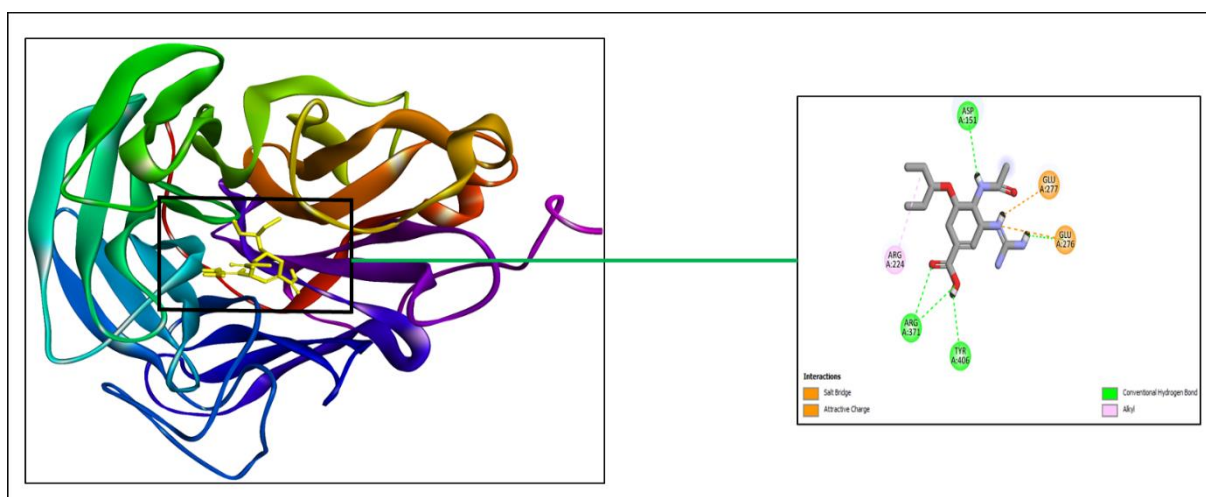


Figure VI. 1. Binding interaction illustration of Neuraminidase in complex with 1SJ.

2.6 Prediction of ADMET Properties

Following the molecular docking of the designed compounds for influenza Neuraminidase inhibition, the absorption, distribution, metabolism, and elimination are estimated using the SwissADME web server [40]. Furthermore, the ProToxII-II VEGA QSAR platforms were used to assess potential toxicity [41, 42].

3. Results and Discussions

3.1 Molecular alignment of dataset

Molecular alignment is one of the most important factors influencing the performance of 3D-QSAR approaches [43]. The database was aligned for this phase using SYBYL-X 2.0 software, with the most active compound (compound 24, pIC₅₀ = 6.780) serving as the structural template for the other compounds' alignment. **Figure VI. 2** shows the alignment of all molecules in the database (training and test set).

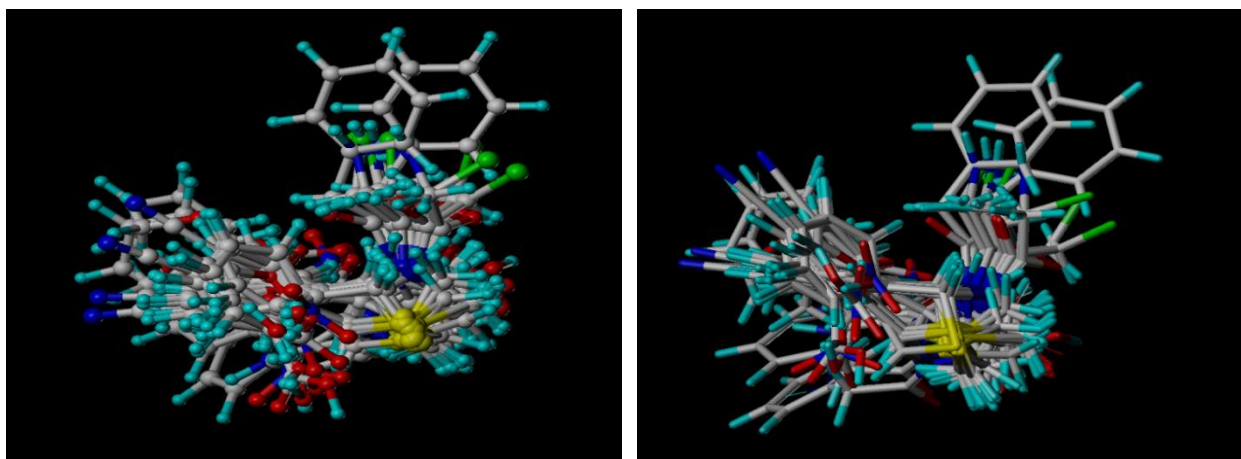


Figure VI. 2. The alignment of all molecules in the database.

3.2 3D-QSAR Model and Validations

The comparative molecular field method is used to establish a quantifiable link between the 3D structure of the compounds and their biological activity. **Table VI. 2** shows the statistical results of the PLS analysis for the CoMFA model. This CoMFA model has an extremely high R^2 value of 0.997, the optimal number of components of 5, and an F-value of 883.433. Furthermore, the built model had a cross validated coefficient of Q^2 of 0.708, with a very small standard error of estimation (SEE) of 0.050. The significant R^2 and Q^2 values, as well as the low SEE value, suggest that the CoMFA model developed is stable and has excellent predictive power.

Table VI. 2. Statistical parameters of partial Least Squares (PLS) analysis on the comparative molecular field analysis (CoMFA) model.

Model	Q^2	R^2	SEE	F	N	Fraction	
						Steric	Electrostatic
CoMFA	0.708	0.997	0.050	883.433	5	0.412	0.588

Second, **Table VI. 3** shows the results of the CoMFA model's external validation. A high R^2_{pred} value greater than 0.6 indicates that the CoMFA model has good predictive power, and an R^2_m value of 0.778 indicates that the model has good predictive ability. Also, all values of r^2_0 and r'^2_0 are close to r^2 , $[r^2-r^2_0]/r^2$ and $[r^2-r'^2_0]/r^2$ have values very less than 0.1.

Table VI. 3. Assessing the predictive performance by statistical parameters of external validation for the comparative molecular field analysis (CoMFA) model.

R^2_{pred}	r^2	r^2_0	r'^2_0	K	K'	$[r^2-r^2_0]/r^2$	$[r^2-r'^2_0]/r^2$	r^2_m
0.674	0.957	0.922	0.955	1.016	0.982	0.036	0.001	0.778

The PLS results and the external validation show that the CoMFA model is reliable and statistically significant. The actual and predicted pIC50 values, as well as the residual values determined by the CoMFA model, are shown in Table S2. **Figure VI. 3**, depicts the excellent correlation between actual and predicted activity, demonstrating the 3D-QSAR model's superior predictive ability.

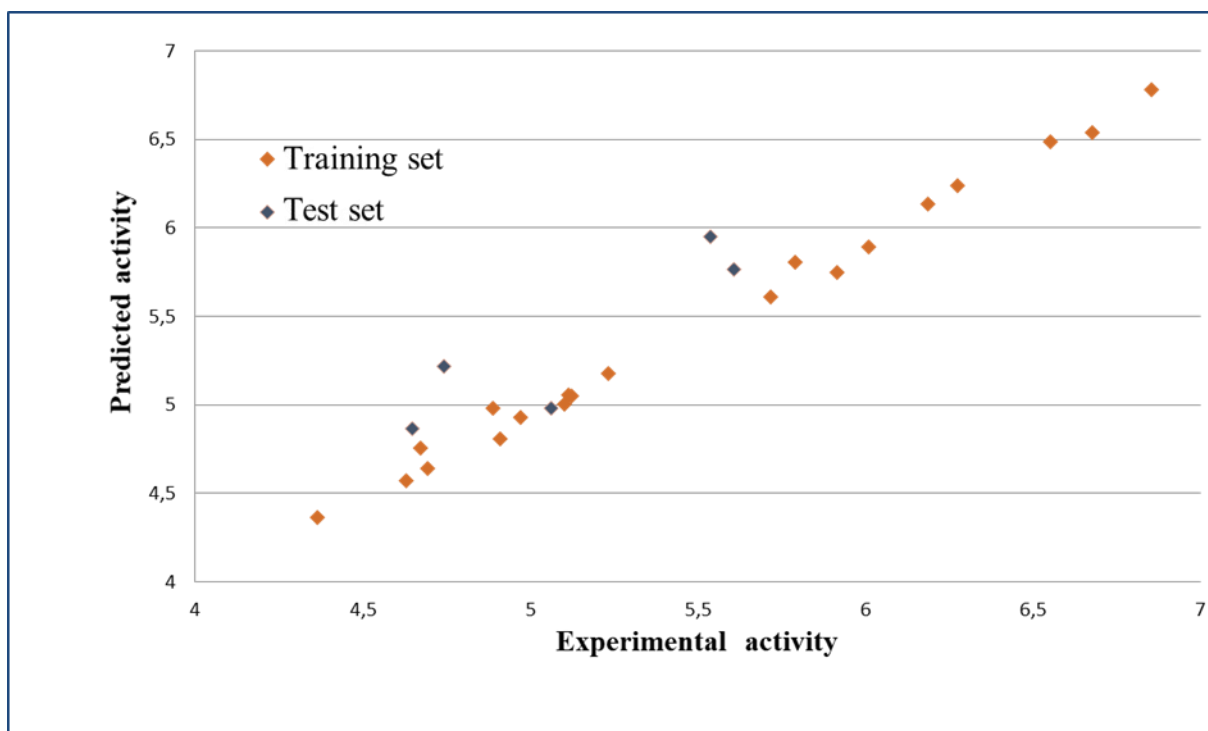


Figure VI. 3. The plot of the correlation between the experimental and predicted activity using 3D-QSAR model of training and test set.

3.3 CoMFA Contour Map

The collected data were used to illustrate the favorable and unfavorable regions during which the structural changes of the compound result in an increase or decrease in biological activity for this critical phase. The steric and electrostatic contour maps generated by CoMFA modelling for the most active compound are shown in **Figure VI. 4**. The green contours represent areas where bulky groups have a positive influence on Neuraminidase inhibitory activity, whereas the yellow contours represent areas where bulky groups have a negative influence on inhibitory activity. Steric contour maps show the spatial volume of substituted groups in a variety of locations. Because of the presence of bulky groups in advantageous locations, it is possible that the steric effect influences the inhibitory activity of compounds 22, 23, and 24.

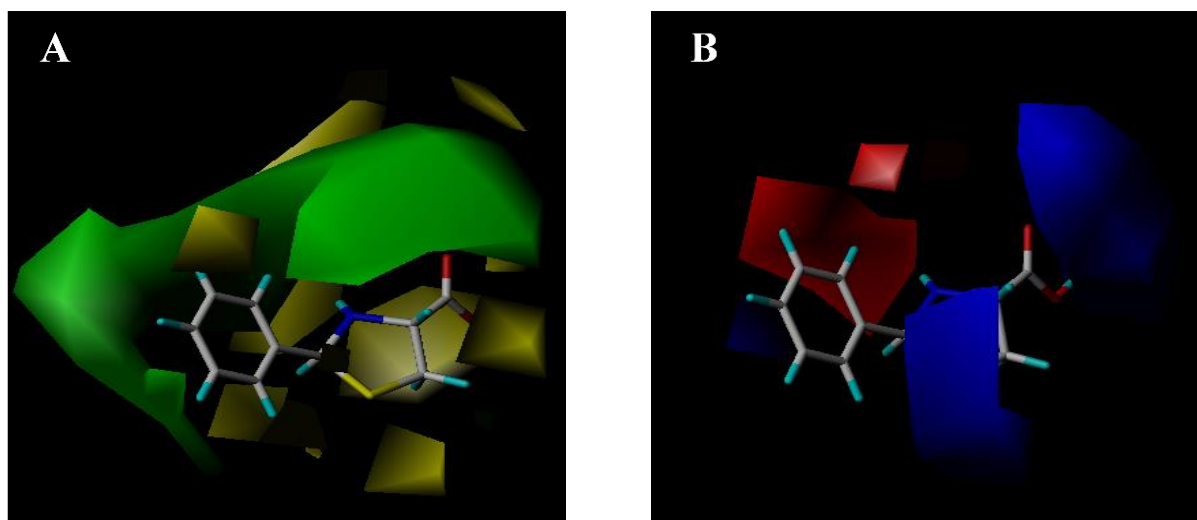


Figure VI. 4. CoMFA contour plot of compound binding to target: Visualization of (A) Steric and (B) Electrostatic Fields. Blue and green regions are favorable for inhibitory activity, red and yellow green regions are unfavorable for inhibitory activity.

The blue contours indicate locations where electronegative groups positively influence Neuraminidase inhibitory activity, whereas the red contours indicate locations where electronegative groups negatively influence inhibitory activity. The contour map shows the presence of two large blue contour maps located between the nitrogen and sulphur atoms of the thiazolidine ring, as well as medium-sized contours near the aromatic ring. This helps to explain the higher activity of compound 24 with a methoxy group near the aromatic ring and the thiazolidine's $\text{NH}_2\text{CH}_2\text{CO}$ - radical. This demonstrates that electronegative groups in these zones enhance the inhibitory activity of influenza virus. From these observations, it can be explained why the inhibitory activity of the best compounds to inhibit the vital function of Neuraminidase.

3.4 Design for New Neuraminidase Inhibitors

This study's primary goal is to develop new anti-influenza thiazolidine inhibitors. The CoMFA model contour map analysis provides useful information on structural properties for improving Neuraminidase inhibitory activity. **Figure VI. 5** depicts the collection of all orientations obtained from the CoMFA contour map, which proved to be a dependable and effective optimization strategy for the design of novel thiazolidines with high-predicted inhibitory activity. Using a comparative molecular field, we created six (Th1-Th6) novel anti-influenza thiazolidine derivatives. Six molecules were optimized and aligned, with the most active compound acting as a structural template. **Table VI. 4** summarizes the chemical structures and predicted pIC50 values of the novel compounds proposed. All six proposed compounds have higher predictive pIC50 values than the most active molecule (predictive pIC50 = 6,780 for the most active compound). These molecules can be thoroughly investigated. Finally, as shown in **Figures VI. 6** and **VI. 7**, we proposed a reaction mechanism for synthesizing these new molecules.

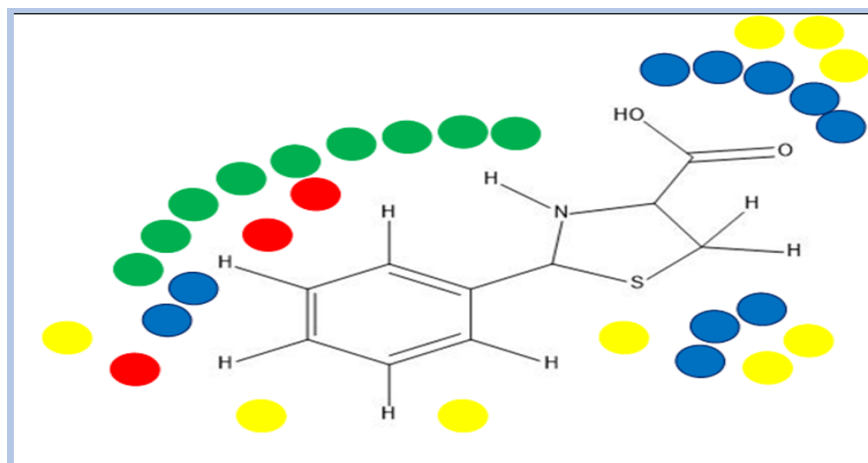


Figure VI. 5. Structural characteristics derived from CoMFA contour Map: Analysis of favorable and unfavorable regions for inhibitory activity. Blue and green regions are favorable for inhibitory activity, red and yellow green regions are unfavorable for inhibitory activity.

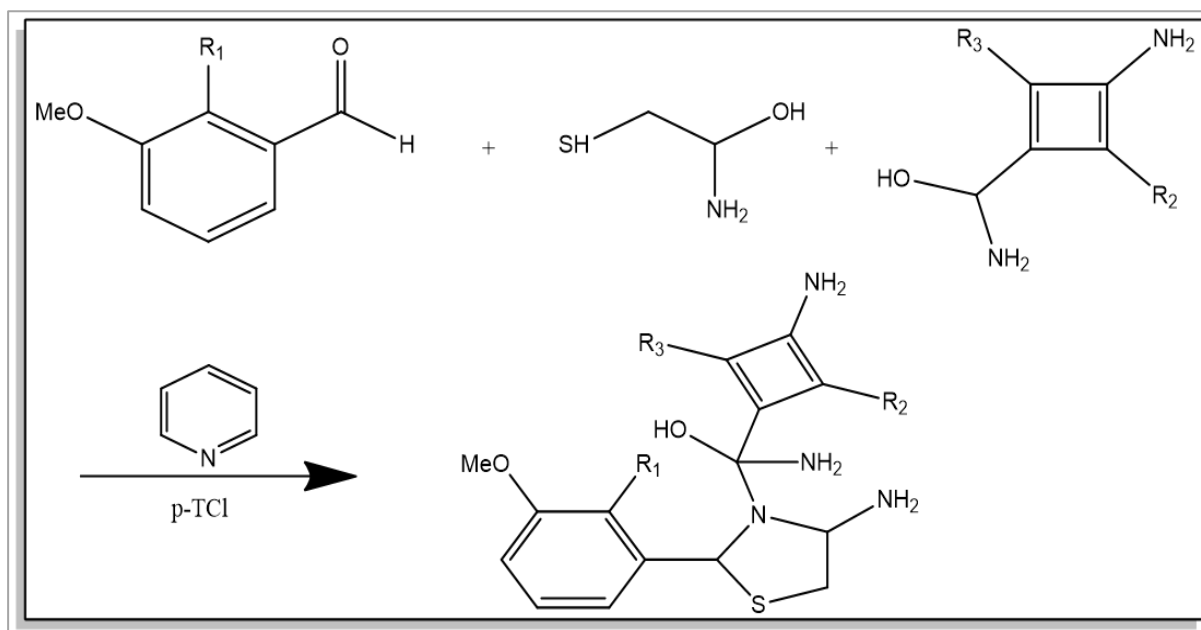


Figure VI. 6. Proposed reaction: General form and chemical equations.

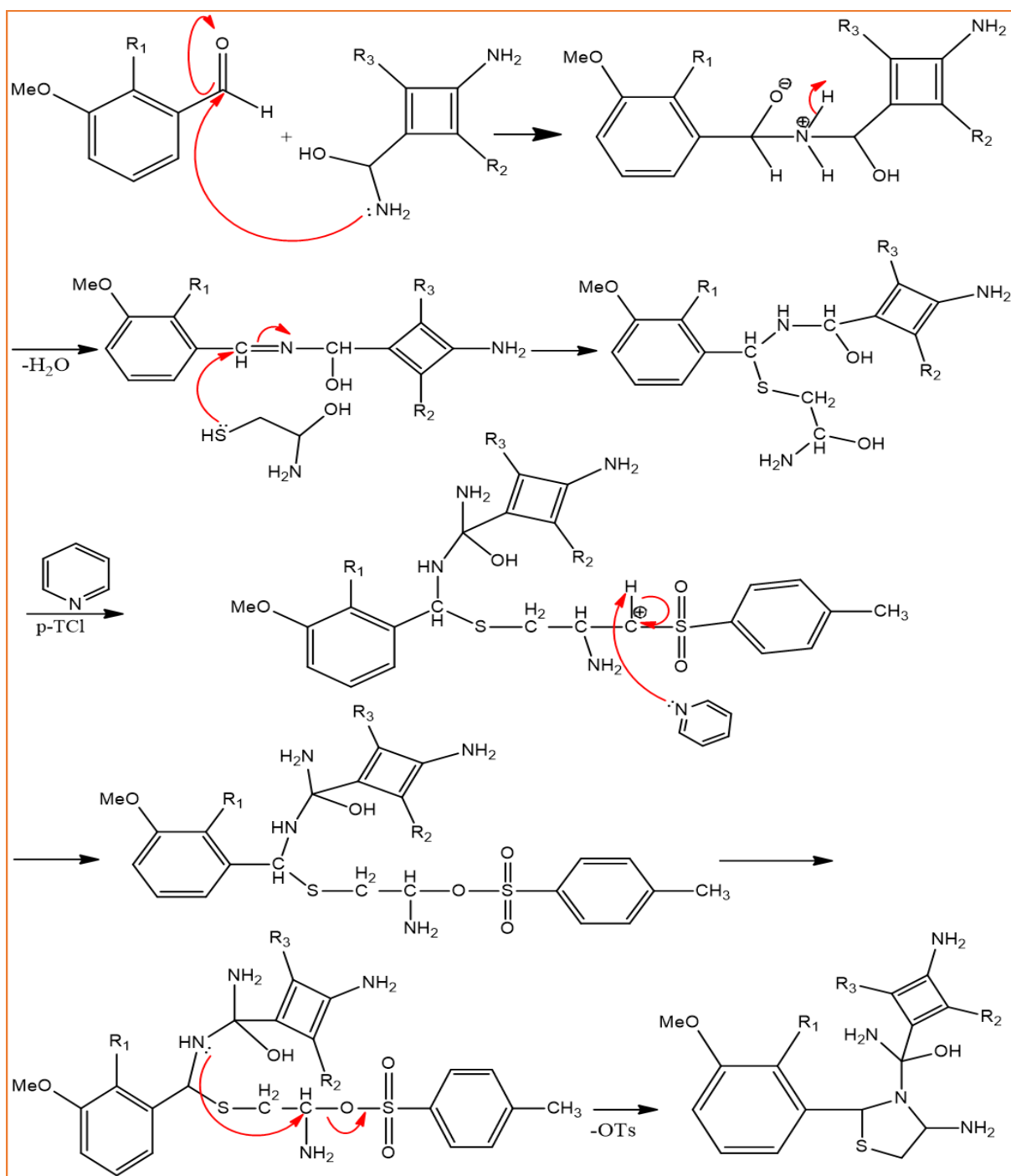
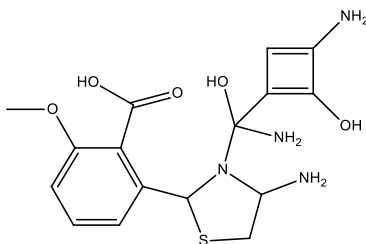


Figure VI. 7. Proposed general mechanism for synthesizing the six compounds: Insights into reaction pathways and synthetic strategies.

Table VI. 4. Structures and pIC_{50} values of novel molecules predicted by the CoMFA model.

Compound	Chemical structures	pIC_{50} predictive
		CoMFA
Th1		7.036
Th2		7.638
Th3		7.090
Th4		7.211
Th5		7.347

Th6



7.223

3.5 Molecular docking

We performed molecular docking for the six designated molecules (Th1-Th6) to gain a better understanding of how the molecules obtained by 3D-QSAR inhibit the vital function of influenza virus Neuraminidase, as well as the binding energy and types of interactions. Furthermore, we docked *Oseltamivir* with Neuraminidase to get a better estimate of the inhibitory efficacy of the proposed compounds (as another reference molecule). The docking modelling results for all proposed molecules and the Neuraminidase inhibitor are presented in **Table VI. 5**, and their types of interactions with the Neuraminidase active site are shown in **Figure VI. 8**. The results show that the designed compounds have binding affinity values ranging from -6.6 to -7.5 kcal/mol, while the binding affinity value of the reference compound (1SJ) is -6.6 kcal/mol, and the binding affinity value of *Oseltamivir* into Neuraminidase is -6.6 kcal/mol. The interaction of the reference molecule (1SJ) and *Oseltamivir* with the active site of Neuraminidase is depicted in **Figure VI. 9**. Th1, Th2, Th4, Th5, and Th6 have lower binding affinities than the reference molecule, indicating that this molecule is significantly more stable in the active site of Neuraminidase. All of the molecules, including the reference compound, interacted with the amino acids Glu119, Asp151, Glu276 and Glu277 via Salt Bridge and Attractive Charge interactions.

We observed a similarity of interaction for the two molecules with the highest binding affinity (Th2 and Th6), which interact with the amino acids Glu119, Trp178, Asp227, Glu277, and Tyr406. The reference molecule only interacts with the active site via a conventional hydrogen bond formed by the amino acids Asp151, Glu276 and Tyr406. It should be noted that conventional hydrogen bond interaction with the amino acids Glu119, Trp178, and Asp227 is critical for inhibiting the vital function of Neuraminidase. The designed molecules Th1, Th2, Th4, Th5, and Th6 demonstrate significant binding to the active site of Neuraminidase, confirming the 3D-QSAR model's good predictive power. Finally, our findings regarding the interactions between the six proposed molecules and the active site of Neuraminidase agree with the findings of *Gracy Fathima Selvaraj et al* [44].

Table VI. 5. Binding interactions and affinity values of six Neuraminidase inhibitors within the active site.

Ligand	Binding affinity (Kcal/mol)	Conventional Hydrogen Bond	Salt Bridge	Attractive Charge
Th1	-7.1	Asp151	Glu277	Asp151, Glu276, Glu277
Th2	-7.5	Asp277, Trp178, Glu277, Tyr406	Glu277	Asp151, Glu276, Glu277
Th3	-6.6	Glu276, Glu277, Tyr347, Tyr406	Asp151, Glu277	Glu119, Asp151, Glu277
Th4	-7.0	Asp151, Glu277, Tyr406	-	-
Th5	-6.9	Ala246, Tyr406	Asp151, Glu119, Glu277	Asp151, Glu119, Glu277
Th6	-7.5	Glu119, Trp178, Tyr406	Glu277	Asp151, Glu277
<i>ISJ</i> ^{ref}	-6.6	Asp151, Glu276, Tyr406	Glu277	Glu277
<i>Oseltamivir</i>	-6.6	Tyr406	-	Asp151, Glu119, Glu277

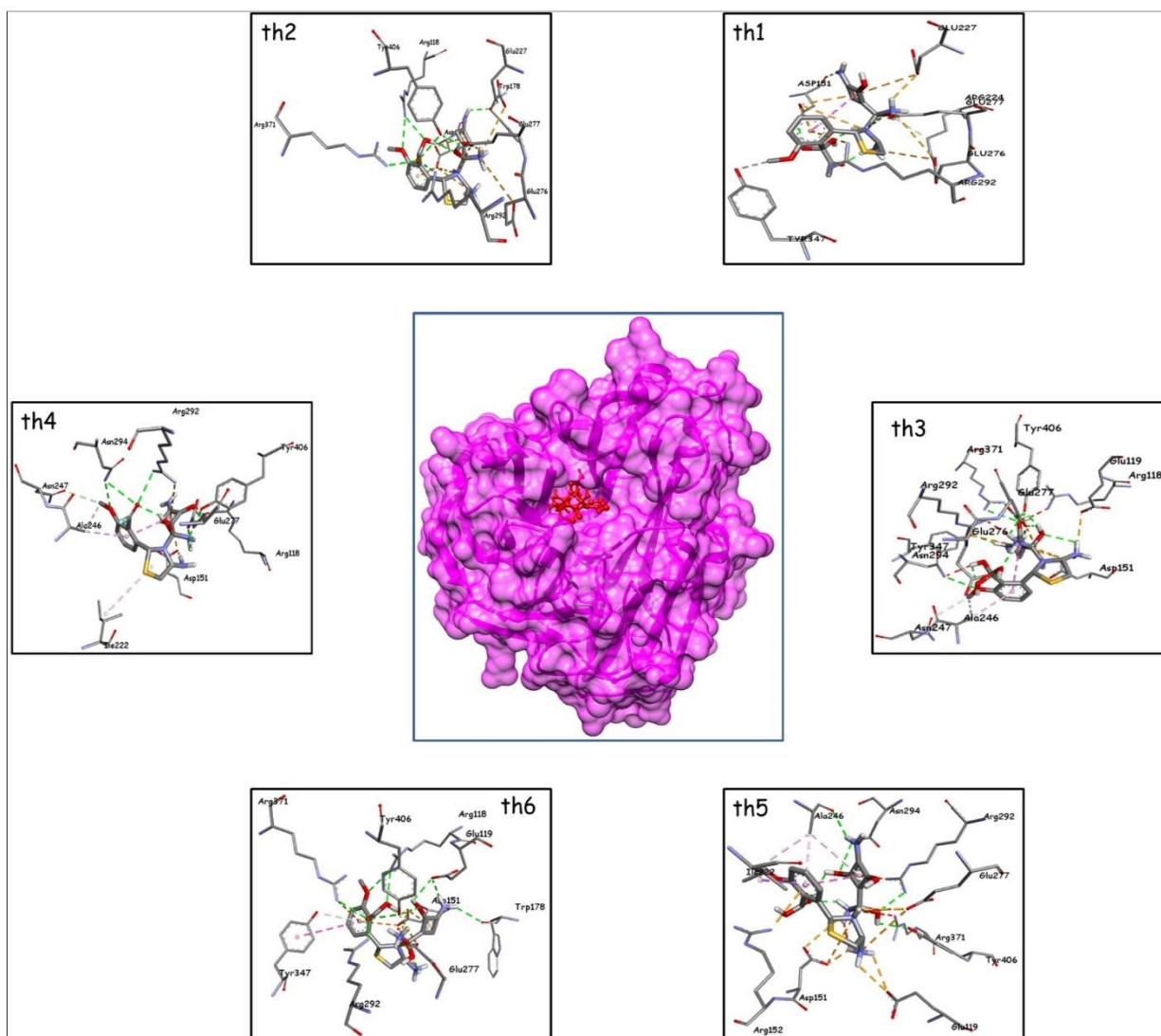


Figure VI. 8. Insights into ligand binding modes: Interactions of six designed compounds with Neuraminidase active site.

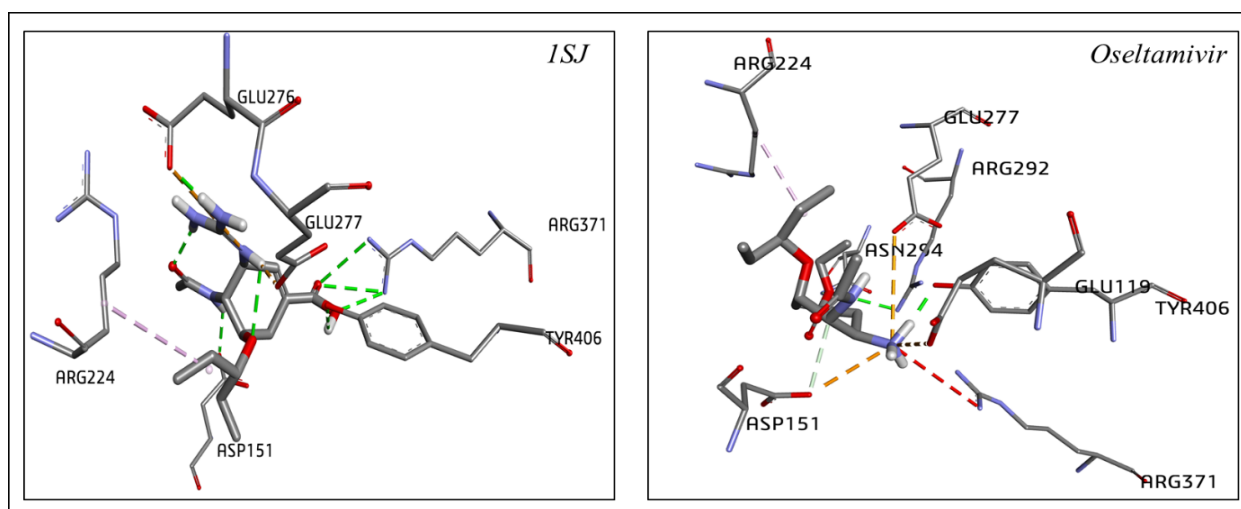


Figure VI. 9. Comparative analysis of ligand binding modes: Interactions of 1SJ and Oseltamivir with Neuraminidase

3.6 ADMET and bioavailability prediction

This study was conducted to determine the critical pharmacokinetic parameters for the six designated molecules. The results obtained by SwissADME are shown in **Table VI. 6**. All the molecules have LogP values between -1.30 and 0.06, these values indicate that all the molecules designed have good permeability towards biological membranes. For aqueous solubility, the six molecules have Log S values between -1 and 0, which means that all the molecules are easily soluble in aqueous media, according to these two parameters all the compounds have a good distribution. The six designed molecules (Th1–Th6) were estimated in silico using the five rules of Lipinski. It was that all molecules follows the Lipinski's rule. For the interactions with hepatic cytochrome P450, we did not record any interaction with them, which means that both molecules have a good metabolism. Another important parameter to quantify the pharmacokinetics of these designated molecules is the bioavailability score, the six molecules have the same bioavailability score (0.55), this value indicates that all the molecules will reach the blood circulation by the oral route (That is, both molecules are well absorbed.). For elimination, due to the aqueous solubility of six proposed compounds, they are readily eliminated renally. Also good LogKp (skin permeation) values between -10.94 and -8.55. Finally, all the proposed molecules are moderately easy to synthesize (the six molecules have synthetic accessibility values lower than 4.75).

Table VI. 6. ADME properties of newly designed compounds: Evaluation of drug-like characteristics.

Compound	MW (g/mol)	Consensus Log P	Log S	CYP3A4 inhibitor	Lipinski	Bioavailability Score	Log Kp (cm/s)	Synthetic accessibility
Th1	424.47	-1.07	-1.25	No	Yes	0.55	-10.00	4.76
Th2	364.42	-0.56	-0.35	No	Yes	0.55	-10.32	4.39
Th3	398.43	-1.30	-0.85	No	Yes	0.55	-10.19	4.63
Th4	382.41	0.06	-2.13	No	Yes	0.55	-8.55	4.53
Th5	378.38	-1.29	0.05	No	Yes	0.55	-10.94	4.31
Th6	361.40	-1.07	0.15	No	Yes	0.55	-10.84	4.32

For a quick assessment of drug-likeness, a bioavailability radar is provided. The Bioavailability radar takes into account six physicochemical properties. Lipophilicity, size, polarity, solubility, flexibility, and saturation are the parameters involved. For all molecules to be drug-like compounds, the bioavailability radar graph must be contained within a pink area. If the graph is in this pink area, the molecule has a drug-like compound. The bioavailability radar plots of the six compounds are shown in **Figure VI. 10**. Th2 and Th4 are pharmaceutical candidates. Although there is a small deviation from area at the point of polar feature, Th1, Th3, Th5, and Th6 molecules are on the verge of being considered as drug candidates. These findings indicate that all molecules have very good bioavailability profiles.

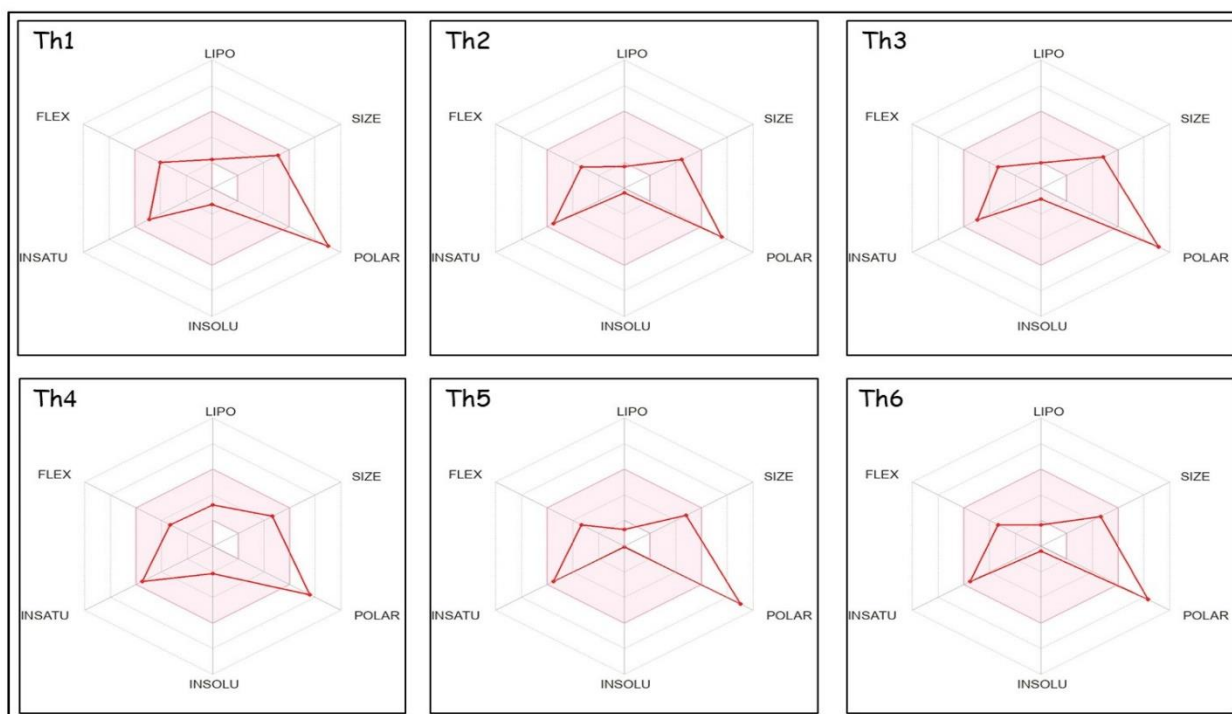


Figure VI. 10. Assessing Drug-like properties: Bioavailability radar graphs of six designed molecules.

We calculated the potential toxicity of these new molecules. **Table VI. 7**, displays the ProToxII results. We found no evidence of toxicity caused by the designed compounds, whether it was Hepatotoxicity, Carcinogenicity, Immunotoxicity, Mutagenicity, or Cytotoxicity. With LD₅₀ predictive values ranging from 230 to 8000 mg/kg and toxicity classes ranging from 2 to 4. We conclude that the molecules proposed using 3D-QSAR are both safe and pharmacologically active.

Table VI. 7. Evaluation of safety profiles: Toxicity prediction of newly designed compounds.

Compound	Hepatotoxicity	Carcinogenicity	Immunotoxicity	Mutagenicity	Cytotoxicity	Predicted LD ₅₀ (mg/kg)	Class
Th1	Inactive	Inactive	Inactive	Inactive	Inactive	230	3
Th2	Inactive	Inactive	Inactive	Inactive	Inactive	8000	4
Th3	Inactive	Inactive	Inactive	Inactive	Inactive	900	4
Th4	Inactive	Inactive	Inactive	Inactive	Inactive	900	4
Th5	Inactive	Inactive	Inactive	Inactive	Inactive	900	4
Th6	Inactive	Inactive	Inactive	Inactive	Inactive	900	4

We estimated Mutagenicity (Ames test) model (CAESAR) 2.1.14, Developmental Toxicity (CAESAR) 2.1.8, Skin Irritation (CONCERT/Kode) 1.0.0, Plasma Protein Binding (- LogK, IRFMN) 1.0.0, P-Glycoprotein activity model (NIC) 1.0.1, and finally total body elimination half-life (QSARINS) 1.0.1 using VEGA QSAR. All of the obtained results are shown in **Table VI. 8**.

All predictions show that the six designed compounds are not mutagenic or toxic to development. Aside from that, none of these molecules causes skin irritation or infection. All molecules had plasma protein binding values ranging from -0.3285 to -0.0484. Furthermore, none of the six proposed compounds interacts with P-Glycoprotein, which is found on the surface of biological cells. Furthermore, because their total body elimination half-life ranges between 1.533 and 2.837 hours, renal elimination of these molecules will be simple. The predicted toxicity study results show that all six proposed compounds are both safe and pharmacologically active.

Table VI. 8. All the results obtained from VEGA QSAR.

Compound	Mutagenicity (Ames test)	Developmental Toxicity	Skin Irritation	Plasma Protein Binding	P-Glycoprotein activity	Total body elimination half-life (hour)
Th1	Non-Mutagenic	Non-Toxicant	Non-Sensitizer	-0.3285	Non Active	2.124
Th2	Non-Mutagenic	Non-Toxicant	Non-Sensitizer	-0.099	Non Active	2.296
Th3	Non-Mutagenic	Non-Toxicant	Non-Sensitizer	-0.2242	Non Active	1.959
Th4	Non-Mutagenic	Non-Toxicant	Non-Sensitizer	-1.1011	Non Active	2.837
Th5	Non-Mutagenic	Non-Toxicant	Non-Sensitizer	-0.0484	Non Active	1.865
Th6	Non-Mutagenic	Non-Toxicant	Non-Sensitizer	-0.2455	Non Active	1.533

4. Conclusion

A 3D-QSAR analysis of 25 thiazolidine-4-carboxylic acid derivatives was constructed in this study. This analysis was carried out by creating a 3D-QSAR model using the CoMFA methodology. The derived 3D-QSAR models were validated using an external validation technique. We proposed six novel compounds with predicted inhibitory activity (pIC₅₀) greater than the most active compound based on the information provided by the contour maps. All of the proposed compounds are more stable in the active site of Neuraminidase than the reference molecule; however, *Oseltamivir* is more stable in the active site of Neuraminidase (as second reference molecule). The molecular docking analysis confirms the 3D-QSAR model's excellent prediction ability. Furthermore, we investigated the pharmacokinetic profile and potential toxicity of the six proposed compounds, and the results showed that each molecule follows Lipinski's rule and can be considered pharmacologically active and safe. We also presented a reaction mechanism for synthesizing these chemicals in order to conduct experimental research on their ability to suppress the critical function of Neuraminidase and assess their efficacy in vitro and in vivo.

5. References

- [1] Lipničanová, S., Legerská, B., Chmelová, D., Ondrejovič, M., & Miertuš, S. (2022). Optimization of an inclusion body-based production of the influenza virus neuraminidase in *Escherichia coli*. *Biomolecules*, *12*(2), 331.
- [2] Mauskopf, J., Klesse, M., Lee, S., & Herrera-Taracena, G. (2013). The burden of influenza complications in different high-risk groups: a targeted literature review. *Journal of medical economics*, *16*(2), 264-277.
- [3] Yoshida, R., Igarashi, M., Ozaki, H., Kishida, N., Tomabechi, D., Kida, H., ... & Takada, A. (2009). Cross-protective potential of a novel monoclonal antibody directed against antigenic site B of the hemagglutinin of influenza A viruses. *PLoS pathogens*, *5*(3), e1000350.
- [4] Smith, G. J., Vijaykrishna, D., Bahl, J., Lycett, S. J., Worobey, M., Pybus, O. G., ... & Rambaut, A. (2009). Origins and evolutionary genomics of the 2009 swine-origin H1N1 influenza A epidemic. *Nature*, *459*(7250), 1122-1125.
- [5] Seniya, C., Khan, G. J., Misra, R., Vyas, V., & Kaushik, S. (2014). In-silico modelling and identification of a possible inhibitor of H1N1 virus. *Asian Pacific Journal of Tropical Disease*, *4*, S467-S476.
- [6] Lackenby, A., Besselaar, T. G., Daniels, R. S., Fry, A., Gregory, V., Gubareva, L. V., ... & Meijer, A. (2018). Global update on the susceptibility of human influenza viruses to neuraminidase inhibitors and status of novel antivirals, 2016–2017. *Antiviral research*, *157*, 38-46.
- [7] Ison, M. G. (2017). Antiviral treatments. *Clinics in chest medicine*, *38*(1), 139-153.
- [8] Jefferson, T., Demicheli, V., Di Pietrantonj, C., Rivetti, D., & Cochrane Acute Respiratory Infections Group. (1996). Amantadine and rimantadine for influenza A in adults. *Cochrane Database of Systematic Reviews*, *2012*(7).
- [9] Veselovsky, A. V., & Ivanov, A. S. (2003). Strategy of computer-aided drug design. *Current Drug Targets-Infectious Disorders*, *3*(1), 33-40.
- [10] Verma, J., Khedkar, V. M., & Coutinho, E. C. (2010). 3D-QSAR in drug design-a review. *Current topics in medicinal chemistry*, *10*(1), 95-115.
- [11] Weaver, S., & Gleeson, M. P. (2008). The importance of the domain of applicability in QSAR modeling. *Journal of Molecular Graphics and Modelling*, *26*(8), 1315-1326.
- [12] Lavecchia, A., & Di Giovanni, C. (2013). Virtual screening strategies in drug discovery: a critical review. *Current medicinal chemistry*, *20*(23), 2839-2860.

- [13] Nikolic, K., Mavridis, L., Djikic, T., Vucicevic, J., Agbaba, D., Yelekci, K., & Mitchell, J. B. (2016). Drug design for CNS diseases: polypharmacological profiling of compounds using cheminformatic, 3D-QSAR and virtual screening methodologies. *Frontiers in neuroscience*, *10*, 265.
- [14] Asadollahi-Baboli, M., & Mani-Varnosfaderani, A. (2013). Molecular docking, molecular dynamics simulation, and QSAR model on potent thiazolidine-4-carboxylic acid inhibitors of influenza neuraminidase. *Medicinal Chemistry Research*, *22*, 1700-1710.
- [15] Liu, Y., Jing, F., Xu, Y., Xie, Y., Shi, F., Fang, H., ... & Xu, W. (2011). Design, synthesis and biological activity of thiazolidine-4-carboxylic acid derivatives as novel influenza neuraminidase inhibitors. *Bioorganic & medicinal chemistry*, *19*(7), 2342-2348.
- [16] Weber, H. U., Fleming, J. F., & Miquel, J. (1982). Thiazolidine-4-carboxylic acid, a physiologic sulfhydryl antioxidant with potential value in geriatric medicine. *Archives of gerontology and geriatrics*, *1*(4), 299-310.
- [17] Dowlati Beirami, A., Hajimahdi, Z., & Zarghi, A. (2019). Docking-based 3D-QSAR (CoMFA, CoMFA-RG, CoMSIA) study on hydroquinoline and thiazinan-4-one derivatives as selective COX-2 inhibitors. *Journal of Biomolecular Structure and Dynamics*, *37*(11), 2999-3006.
- [18] TRIPOS Associates, Inc. 2012, Sybyl-X molecular modeling software packages, version 2.1.1. <https://www.certara.com/pressreleases/certaraenhances-sybyl-x-drug-designand-discovery-software-suite/>
- [19] Yuan, H., Zhuang, J., Hu, S., Li, H., Xu, J., Hu, Y., ... & Lu, T. (2014). Molecular modeling of exquisitely selective c-Met inhibitors through 3D-QSAR and molecular dynamics simulations. *Journal of Chemical Information and Modeling*, *54*(9), 2544-2554.
- [20] Clark, M., Cramer III, R. D., & Van Opdenbosch, N. (1989). Validation of the general purpose tripos 5.2 force field. *Journal of computational chemistry*, *10*(8), 982-1012.
- [21] Hong, H., Fang, H., Xie, Q., Perkins, R., Sheehan, D. M., & Tong, W. (2003). Comparative molecular field analysis (CoMFA) model using a large diverse set of natural, synthetic and environmental chemicals for binding to the androgen receptor. *SAR and QSAR in Environmental Research*, *14*(5-6), 373-388.
- [22] Zięba, A., Laitinen, T., Patel, J. Z., Poso, A., & Kaczor, A. A. (2021). Docking-based 3D-QSAR studies for 1, 3, 4-oxadiazol-2-one derivatives as FAAH inhibitors. *International journal of molecular sciences*, *22*(11), 6108.

- [23] Ståhle, L., & Wold, S. (1988). 6 multivariate data analysis and experimental design in biomedical research. *Progress in medicinal chemistry*, 25, 291-338.
- [24] Baroni, M., Costantino, G., Cruciani, G., Riganelli, D., Valigi, R., & Clementi, S. (1993). Generating optimal linear PLS estimations (GOLPE): an advanced chemometric tool for handling 3D-QSAR problems. *Quantitative Structure-Activity Relationships*, 12(1), 9-20.
- [25] El Mchichi, L., El Aissouq, A., Kasmi, R., Belhassan, A., El-Mernissi, R., Ouammou, A., ... & Bouachrine, M. (2021). In silico design of novel Pyrazole derivatives containing thiourea skeleton as anti-cancer agents using: 3D QSAR, Drug-Likeness studies, ADMET prediction and molecular docking. *Materials Today: Proceedings*, 45, 7661-7674.
- [26] Golbraikh, A., & Tropsha, A. (2002). Beware of q^2 !. *Journal of molecular graphics and modelling*, 20(4), 269-276.
- [27] Kalhapure, R. S., Salunke, C. L., & Akamanchi, K. G. (2012). QSAR model for chemical penetration enhancers containing long hydrocarbon chain. *Chemometrics and Intelligent Laboratory Systems*, 118, 267-270.
- [28] Roy, K. (2007). On some aspects of validation of predictive quantitative structure–activity relationship models. *Expert Opinion on Drug Discovery*, 2(12), 1567-1577.
- [29] Rücker, C., Rücker, G., & Meringer, M. (2007). γ -Randomization and its variants in QSPR/QSAR. *Journal of chemical information and modeling*, 47(6), 2345-2357.
- [30] Dias, R., de Azevedo, J., & Walter, F. (2008). Molecular docking algorithms. *Current drug targets*, 9(12), 1040-1047.
- [31] Fan, J., Fu, A., & Zhang, L. (2019). Progress in molecular docking. *Quantitative Biology*, 7, 83-89.
- [32] Prieto-Martínez, F. D., López-López, E., Juárez-Mercado, K. E., & Medina-Franco, J. L. (2019). Computational drug design methods—current and future perspectives. *In silico drug design*, 19-44.
- [33] Trott, O., & Olson, A. J. (2010). AutoDock Vina: improving the speed and accuracy of docking with a new scoring function, efficient optimization, and multithreading. *Journal of computational chemistry*, 31(2), 455-461.
- [34] Temml, V., & Kutil, Z. (2021). Structure-based molecular modeling in SAR analysis and lead optimization. *Computational and Structural Biotechnology Journal*, 19, 1431-1444.

- [35] Acharya, B., Ghosh, S., & Manikyam, H. K. (2016). NATURE'S RESPONSE TO INFLUENZA: A HIGH THROUGHPUT SCREENING STRATEGY OF AYURVEDIC MEDICINAL PHYTOCHEMICALS. *International Journal of Pharmaceutical Sciences and Research*, 7(6), 2699.
- [36] Tan, Q., Duan, L., Ma, Y., Wu, F., Huang, Q., Mao, K., ... & Jin, Y. (2020). Is oseltamivir suitable for fighting against COVID-19: In silico assessment, in vitro and retrospective study. *Bioorganic chemistry*, 104, 104257.
- [37] Seeliger, D., & de Groot, B. L. (2010). Ligand docking and binding site analysis with PyMOL and Autodock/Vina. *Journal of computer-aided molecular design*, 24(5), 417-422.
- [38] Jug, G., Anderluh, M., & Tomašič, T. (2015). Comparative evaluation of several docking tools for docking small molecule ligands to DC-SIGN. *Journal of Molecular Modeling*, 21, 1-12.
- [39] Sharma, S., Kumar, P., & Chandra, R. (2019). Applications of BIOVIA materials studio, LAMMPS, and GROMACS in various fields of science and engineering. *Molecular dynamics simulation of nanocomposites using BIOVIA materials studio, Lammops and Gromacs*, 329-341.
- [40] Daina, A., Michielin, O., & Zoete, V. (2017). SwissADME: a free web tool to evaluate pharmacokinetics, drug-likeness and medicinal chemistry friendliness of small molecules. *Scientific reports*, 7(1), 42717.
- [41] Banerjee, P., Eckert, A. O., Schrey, A. K., & Preissner, R. (2018). ProTox-II: a webserver for the prediction of toxicity of chemicals. *Nucleic acids research*, 46(W1), W257-W263.
- [42] Benfenati E, Manganaro A, Gini G. 2013, 1107,21–28. <http://www.vegahub.eu/portfolio-item/vega-qsar/>. Accessed 12 April 2019.
- [43] Zięba, A., Laitinen, T., Patel, J. Z., Poso, A., & Kaczor, A. A. (2021). Docking-based 3D-QSAR studies for 1, 3, 4-oxadiazol-2-one derivatives as FAAH inhibitors. *International journal of molecular sciences*, 22(11), 6108.
- [44] Selvaraj, G. F., Piramanayagam, S., Devadasan, V., Hassan, S., Krishnasamy, K., & Srinivasan, S. (2020). Computational analysis of drug like candidates against Neuraminidase of Human Influenza A virus subtypes. *Informatics in Medicine Unlocked*, 18, 100284.

General Conclusion

The influenza virus infects the nose, throat and lungs. It can cause mild to severe disease and, in extreme cases, death. The easiest approach to avoiding flu is to obtain a flu vaccine every year. In this study, we combined multiple computational and bioinformatics techniques for drug discovery to create a new and effective treatment for influenza and its consequences. Pharmacophore-based virtual screening, 3D-QSAR, fragment-based drug design, breed De Novo hybridization, molecular docking, ADMET investigations, molecular dynamics simulations and MM-PBSA calculations are the approaches that were applied.

Generally, in comparison to the clinical inhibitors (*Zanamivir*, *Oseltamivir* and *Peramivir*) all of the proposed compounds bind strongly to Neuraminidase and form extremely stable complexes with it. At the pharmacokinetics level, the developed compounds have very good pharmacological profiles such as bioavailability, solubility, permeability, interactions with P-Glycoprotein and total body elimination half-life. On other hand, the proposed compounds were quickly metabolized in the liver and did not create toxic compounds, and no inhibition of cytochrome P450 such as CYP 3A4 was found. Furthermore, we assessed the potential toxicity (Mutagenicity, Developmental Toxicity, Hepatotoxicity, Immunotoxicity and Cytotoxicity) of such compounds and found that it was within an acceptable range.

Another critical consideration is the molecular stability of the proposed molecules within the Neuraminidase receptor. Following the interpretation of molecular dynamics simulation data and evaluation of RMSD, RMSf, Rg, H-bonds, SASA, and MM-PBSA calculations for each proposed molecule, we concluded the great stability of the formed complexes between the designed molecules and the active site of Neuraminidase, and we clearly saw insignificant atomic shift and the continuation of structural stability. During 100 ns of simulation, the findings validate the biomolecular structural stability of the proposed molecules within the Neuraminidase receptor.

Finally, we provided a chemical mechanism for synthesizing some of the proposed compounds in order to test their inhibitory activity *in vitro* and *in vivo*. These findings could play a role in the creation of new and powerful neuraminidase inhibitor for the treatment of influenza, as well as provide researchers with the chance to investigate these created compounds for the treatment of flu and its complications.